CZECH TECHNICAL
UNIVERSITY
IN PRAGUE

FACULTY
OF MECHANICAL
ENGINEERING

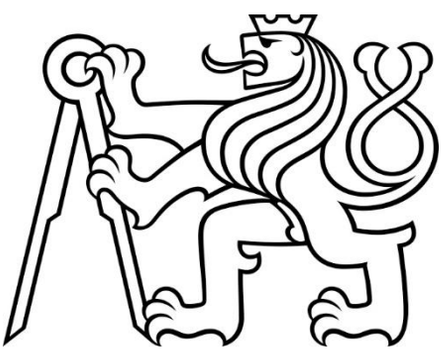

MASTER'S THESIS

2020

JAKUB
RYBÍN

ZADÁNÍ DIPLOMOVÉ PRÁCE

I. OSOBNÍ A STUDIJNÍ ÚDAJE

Příjmení: **Rybín** Jméno: **Jakub** Osobní číslo: **462166**

Fakulta/ústav: **Fakulta strojní**

Zadávající katedra/ústav: **Ústav strojírenské technologie**

Studijní program: **Strojní inženýrství**

Studijní obor: **Výrobní a materiálové inženýrství**

II. ÚDAJE K DIPLOMOVÉ PRÁCI

Název diplomové práce:

Plazmové navařování wolframu pro fúzní aplikace

Název diplomové práce anglicky:

Plasma overlays of tungsten for fusion application

Pokyny pro vypracování:

Provést rešerši na téma fúzní energetiky, plazmového navařování, materiály pro první stěnu (PFM), funkčně gradované materiály
Experimentálně ověřit možnost navaření směsi titanu a wolframu na kovovou podložku
Popsat základní vlastnosti směsných návarů
Zhodnotit výsledky a doporučit další postup

Seznam doporučené literatury:

ELIEZER, Yaffa. a Shalom. ELIEZER. The fourth state of matter: an introduction to plasma science. 2nd ed. Philadelphia: IOP, 2001.
MATĚJÍČEK, J. Materials for Fusion Applications. Acta Polytechnica [online]. Praha: České vysoké učení technické v Praze, 2013
D'OLIVEIRA, A., R. PAREDES a R. SANTOS. Pulsed current plasma transferred arc hardfacing. Journal of materials processing technology. Amsterdam: Elsevier Science Publishers, 2006
NAEBE, Minoo a Kamyar SHIRVANIMOGHADDAM. Functionally graded materials: A review of fabrication and properties. Applied Materials Today [online]. 2016

Jméno a pracoviště vedoucí(ho) diplomové práce:

Ing. Pavel Rohan, Ph.D., ústav strojírenské technologie FS

Jméno a pracoviště druhé(ho) vedoucí(ho) nebo konzultanta(ky) diplomové práce:

Datum zadání diplomové práce: **29.04.2020** Termín odevzdání diplomové práce: **31.07.2020**

Platnost zadání diplomové práce: **31.12.2020**

Ing. Pavel Rohan, Ph.D.	doc. Ing. Ladislav Kolařík, Ph.D.	prof. Ing. Michael Valášek, DrSc.
podpis vedoucí(ho) práce	podpis vedoucí(ho) ústavu/katedry	podpis děkana(ky)

III. PŘEVZETÍ ZADÁNÍ

Diplomant bere na vědomí, že je povinen vypracovat diplomovou práci samostatně, bez cizí pomoci, s výjimkou poskytnutých konzultací. Seznam použité literatury, jiných pramenů a jmen konzultantů je třeba uvést v diplomové práci.

12.06.2020
Datum převzetí zadání

Podpis studenta

Annotation Record

Author's name:	Jakub Rybín
Title of master's thesis:	Plasma overlays of tungsten for fusion applications
Název diplomové práce:	Plazmové navařování wolframu pro fúzní aplikace
Academic year:	2019/2020
Programme of study:	Mechanical engineering
Field of study:	Production and Materials Engineering
Institution:	Department of Manufacturing Technology
Master's thesis supervisor:	Ing. Pavel Rohan, Ph. D.
Bibliographic information:	Number of pages: 112 Number of tables: 17 Number of figures: 60 Number of appendices: 2

This work was written in cooperation with the Institute of Plasma Physics of the Czech Academy of Sciences, a public research institute.

Tato práce vznikla ve spolupráci s Ústavem fyziky plazmatu Akademie věd České republiky, v. v. i.

FACULTY OF MECHANICAL ENGINEERING CTU IN PRAGUE

Department of Manufacturing Technology

IPP

Abstract

This work explores the possibilities of manufacturing and using a functionally graded material of titanium and tungsten for applications in plasma facing components of fusion reactors. In its theoretical part, it provides an overview of the current status of nuclear fusion research and nuclear fusion devices. Emphasis is placed on the problematics of plasma facing components and especially plasma facing materials. The properties of titanium, tungsten and their alloys are discussed, as is the concept of functionally graded materials. Finally, the technology of plasma transferred arc cladding is addressed. In its practical part, this work describes the experimental manufacturing of a titanium-tungsten functionally graded material by the plasma transferred arc method. The results achieved on a total of five experimental samples are presented and discussed. The results show that a titanium-tungsten functionally graded material can be successfully manufactured by the plasma transferred arc method. Furthermore, results show that the resultant material is suitable for further research on its specific properties, with regards to the use of such material in future nuclear fusion reactors.

Abstrakt

Tato práce se zabývá možnostmi výroby a použití funkčně gradovaného materiálu titanu a wolframu pro aplikace v komponentech vystavených plazmatu ve fúzních reaktorech. V teoretické části podává přehled o současném stavu výzkumu v oblasti jaderné fúze a fúzních zařízení. Důraz je kladen zejména na problematiku komponent a materiálů přímo vystavených plazmatu. V práci jsou dále popsány vlastnosti titanu, wolframu, a jejich slitin. Následně se práce věnuje problematice funkčně gradovaných materiálů a také technologii *plasma transferred arc*. V praktické části je pak popsána experimentální výroba funkčně gradovaného materiálu titanu a wolframu metodou *plasma transferred arc*. Celkem jsou prezentovány a popsány výsledky, kterých bylo dosaženo na pěti experimentálních vzorcích. Výsledky ukazují, že je možné vyrobit funkčně gradovaný materiál titanu a wolframu metodou *plasma transferred arc*. Výsledky dále naznačují vhodnost vyrobeného materiálu k dalšímu zkoumání jeho konkrétních vlastností ve vztahu k možnému využití tohoto materiálu v budoucích fúzních reaktorech.

Keywords

functionally graded material, plasma facing material, plasma facing component, nuclear fusion, fusion reactor, plasma transferred arc, cladding, overlays, titanium, tungsten, FGM, PFM, PFC, PTA

Klíčová slova

funkčně gradovaný materiál, materiál vystavený plazmatu, komponent vystavený plazmatu, jaderná fúze, fúzní reaktor, plasma transferred arc, navařování, návary, titan, wolfram, FGM, PFM, PFC, PTA

Sworn statement

I declare that I have prepared and written this master's thesis independently, with the contribution of expert consultations and the literature listed below.

Praha, 20.8.2020.

.....

Acknowledgements

I would like to take this opportunity to sincerely thank the supervisor of this thesis, Pavel Rohan, for his professional supervision, assistance, and overall support during the completion of this work. I would also like to thank Jiří Matějíček of the Institute of Plasma Physics, for his valued help in analysing samples and providing priceless professional insight. Finally, I would like to thank the employees of the Czech Technical University, who helped with the preparation of materials, samples, and equipment for this work.

Table of Contents

List of Figures

List of Tables

List of Appendices

List of Abbreviations

FGM	Functionally Graded Material
PTA	Plasma Transferred Arc
D-T	Deuterium-Tritium
ITER	International Thermonuclear Experimental Reactor
PFC	Plasma Facing Component
PFM	Plasma Facing Material
DBTT	Ductile-to-Brittle Transition Temperature
JET	Joint European Torus
VPS	Vacuum Plasma Spraying
RSUHP	Resistance Sintering Under Ultra-High Pressure
PVD	Physical Vapour Deposition
CVD	Chemical Vapour Deposition
Ti-W	Titanium-tungsten
α-Ti	α-Titanium
β-Ti	β-Titanium
ω-Ti	ω-Titanium
BCC	Body-centred cubic
HCP	Hexagonally close-packed
PAW	Plasma Arc Welding
TIG	Tungsten Inert Gas
SEM	Scanning Electron Microscope
EDS	Energy Dispersive Spectroscopy
XRD	X-Ray Diffraction
I/F	Interface

PLASMA OVERLAYS OF TUNGSTEN FOR FUSION APPLICATIONS

P R A H A

2020

1 Introduction

Ever since the emergence of humankind as an intelligent, dominant, and motivated species, people have been driven in the search for sources of energy that would ultimately lead to the growth of an entire civilization. From the most primitive sources of energy such as animal power, wood burning or through the taming of watercourses, humankind has come a long way to reach the level of technology that is familiar to us today; be it in nuclear power plants, geothermal plants, impressive hydroelectric works, or any other of the vast array of energy sources that are currently being utilised - and in some ways, exploited.

The fact that throughout the centuries, different energy sources have allowed our civilization to sustain, grow, and further increase its wealth and standard of living is without question, however all of the historically and currently utilised sources of energy are not without drawbacks. Despite the great technological advancements, made especially in the 19th and 20th centuries, there is always a trade-off to be considered – air and water pollution, risk of a nuclear accident, devastation of vast areas of nature. Given the unprecedented rise in the global population, standard of living, consumption of non-renewable resources and the dependence on electric power in the post-WWII era, the ultimate conclusion is, given the current situation and future prognosis, that all currently utilised energy sources of significance are ultimately unsustainable, or greatly impractical.

One energy source, however, has not yet been conquered by humankind – nuclear fusion. The energy source that is the driving force of the universe, that is ever-present in every aspect of life on Earth, yet is so difficult to attain and utilise in the available conditions. Dubbed the *Holy Grail of Energetics*, nuclear fusion would effectively suffice in satisfying all of humanity's energy needs until the cessation of life on Earth, and yet presents few drawbacks (especially in terms of the ill-effects on the environment) in comparison to current alternatives. The biggest drawback of nuclear fusion is the sheer difficulty of its realization in the confined conditions on Earth, as evidenced by the decades of research that have to date not resulted in a viable energy source. [1]

One hundred and fifteen years after Albert Einstein laid down the groundworks for the special theory of relativity, nuclear fusion is now understood and described to a satisfactory level. Nevertheless, the technical aspects of realizing a controlled, sustained and significantly energetically profitable fusion reaction present a vast challenge.

One of the greatest difficulties in the construction of a thermonuclear fusion reactor is the fact that primarily the components inside the reactor itself, directly exposed to plasma, have to be able to withstand extreme conditions, in all respects, for prolonged periods of time. To this effect, the materials used for in-reactor plasma facing applications have to satisfy strict requirements that are presented by the nature of their application, in conditions that are practically unprecedented and unimaginable in any other environment on this planet.

It is becoming clear that conventional materials are not able to, or will soon not be able to, hold up to this challenge, and new materials and their combinations are therefore the subject of research. In this respect, functionally graded materials, or FGMs, present an interesting possible solution, as they allow the full utilisation of properties of multiple materials in a single application, without the need for compromise, in a *best of both worlds* setting. [2]

This master's thesis aims to explore the possibilities of FGMs, specifically a combination of titanium and tungsten, in fusion reactor, plasma facing applications. In its theoretical part, this master's thesis will provide a brief introduction to the concept of nuclear fusion reactors and their components, with emphasis on plasma facing components, and most importantly, plasma facing materials. The concept of functionally graded materials will be explored, as will plasma transferred arc (PTA) technology, which will be used in the practical experiment. The experimental part of this master's thesis aims to utilise plasma transferred arc technology in fabricating a functionally graded material of titanium and tungsten, and evaluate the resulting material, with consideration for its application in nuclear fusion reactors.

2 Controlled Thermonuclear Fusion as a Source of Energy

The past decades have witnessed an unprecedented rise in energy consumption, which, when contrasted with the realization that fossil fuels will inevitably be depleted, leads to an increased demand for a new energy source. This demand is currently partially met with a variety of "renewable" energy sources, heralded with utopic visions of the future energy-neutral existence of humankind, which many are naturally beginning to doubt. At such a time, it seems that nuclear fusion is realistically the only energy source capable of satisfying the ever-increasing demand for energy, and reducing the growing energy deficit of humankind, while at the same time completely eliminating many of the shortcomings of other conventional or renewable sources of energy. [1] [3]

2.1 Comparison of a Nuclear Fusion Reaction to Other Sources of Energy

In principle, most of the energy available on Earth in any form originates from nuclear fusion and has gone through a finite number of transformations to finally be utilised, all indirectly, with minimum efficiency. In contrast, a fusion reactor would allow for the energy released in a fusion reaction to be utilised directly, with an efficiency 10 000 000 times greater than that of any chemical reaction. [1]

The primary fuel for current, as well as likely future fusion reactors is deuterium, one of two stable isotopes of hydrogen (the other being protium), which can be found in nearly all compounds of hydrogen, including water, of which there is (and will be) an abundance in the Earth's oceans. This abundance is made clear by the fact that while crude oil supplies are estimated to last centuries, deuterium (in the amount available and given the current energy consumption) would last for as long as eight billion years. The energy density as well as specific energy of the deuterium/tritium fuel[1] is also significantly higher than that of any other fuel, as illustrated in the following Table 2.1.[2] [1] [4] [5]

[1] Deuterium/tritium – see Part 2.2.
[2] Simplified, illustrative comparison of fuels used in fundamentally different reactions and circumstances.

Table 2.1: Specific energy and energy density of different fuels [5]

Fuel [-]	Specific energy [MJ.kg^{-1}]	Energy density [MJ.m^{-3}]
Wood	1.6 x 10^{1}	1 x 10^{4}
Coal	2-6 x 10^{1}	2-6 x 10^{9}
Gasoline	4.5 x 10^{1}	3.5 x 10^{7}
Water (falling from 100m)	1 x 10^{-3}	1 x 10^{3}
Natural gas (at atmospheric pressure)	5.5 x 10^{1}	3.5 x 10^{4}
Uranium (for fission reaction)	8 x 10^{7}	1.5 x 10^{15}
Deuterium/tritium (for fusion reaction)	3 x 10^{8}	6 x 10^{15}

Furthermore, unlike uranium fuel used in nuclear fission reactors, the fuel for a fusion reactor is not radioactive, and given the nature of the reaction, neither is the "waste product", which is, in effect, pure helium – a non-toxic, inert gas, of which there is an overall shortage. A future nuclear power plant will thus be, in principle, emission free. Finally, it cannot go unmentioned, that unlike a nuclear fission reaction, a fusion reaction cannot be sustained without the active support of auxiliary systems. This quality, combined with the fact that at any one time, a reactor will only contain grams of fuel, makes a nuclear fusion reactor inherently internally stable. In effect, should auxiliary systems fail or should control be lost, the ongoing reaction will self-extinguish, which effectively eliminates any risk of a severe nuclear accident. [1] [4]

2.2 Fundamentals of Nuclear Fusion and Plasma

Fusion is one of two fundamental nuclear reactions, the other being fission. In a fusion reaction, two nuclei of lighter element atoms are brought together to approximately 10^{-14} m, which is sufficient to overcome the potential barrier of repulsive Coulomb forces between nuclei and is within range of the nuclear force. The nuclear force then prevails over the repulsive Coulomb forces, and the nuclei are fused together, with the mass of the products of the reaction being lower than the mass of the original constituents. In his *annus mirabilis* papers, Albert Einstein came to the indispensable realization that any body of any mass possesses an equivalent amount of energy, and *vice versa*. This mass-energy equivalence stipulates that the difference in mass, observed between the original constituents

and the reaction products, was “released” resulting in a substantial discharge of energy during the reaction, in accordance with Einstein’s - now iconic - equation; $E = m \cdot c^2$. [1] [6]

The reaction between deuterium and tritium, schematically shown below in Figure 2.1, is one of almost eighty possible fusion reactions, and is currently the most feasible in the context of first-generation fusion reactors. During this reaction, 80% of the discharged energy is released as the kinetic energy of the neutron, while the remaining 20% is released as the kinetic energy of the alpha-particle, as described by Equation 1. [1] [7]

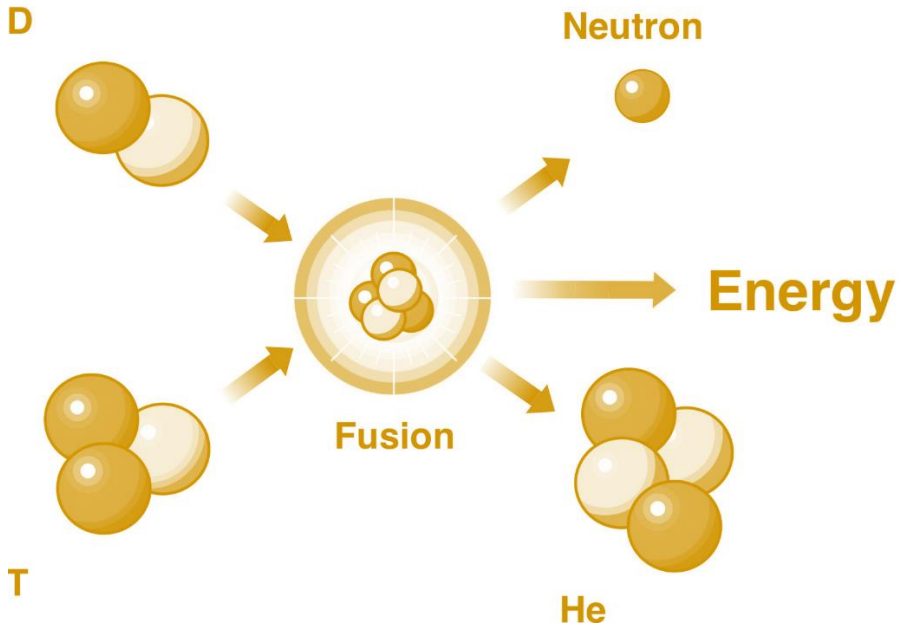

Figure 2.1: Fusion reaction between deuterium (D) and tritium (T) [8]

$$D + T \rightarrow {}^{4}He(3.52\ MeV) + n(14.07\ MeV) \qquad (1)$$

where:

D.....deuterium,
T.....tritium,
${}^{4}He$....helium-4, and
n.....neutron.

In order to overcome the repulsive forces between the nuclei and to bring them close enough together, significant energy must be delivered. This energy can be delivered in one of two ways; either in the form of kinetic energy, when nuclei

are collided in a particle accelerator, or in the form of heat, when the nuclei are heated to a high temperature. Due to the immense energetic requirements of accelerating the nuclei, it is not possible to achieve a positive energy balance this way, and the second – thermonuclear – approach will therefore be utilised in fusion power plants, as it is in current experimental devices. The optimum temperature for the deuterium-tritium (D-T) fusion is approximately 163 000 000 °C, at which the atoms of all elements are in a state of matter, in which their atoms are ionised – the state of plasma. In this state, the negatively charged electrons and the positively charged ions move independently, as schematically shown in Figure 2.2, in a quasi-neutral environment, giving this state its unique properties. [4] [9] [10] [11]

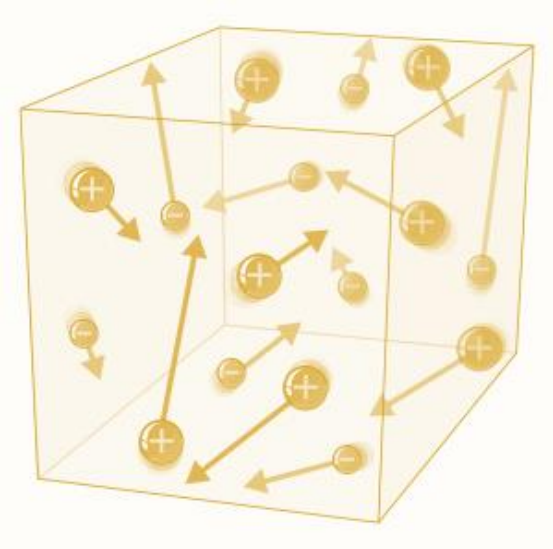

Figure 2.2: Quasi-neutral model of plasma [12]

In most materials, the dynamics of their movement are described by forces acting between neighbouring regions of the material. Plasma displays collective behaviour and electric neutrality on a macroscopic level, but the independent movement of charged particles creates electric fields, electric currents, and consequently, magnetic fields, on a microscopic level. As a result, plasma can be confined entirely in an appropriate magnetic field; a property of paramount significance for the construction of magnetic confinement fusion reactors. [11] [13]

2.3 Magnetic Confinement Fusion Reactors

For a fusion reaction to be energetically profitable, the product of plasma density and confinement time must essentially amount to a certain value. This figure of merit, now called the Lawson Criterion, was formulated in 1955 by John D. Lawson, and takes the form of Equation 2 below: [4] [14]

$$n \cdot \tau_E \geq f(T) \qquad (2)$$

where:

n..... plasma density [m^{-3}],
τ_E ..... confinement time [s], and
T..... temperature [K].

Two approaches arise from the Lawson Criterion; either confine plasma at low density for an extended period of time, or confine plasma at very high density for a brief moment. Magnetic confinement utilises the first approach (as opposed to inertial confinement), and makes use of the electromagnetic properties of plasma, as described in in Part 2.2.

In a magnetic confinement, a combination of magnets and electric currents within the plasma produces a geometrically specific magnetic field (shown below in Figure 2.3), used to confine the plasma, and prevent it from colliding with reactor walls as a result of particle drift.

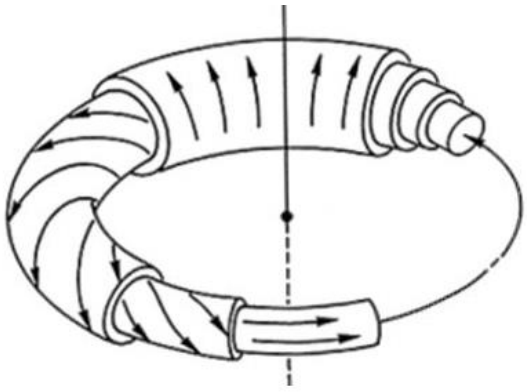

Figure 2.3: Magnetic field for plasma confinement [1]

2.4 Technological Aspects of Magnetic Confinement Fusion Reactors

Currently, the most promising type of fusion reactor with magnetic confinement is the *tokamak* (by transcription from Russian; ***то**роидальная **ка**мера с **ма**гнитными **ка**тушками*). The tokamak is essentially a transformer core, surrounded by a toroidal vessel holding hydrogen plasma, which acts as the secondary winding of a single-threaded transformer, as shown below in Figure 2.4.

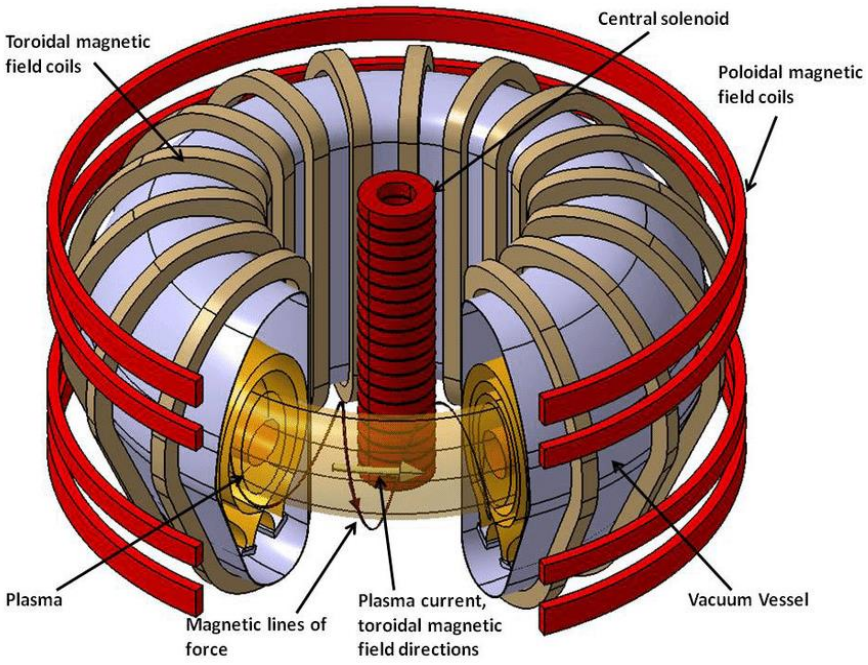

Figure 2.4: Schematic of a tokamak [15]

The resultant magnetic field of the tokamak is the product of superposing the toroidal component generated by the magnetic coils, and the poloidal component generated by a current induced in the plasma. Given the specific nature of the tokamak, with a current being induced in the plasma, it principally operates in a pulsed nature; corresponding to the saturation of the transformer core – the solution to this problem is the subject of concurrent research. [1] [16]

Owing to the significant electrical resistance of the hydrogen gas, through which the induced current is flowing, the plasma is effectively heated by the resulting Joule heat, as per the Joule-Lenz law. In addition, external methods of heating are used at higher temperatures, as the ohmic resistance decreases. Two

currently researched and promising methods, intended for the ITER[3] project, are heating by neutral particle beams, making use of a significant amount of energy carried by particles injected into the plasma, and heating by absorbing electromagnetic waves, in a manner not unfamiliar from microwave ovens. [16] [17]

The reactor vessel itself houses the plasma and the ongoing reaction, and acts as the primary barrier against the radiation it contains, as such it is classified as a safety-important component. It is ring-shaped, with a cross-section resembling the letter D, on most contemporary tokamaks. The vessel supports high vacuum, and is itself (on ITER) enclosed in a vacuum cryostat; in place to prevent losses in the superconducting magnets contained within at a temperature of around 4.5 K. The reactor vessel also supports the in-reactor components, directly exposed to the plasma; namely the *blanket* with the *first wall*, and the *divertor*, which will be described in greater detail in the following Part 2.5. The entire tokamak as a functional unit is depicted below in Figure 2.5 for clarity; note the blanket (❹) and divertor (❺) inside the vacuum vessel. The depicted tokamak is the ITER, however a similar setup, albeit at different scales, is characteristic of nearly all tokamaks. [16] [17]

[3] World's largest tokamak, currently under construction in Cadarache, France, as of 2020.

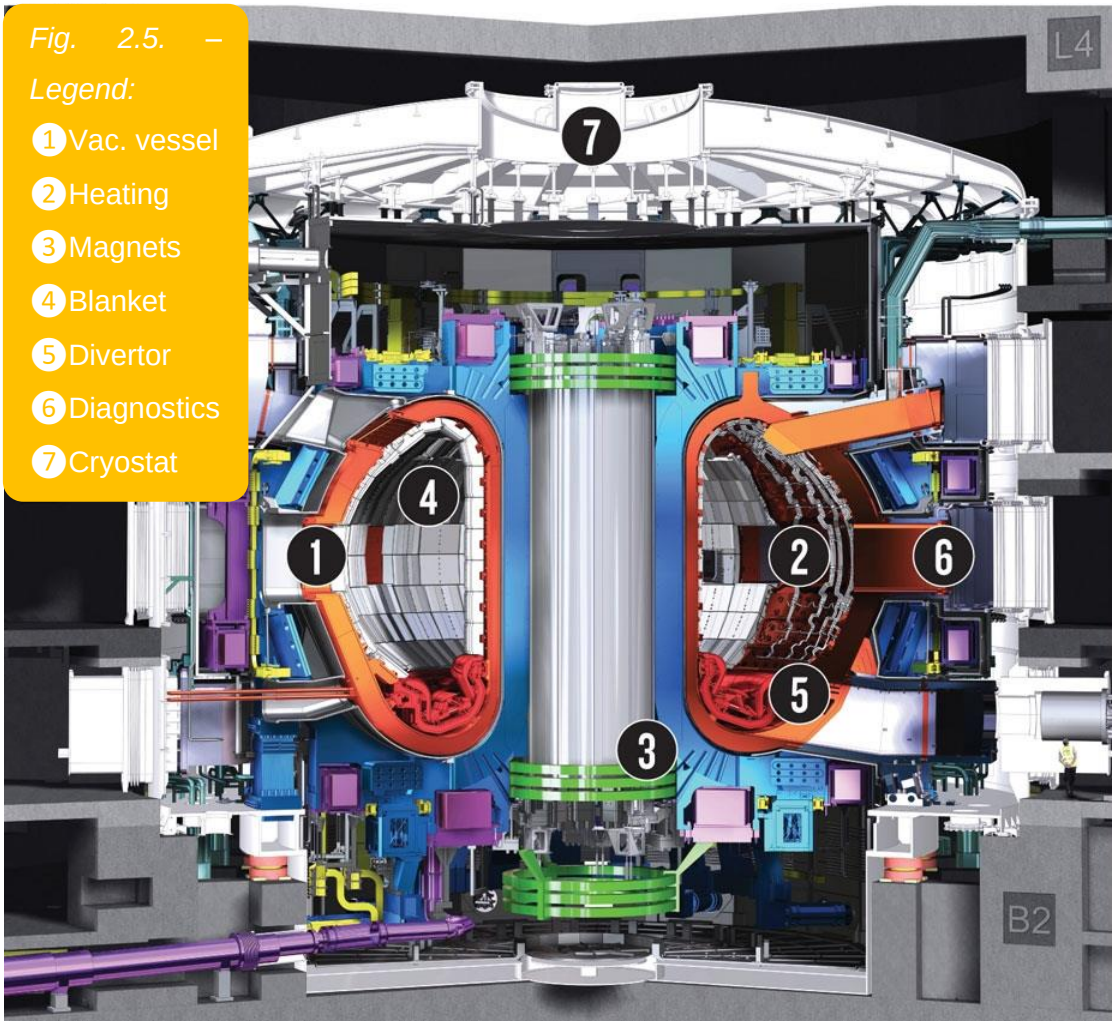

Figure 2.5: Conceptual visualisation of the ITER tokamak [16]

2.5 Plasma Facing Components of Magnetic Confinement Fusion Reactors

Within the reaction vessel housing the fusion reaction are components, which are directly exposed to the plasma – as such called plasma facing components; PFCs. They are the divertor, found at the bottom of the vacuum vessel, and the blanket with the first wall, which line the vacuum vessel – see Figure 2.5 above. Given the extreme conditions within the vacuum vessel that these components have to endure, their design, especially in terms of material engineering, is currently one of the greatest technological challenges to overcome on the path to a future fusion power plant, and is one of the eight strategic tasks outlined in the "Fusion Roadmap"[4]. [10]

[4] Basis for EUROfusion and Fusion for Energy programmes, provides a structured way to commercial electricity from nuclear fusion.

2.5.1 Divertor

The divertor (ITER divertor cassette depicted on the following page, in Figure 2.7), is usually installed at the bottom of the reactor vessel, but some designs may also implement a divertor at the top of the vessel in tandem. The primary purpose of the divertor is the removal of impurities contaminating the plasma, and adversely affecting its quality. These are, in particular, the helium nuclei (alpha-particles) – helium ash, eroded parts of the PFCs and reactor vessel, as well as any unburnt fuel still present in the plasma. The build-up of such impurities would result in the dilution of the plasma, and ultimately halt the reaction. Furthermore, the divertor is an evolution in setting the plasma boundary and came to replace a mechanical limiter that defined the plasma edge in prior designs. In a divertor configuration, plasma is defined by a singularity of the magnetic geometry; the X-point (see Figure 2.6 below), resulting in the formation of a high density, relatively cold plasma, separated from the plasma core below the X-point, and striking the divertor target plates, as a result of the diverting magnetic fields. Consequently, the divertor is directly and continually exposed to the ill-effects of the plasma, making it the single most strained component of the reactor. [10] [18] [19]

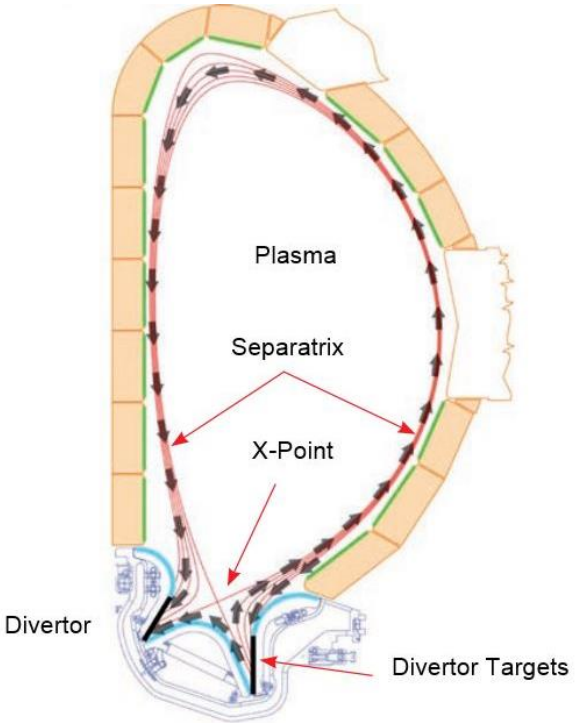

Figure 2.6: Divertor operation plasma geometry [10]

The divertor of the ITER is made of a series of modules - cassettes, each consisting of the load-bearing cassette proper, an outer and inner target, and a central dome. The cassettes are cooled by through-going cooling ducts, and are manufactured to be dismountable, in order to allow for the replacement of targets, consequently minimising secondary radioactive waste. [16]

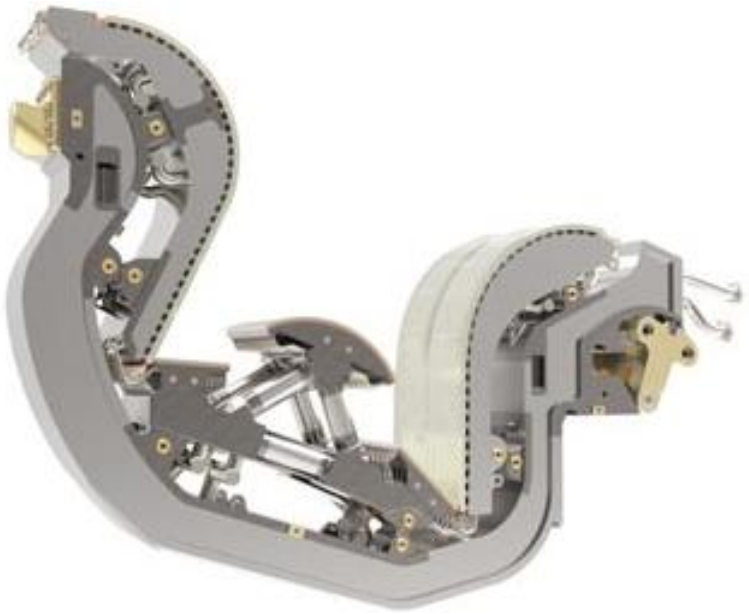

Figure 2.7: ITER divertor cassette [16]

2.5.2 Blanket and the First Wall

The blanket modules, as seen in Figure 2.8 on the following page, completely cover the inner wall of the reactor vessel. The primary purpose of the blanket is to act as a barrier, protecting the reactor vessel and superconducting magnets placed behind it from high-energy neutrons. These are products of the fusion reaction, and due to their neutrality cannot in principle be contained by the magnetic field. Upon collision with the blanket, the kinetic energy of the neutrons is absorbed by the blanket module as heat, which is dissipated through cooling ducts inside the blanket. The vast amount of energy absorbed by the blanket creates a technological challenge in cooling down the module, and the material of the blanket thus has to be chosen accordingly. [16] [17]

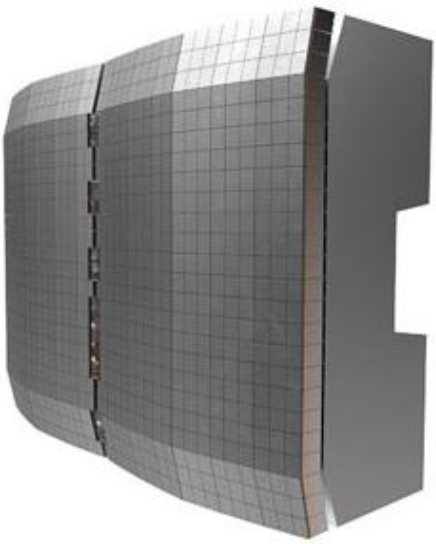

Figure 2.8: ITER blanket module [16]

In contemporary experimental devices, this heat is merely a waste product. In future fusion power plants however, it is this energy that will be used to heat the steam to drive turbines connected to generators, in the non-nuclear section of the facility, and generate electric power in the manner familiar today from fission, coal and gas-fired, or geothermal power plants. For a D-T fusion reaction to be self-sufficient, the neutrons, reacting with an appropriate material of the blanket will concurrently stimulate the "breeding" of tritium in a secondary nuclear reaction. For a blanket containing lithium, this secondary reaction is described by Equation 3, and depicted in Figure 2.9. [17] [20]

$$^{6}Li + n \rightarrow {}^{4}He + T + 4.78MeV \qquad (3)$$

where:

T..... tritium,
^{4}He helium-4,
^{6}Li lithium-6, and
n..... neutron.

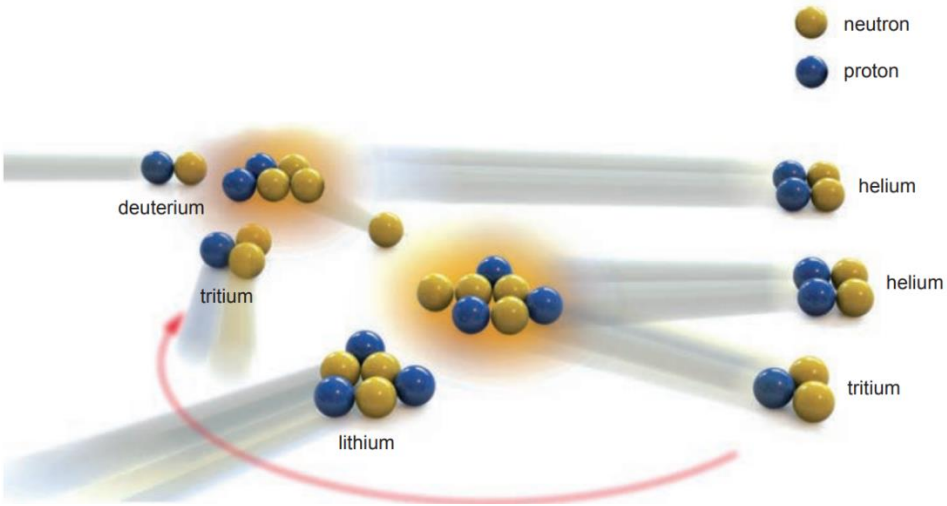

Figure 2.9: Reaction between a neutron and lithium [10]

The first wall is the inner lining of the reactor, directly exposed to the plasma. The purpose of the first wall is the protection of the reactor components under nominal conditions, as well as during abnormal behaviour of the plasma, resulting in increased loads (see Part 3). Conceptually, it may either be the in-facing wall as an integral part of the blanket, or a separate structure mounted in front of the blanket. The first wall may also utilise an independent cooling system, with cooling ducts directly within the wall. It is continuously degraded by the effects of the plasma, and the independent design thus allows for more convenient replacement with the use of robotic technology, thereby also contributing to the reduction of secondary radioactive waste, as in the case of dismountable divertor designs. [10] [16]

3 Plasma Facing Materials

As outlined in Part 2.5, one of the most formidable technological challenges in constructing a fusion power plant is the design of the in-reactor, plasma facing components. This is especially true for the material aspect of the design, given the conditions to which the plasma facing materials (PFMs) are exposed, and the issues that arise from this exposure.

One significant issue in the design of PFMs is the extreme heat flux incident on the PFCs. The divertor targets of the DEMO[5] future fusion plant, for example, are expected to endure a nominal heat flux (density) in the order of tens of $MW \cdot m^{-2}$, with significant upsurges during instabilities of the plasma. Similarly, the nominal load on the first wall of the DEMO is expected to be about 0.5 $MW \cdot m^{-2}$, and even up to 7 $MW \cdot m^{-2}$ when transients are considered. Consequently, a steady temperature of 1 200 °C is typical for conditions at the divertor targets, while temperatures at the first wall usually fall within a 400 – 500 °C range. Further considering component cooling, the resulting temperature gradients of 25 °C per 1mm of material lead to an extreme thermal stress on the materials. [19] [21] [22] [23]

PFMs are in constant interaction with the plasma on an atomic and subatomic level, resulting in further adverse effects on the materials. Neutrons present a specific strain, as they irradiate the PFM, and necessitate considerations for material activation and transmutation, as well as the subsequent radioactivity of the material, and associated radiation hazards. Furthermore, particles striking the PFM can displace surface atoms, leading to displacement damage, blistering and flaking at the surface, given they are sufficiently energetic. Reciprocally, any impurities knocked from the PFM into the plasma lead to its cooling through radiation losses. PFMs are also subject to erosion by melt layer loss, brittle destruction, evaporation, sublimation and ablation. The eroded material can be further re-deposited by the splashing of molten material, implantation, or transport along magnetic field lines. [10] [19] [24]

[5] The DEMO is a project directly following the ITER. It is a proposed nuclear fusion power plant intended for demonstration purposes.

The effects of the above described environment, to which the PFMs are exposed, in combination with more "mundane" necessities imposed by manufacturing, maintenance, health, and economic limitations, lead to complex requirements, which are formulated in the following Part 3.1.

3.1 Requirements for Plasma Facing Materials

Given the nature of the operation of PFCs, it is evident that any solution in terms of materials will inevitably be a compromise, as it is not possible to completely satisfy all requirements without omission. Below is an outline of the fundamental properties required of plasma facing materials: [10] [15] [21] [19] [24]

In terms of in-vessel interactions:

- PFMs must be capable of withstanding severe heat fluxes during nominal operations, as well as at peaks during abnormalities in the plasma.
- PFMs must withstand damage from neutrons and other high-energy particles, while at the same time minimising plasma contamination by particles of PFM origin.
- PFMs must withstand intense surface erosion by various means caused by the plasma.
- PFMs must be able to cope with the gradual change in their properties caused by long-term irradiation.
- PFMs should be characterised by a low atomic number, in order to minimise energy losses in the plasma, as well as neutron activation and hydrogen absorption.
- PFMs must be overall compatible with the processes within the plasma, during normal and abnormal events, including circumstances that may induce large electromagnetic forces.

In terms of basic material properties:

- PFMs must be able to withstand extreme temperatures for extended periods of time; they should have a high melting point and should not be prone to evaporation.

- PFMs must be resistant to thermal shocks and should possess sufficient strength.
- PFMs must be highly thermally conductive to allow effective heat dissipation and minimise thermomechanical tension in the material.
- PFMs must be compatible with other construction materials, and operational mediums, such as coolants.
- The input raw materials for manufacturing should be reasonably available, the manufacturing process should not be overly complicated in terms of technological requirements, and the manufacturing price should be acceptable.
- It must be possible to process the materials to a sufficient degree of precision, to satisfy the need to manufacture geometrically complex components with respect to the reactor geometry.
- PFMs should not pose a health risk.

3.2 Overview of Contemporary Plasma Facing Material Options

The materials used for the PFCs are mostly carbon, beryllium, or tungsten-based in contemporary fusion reactors, and a brief overview of each material group follows below:

3.2.1 Carbon-based PFMs

Carbon based PFMs are characterised by a low atomic number of 6 and are thus suitable in terms of interaction with the plasma, while being capable of withstanding severe heat fluxes and offering superior performance under thermal stress. Furthermore, they offer a good thermal conductivity, which is however, like other properties of the material, anisotropic in the case of carbon composites. Significantly, carbon has a low coefficient of thermal expansion, possibly making interaction with other materials difficult at interfaces (see Part 4.2). Carbon composites possess higher strength as well as elastic moduli, and can therefore offer improved performance under thermal stress, as well as sufficient toughness through thermal cycling. [19] [24]

Carbon offers low activation by incident neutrons and is also resistant to radiation swelling – however, exposure may lead to a loss of thermal conductivity and consequently increased erosion during abnormalities. Carbon based materials are limited to a maximum temperature of about 1300 °C, due to radiation enhanced sublimation, and are relatively prone to erosion, particularly chemical, which can be reduced by the addition of dopants such as silicone or boron. Significantly however, the high retention of tritium poses problems for use in future reactors, due to the radioactivity of tritium, and therefore the carbon material in which it is retained. Furthermore, tritium sputtering back into the plasma leads to an oversupply of the plasma edge with fuel. [19] [24]

Carbon-based PFMs, especially fine-grain graphite and carbon-fibre composite tiles have been used extensively in large tokamaks, in both divertor and first wall applications. [23]

3.2.2 Beryllium-based PFMs

Beryllium-based materials are similarly characterised by a low atomic number of 4. They offer desirable interaction with the plasma, and furthermore, the ability to getter oxygen from the plasma. Beryllium has a satisfying thermal conductivity, a low activation, and is not prone to chemical sputtering. [19] [24]

It is, however, very prone to erosion - especially physical sputtering - which poses a key obstacle in the use of beryllium-based materials. Beryllium is also constrained by its relatively low melting point of 800 °C, limiting its use to first wall applications only. Furthermore, the mechanical properties of beryllium are subject to degradation as the material is irradiated by neutrons, and beryllium further reacts with steam. The hydrogen retention properties, combined with slow tritium release kinetics, are further obstacles in the use beryllium as a PFM. [19] [24]

Beryllium is a highly chemically reactive material and forms very stable, very toxic oxides. These further increase the retention rate for tritium. The surface of beryllium is often covered by a chemically protective oxide film due to the affinity to oxygen. In this way, the use of beryllium benefits the removal of any oxygen

impurities from the plasma. Being highly reactive with almost all metals, the in-vessel interaction with other materials is also problematic. [19]

There is experience with the use of beryllium on the Joint European Torus - JET[6] - tokamak, and it is intended as the PFM of the first wall in the candidate designs for the ITER. It is also foreseen as a neutron multiplier in breeding blankets (see Part 2.5.2). [16] [19] [24]

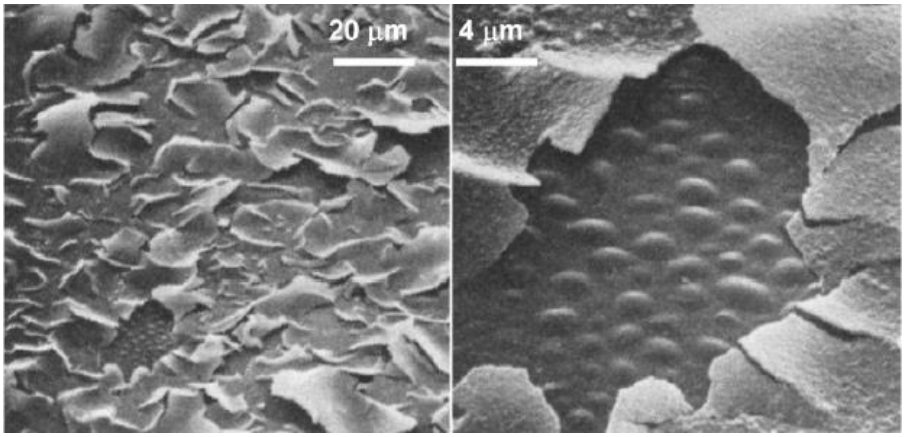

Figure 3.1: Radiation damage on a beryllium surface [19]

3.2.3 Tungsten-based PFMs

Tungsten-based materials are considered primary candidates for use in both first wall and divertor applications in future power plants, including the DEMO. Concurrently, tungsten is a candidate material for the ITER divertor. [24]

Significantly, tungsten offers an extremely high melting point of 3 410°C – the highest of all metals. Furthermore, it has a low coefficient of thermal expansion, as well as adequate thermal conductivity and strength at high temperatures. The optimum operational range for the material is between 800 °C and 1300 °C. Tungsten-based materials offer a high energy threshold for physical sputtering and overall satisfying properties in terms of erosion. Furthermore, tungsten does not form hydrides and co-deposits with tritium. The primary problem of using tungsten

[6] The JET is the largest operational magnetic confinement reactor at Culham, United Kingdom.

is its high atomic number of 74, imposing problems in terms of radiation losses in the plasma as a significant impurity. [19] [24] [25]

Tungsten is inherently relatively brittle and suffers from a high ductile-to-brittle transition temperature (DBTT), which is known to further increase after irradiation. Tungsten is prone to further embrittlement under neutron irradiation, and readily transmutes to rhenium and subsequently osmium - a composition of 91W–6Re–3Os is modelled after a 5-year service life, by which it is very close to crossing into an extremely brittle phase. A possible way to increase fracture toughness is the use of tungsten-fibre reinforced tungsten composite. Tungsten is further limited by a low recrystallization temperature, as well as severe difficulties in machining and welding the material. [19] [24] [25]

Studies of the utilisation of heavy tungsten alloys suggest that the use of such materials in place of pure tungsten is also possible, with the added benefit of a reduction in brittleness, as well as an improvement in machinability and overall manufacturability. [26] [27]

4 Functionally Graded Materials

As made clear in Part 3.1, PFMs are bound by complex requirements in ways that make it impossible to fully satisfy all criteria simultaneously. While advancements have been made in materials science, it is difficult to meet benchmarks with any one material, and the use of composites is preferable in many applications.

4.1 Generic Properties of Functionally Graded Materials

Functionally graded materials – FGMs – provide an opportunity to tailor material properties to very specific applications, by amalgamating the properties of constituent materials. FGMs are best suited to applications requiring material properties to be spatially varied, as they allow for continuous gradation of composition or structure. [2] [28]

FGMs, as schematically illustrated in Figure 4.2, are two (or more) component composites, characterised by a compositional or structural transition from one constituent to the other, in contrast to composites with homogenous structures. The transition from one constituent material to the other allows for the gradual variation of properties, as depicted in Figure 4.1, consequently resulting in a modified response to loads. Surface layers of the FGMs can contain the constituent materials in pure form, which allows the resultant composite to retain the full extent of desirable properties of the constituents in the surface layers. This reduces the need for compromise, characteristic of homogenous composites, as the properties and characteristics of the constituent materials can be fully utilised. [2] [28] [29]

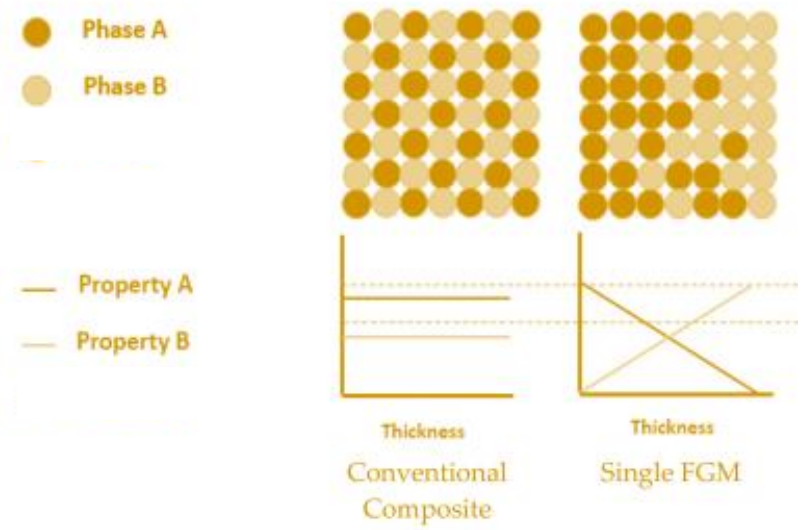

Figure 4.1: Distribution of phases and properties in a FGM [30]-edited

The gradation of composition and structure may occur either continuously from one surface to the other, or in discrete layers; see Figure 4.2 for comparison. In a discretely layered FGM, the material distribution and properties change abruptly at the interface between two layers. Conversely, in a continuously graded FGM, the variation in the material distribution and the material properties is continuous, and is described in the simplest terms by functions related to the volume fraction distribution, of which the power-law model is given below in the form of Equation 4: [29]

$$V_B = \left(\frac{1}{2} + \frac{z}{h}\right)^p \quad \text{for } z \in \langle 0; h \rangle \tag{4}$$

where:

V_B.....volume ratio of const. B [-],
p..... power-law index [-],
z.....material coordinate [mm], and
h..... height (thickness) of material [mm].

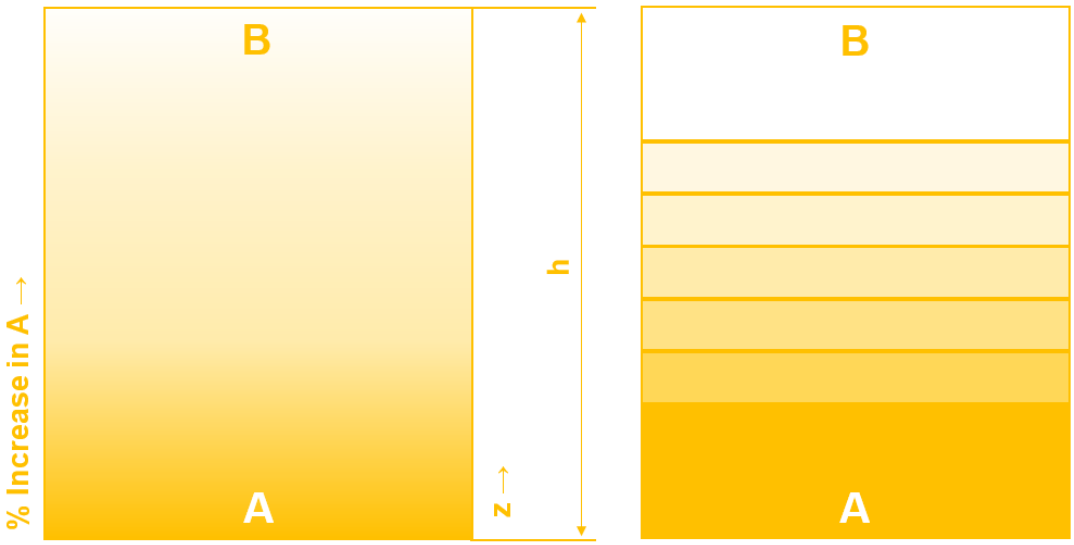

Figure 4.2: Schematic of a continuously graded and discretely layered FGM

4.2 Basis for Utilising FGMs in Plasma Facing Applications

Due to the specific nature of the conditions within the fusion reactor, different properties are of varying significance in different areas of a plasma facing component. While at the innermost layer, properties ensuring optimal interaction with the plasma, such as erosion resistance, are vital, the significance of these properties decreases further outwards from the plasma, where technological properties such as thermal conductivity are of greater significance. Given the unique properties of the materials directly exposed to plasma, they are usually rendered inappropriate for other applications. Furthermore, candidate plasma facing materials, such as tungsten, are brittle at low temperatures, and thus unsuitable for use in colder regions of the structure. As a result, an aspect in the design of in-vessel, plasma facing components is the transition from an "armour material" directly exposed to the plasma, to a "technological material", suitable for the convenient realisation of technical aspects of the component, such as attachment or cooling.

However, the utilisation of two or more materials results in difficulties arising, particularly at the interface between the materials, due to the sudden change of thermal, mechanical, and physical properties that occurs. The problem of thermal expansion is of particular significance, as the armour material, such as tungsten, is

usually characterized by a low coefficient of thermal expansion; while the technological material such as copper, acting as a heat-sink, expands significantly when heated. Consequently, significant stresses are thermally induced at the interface under load, due to the difference in thermal expansion and elastic moduli. This results in the cracking and peeling of PFMs under repeated loads, negatively impacting the lifespan of resultant PFCs. [24] [31] [32]

Such problems can be reduced by utilising a functionally graded material, ensuring gradual transition from one material to the other, in place of an abrupt interface produced by conventional joining methods, such as welding, brazing, sintering, casting, *et cetera*. The key benefit of FGMs in PFC applications is the mitigation of thermally induced stress at the sharp material interface, by dispersing such stress into multiple interfaces at multiple layers, or the elimination of extensive interfaces altogether in the case of continuously graded FGMs. In such an arrangement, not only is the mismatch of material properties alleviated, but the generic benefits of FGM composites, as described in part 4.1, can be utilised to significant benefit. [24] [31] [32]

4.2.1 Basis for a Functionally Graded Titanium-Tungsten PFM

As made clear in previous Parts, the scope and interconnectedness of material requirements, posed by the in-vessel environment, renders all known materials unsuitable in one way or another. Even with the utilisation of FGMs, compromises have to be made in material selection and design, especially when simultaneously considering the limitations of FGM manufacturing methods themselves (see Part 4.3.1).

From the PFM perspective, an FGM containing pure tungsten on one side, transitioning into a “technological” metal on the other side is the optimal result, for the desirable properties of tungsten-based materials as briefly outlined in Part 3.2.3.

An optimal “technological” metal would be characterised by a high thermal conductivity in a heat-sink application, to allow for effective cooling. Copper, as the optimal material in terms of thermal conductivity, is considered for the divertor of

the DEMO power plant; copper is however undesirable in terms of neutron activation. Experimental research on fabricating copper-tungsten FGMs by PTA cladding has shown severe difficulties in layering the two materials, as a result of the significant difference in their melting points (Cu: 1 084°C; W: 3 410°C) and thermal conductivity (Cu: 413 $W.m^{-1}K^{-1}$; W: 197 $W.m^{-1}K^{-1}$). This resulted in the insufficient melting of tungsten and the evaporation of copper. Another possibility that was subjected to research was a combination of nickel and tungsten. This combination, however, proved to have limited applicability, due to the formation of brittle intermetallics at increased temperatures. [33] [34] [35] [36]

The possibilities of manufacturing a titanium-tungsten FGM are investigated in the practical part of this thesis. Such an FGM for plasma facing applications, while offering multiple benefits, is in many ways a result of compromise, following the experience of prior research.

In terms of the technological limitations of PTA welding; titanium is less likely to evaporate than copper, due to its higher melting and boiling points. Furthermore, it can be expected that titanium will not be prone to the formation of brittle intermetallics with tungsten. From a PFM perspective, titanium appears suitable in terms of irradiation properties, radiation damage resistance and activation. A significant drawback in the use of titanium as opposed to copper as a heat sink is its low thermal conductivity of 17 $W.m^{-1}K^{-1}$. This is however relatively comparable to the ~30 $W.m^{-1}K$ thermal conductivity of the low-activated *EUROFER 97* steel, considered for first wall designs of the DEMO power plant. Titanium further alleviates the low DBTT of tungsten, a significant problem in using tungsten for structural parts of the PFCs. Furthermore, experiments were conducted, which demonstrated the viability of using a titanium interlayer in joining W to W-1% La_2O_3, in PFC applications, further pointing to the possibilities of using titanium in PFCs. [22] [35] [36] [37] [38]

Given the potential of titanium in possible PFM applications, and its expected suitability for PTA welding, it was chosen as a promising candidate for the research of FGMs in the experimental part of this master's thesis.

4.3 Methods for the Fabrication of FGMs

It is possible to manufacture FGMs utilising a vast array of known methods and processes. These span over many physical and chemical principles and range from simple techniques to high-tech methods requiring specialised equipment. Within the scope of designated methods, a distinction is made between the following: Gas based methods; which include chemical and physical vapour deposition and surface reaction processes. Liquid phase processes; such as casting, thermal spraying, various other methods of liquid form deposition, directional solidification or sedimentation. Solid phase processes; such as spark plasma sintering and powder metallurgy. Lastly, biopolymeric-based functionally graded structures; such as freeze drying, compression moulding or electrospinning. [28] [30] [39]

4.3.1 Suitability of Fabrication Methods for a Titanium-Tungsten FGM

The following evaluation of methods is based on prior research on steel-tungsten FGMs, however; given the similarities, the conclusions can to some degree be related to an FGM of titanium and tungsten. [39] [40]

Plasma spraying offers promising results for the fabrication of FGMs containing tungsten. Vacuum plasma spraying (VPS) in particular shows promising results in terms of layer thickness, range of gradation, and seems to be an overall feasible method. Plasma spraying also offers the opportunity to control the composition of the coating relatively precisely by the adjustment of powder ratios. Significantly, plasma spraying can cover large areas at a satisfactory rate. However, plasma sprayed FGMs are characterised by a specific lamellar architecture, and imperfect bonding in between layers and splats. This characteristic greatly deteriorates the physical and mechanical properties of the resultant material, such as its thermal conductivity or strength. Laser cladding offers similar results to plasma spraying, albeit at a lower rate, incorporating molten or semi-molten particles into an existing melt pool. [39] [40]

Conventional sintering methods are generally impractical, due to the significant incompatibility of sintering conditions. Experimental hot-pressed FGMs contained brittle intermetallic phases, greatly undermining the prospective application of such

a method. Nonetheless, hot pressing of powders did provide feasible results, as did resistance sintering under ultra-high pressure (RSUHP) and laser sintering. As with other powder metallurgy methods, the size of the resultant composite is severely limited, and covering hundreds of square meters of plasma facing surfaces would be a technological challenge in itself. [39] [40]

The best results are achieved by PVD methods, which can produce a completely smooth FGM, even at an atomic level. Furthermore, the PVD method of magnetron sputtering offers the additional advantage of a full gradation range, and deposition in vacuum. However, all CVD and PVD methods are severely limited by the long deposition time, and as such, only FGMs with a thickness in the order of μm can be fabricated, making these methods less attractive. [39] [40]

Based on the above-stated conclusions, plasma spraying methods - particularly VPS - are identified as eligible and promising for manufacturing FGMs containing tungsten. Given the results achieved by plasma spraying methods and the relative physical similarities of the processes, PTA could provide an alternative to plasma spraying as a manufacturing method for plasma facing FGMs. Furthermore, PTA could be an improvement on plasma spraying methods, as it is not limited by problems with adhesion between layers, as the base material is melted during the PTA process. For these reasons, and the availability of the method, PTA is the base technology for the experimental fabrication of a titanium-tungsten FGM, as presented in Parts 7 and 8. The PTA technology is described in detail in Part 6. [39] [40]

5 Titanium, Tungsten, and Their Alloys

Titanium and tungsten were selected as the constituent materials for the experimental fabrication of an FGM for PFM applications in the experimental part of this thesis, for reasons described in Part 4.2.1. For completeness, an overview of the basic properties of each material as well as of the titanium-tungsten (Ti-W) system is given in the following Parts:

5.1 General Characteristic and Properties of Titanium

Titanium is a Group 4 chemical element. It is a silver-gray transition metal, characterised by its low density, high strength, and corrosion resistance. Titanium constitutes ~0.44 percent of the earth's crust, and its two primary commercial minerals are ilmenite and rutile. Titanium, in pure form, is ductile, has a relatively low thermal and electrical conductivity, and is paramagnetic. Its corrosion resistance is granted mostly by the formation of a passive oxide layer, however at elevated temperatures, titanium is reactive. For its unique properties and relatively high cost, titanium is mostly limited to medical, aerospace or jewellery applications. It is also used as an alloying element in commercially produced steels. The properties of titanium are listed in the following Table 5.1 and
Table 5.2: [41] [42]

Table 5.1: Thermophysical properties of titanium [42] [43]

Density	[kg.m^{-3}]	4 500
Melting point	[°C]	1 660
Boiling point	[°C]	3 287
Specific heat capacity	[J.kg^{-1}.K^{-1}]	523
Thermal conductivity	[W.m^{-1}.K^{-1}]	17.0

Table 5.2: Mechanical properties of titanium [42]

Tensile strength	[MPa]	220
Modulus of elasticity	[GPa]	116
Shear modulus	[GPa]	43
Hardness according to Brinell	[-]	70

Titanium is polymorphous and exists in more stable crystallographic structures; α-Titanium (α-Ti) and β-Titanium (β-Ti). β-Ti exists above 882°C, and in this phase, the crystallographic structure is body-centred cubic (BCC). Below the β-transus temperature of 882°C, β-Ti transforms into the hexagonally close-packed (HCP) α-Ti. Only the α-Ti can exist at room temperature under equilibrium conditions in the case of pure titanium, β-alloys can however be stabilised, even at room temperature, with the use of stabilisers - one of which is tungsten. The formation of ω-Ti nano-sized particles, which are precursors for α-Ti particles precipitation is also possible at high temperatures. [41] [44] [45] [46]

5.2 General Characteristic and Properties of Tungsten

Tungsten is a Group 6 chemical element - a white-to-gray refractory metal. It is used for its exceptionally high strength, which is its defining characteristic in many applications. The metal constitutes ~1.5 ppm of the Earth's crust and is found, among others, in wolframite ores. Tungsten is inert to oxygen at room temperatures, but readily combines with it at increased temperatures. Although relatively brittle at room temperature, it has the highest tensile strength, highest melting point, and the lowest coefficient of thermal expansion among all metals. Tungsten is highly electrically and thermally conductive. It is used to harden blades and drill bits, for high temperature application lubricants, and more commonly, for bulb filaments and heating elements. Unlike titanium, tungsten is not polymorphous, and exists in one crystallographic structure throughout the solid phase. The properties of tungsten are given in the following Table 5.3 and Table 5.4: [47] [48]

Table 5.3: Thermophysical properties of tungsten [43] [49] [47]

Density	[$kg.m^{-3}$]	19 270
Melting point	[°C]	3 410
Boiling point	[°C]	5 555
Specific heat capacity	[$J.kg^{-1}.K^{-1}$]	134
Thermal conductivity	[$W.m^{-1}.K^{-1}$]	196.65

Table 5.4: Mechanical properties of tungsten [49] [47]

Tensile strength	[MPa]	1 725
Modulus of elasticity	[GPa]	400
Shear modulus	[GPa]	145
Hardness according to Brinell	[-]	300

5.3 The Titanium-Tungsten System

Titanium and tungsten can form solid solutions, and exhibit complete mutual solubility under certain conditions. The titanium – tungsten system allows for multiple equilibrium phases, as well as metastable phases, which are described below, in reference to the titanium-tungsten equilibrium diagram presented in Figure 5.1: [45]

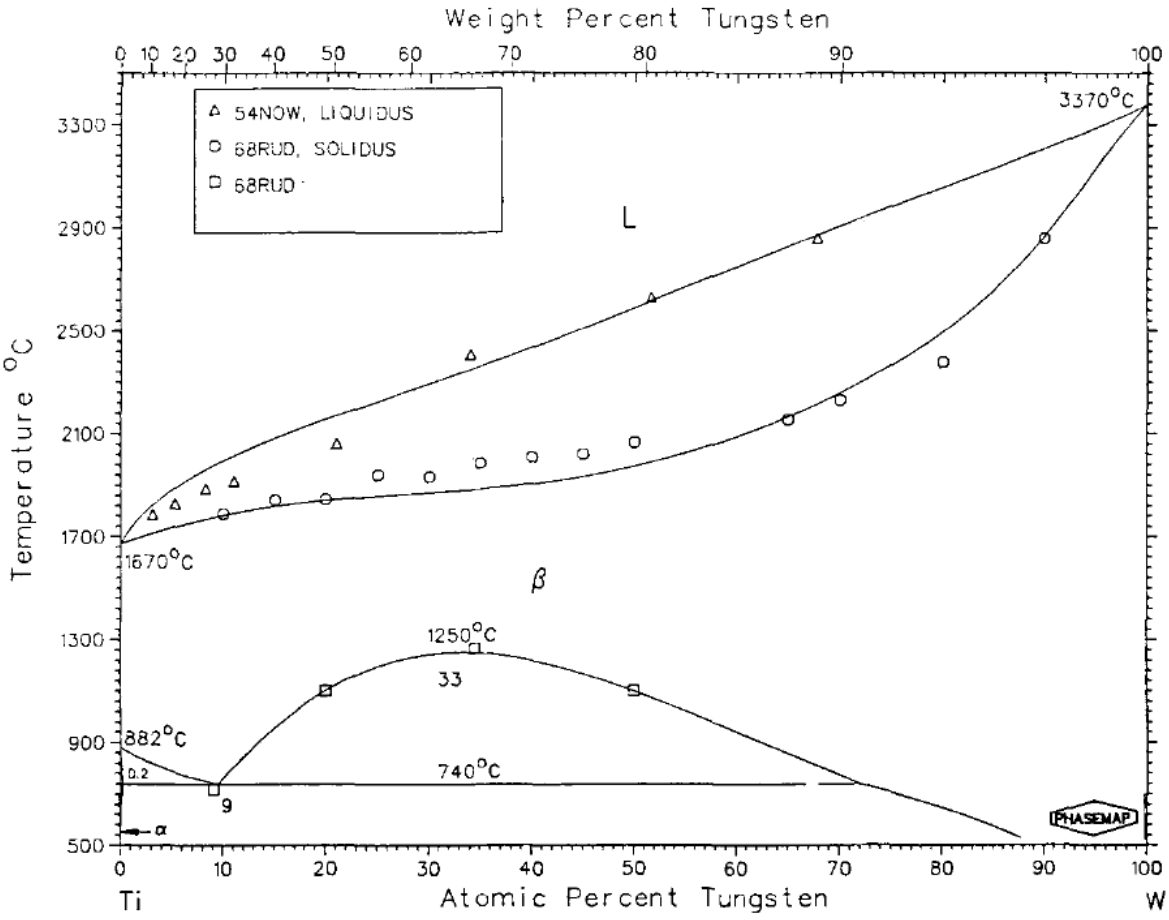

Figure 5.1:Titanium-tungsten equilibrium diagram [45]

5.3.1 Equilibrium Phases

Three equilibrium phases exist in the titanium-tungsten system: [45]

- The liquid, which exists above the temperature of the liquidus,
- a titanium-rich HCP α-phase solid solution, which exists below the β-transus temperature of pure titanium (882°C), and
- a BCC β-phase solid solution of titanium and tungsten.

Titanium and tungsten are completely mutually soluble in the β-phase at temperatures higher than the critical temperature of the miscibility gap (1250°C), below the temperature of the solidus. In the α-phase, tungsten is soluble in titanium in concentrations up to 0.2 at. % at a temperature of 715°C. [45]

5.3.2 Metastable Phases

The following metastable phases can be formed from the β-phase in the titanium-tungsten system during quenching: [45]

- α'-phase, an HCP structured phase formed from titanium rich phases,
- α''-phase, an orthorhombic distortion of the HCP structure formed at higher concentrations of W, and
- ω-phase, an HCP structured transition phase between high temperature α-Ti and the β-phase. The ω-phase is also an equilibrium phase of titanium at high temperatures (see Part 5.1).

5.4 Beneficial Properties of Titanium-Tungsten Alloys

In terms of strength, it was found that a Ti-W[7] alloy displays a linear load-displacement curve until fracture up to 1000°C. In comparison, pure tungsten is brittle, and the load-displacement curve is linear up to the DBTT of 200-400°C, while the curve is non-linear above the DBTT. At room temperature, the Ti-W alloy is stronger than pure tungsten, its strength increases up to 600°C, and then starts to decrease. Pure tungsten maintains ambient temperature strength up to 200°C, above which plastic deformation becomes dominant and yield strength progressively decreases. [50]

[7] Tungsten alloyed with 4 wt. % titanium by isostatic pressing.

The Ti-W alloy further displays higher toughness and hardness than pure tungsten at room temperature. Alloying tungsten with titanium also offers an improvement in ductility, as well as lowering the high DBTT temperature of tungsten. [50]

The mechanical properties can be affected by the presence of metastable phases (see Part 5.3.2), and it was found that some titanium alloys undergo a tensile ductility loss near the β-α transformation. [50] [51]

In terms of helium and deuterium irradiation effects, it was found that Ti-W alloys produced by titanium implantation at 500°C have shown a reduction in the retention of hydrogen. Research on a nanograined Ti-W[8] alloy has shown that in comparison to pure nanograined tungsten, the Ti-W alloy showed a reduction in deuterium retention, as well as having fewer deuterium induced blisters. [51] [52]

[8] 80W-20Ti

6 Plasma Transferred Arc Technology

Plasma arc welding-cladding (PAW) processes represent joining and surface engineering methods, characterised by the utilisation of a highly constricted electric arc, ionising an inert gas, and producing a high-density plasma arc. As such, PAW processes are, in some regards, considered a modification of tungsten inert gas (TIG) welding. Compared to the TIG method, PAW is comparatively more productive, and significantly higher temperatures are reached in the process. Welds and deposited layers are characterised by particularly good penetration, and an optimal width-to-height ratio between 1:1.5 and 1:2.5. The process is used for the welding and cladding of all types of steels, copper, aluminium, titanium, nickel, molybdenum, and their alloys. In PAW processes, the electric arc is formed between a non-consumable tungsten electrode and (depending on whether the arc is transferred or not), either the substrate material or a cooled nozzle. The Plasma Transferred Arc process (PTA) is a specific plasma arc welding-cladding process, employing filler material in solid state in the form of a metal powder, thus differing from the Plasma Arc Welding process, which employs filler in the form of a metal wire. [53] [54] [55] [56]

6.1 Principle of PTA Technology

As mentioned above, PTA is a welding-cladding process characterised by an electric arc ionising a gas and producing a high-density, high-temperature plasma. A depiction of the PTA process is shown below in Figure 6.1:

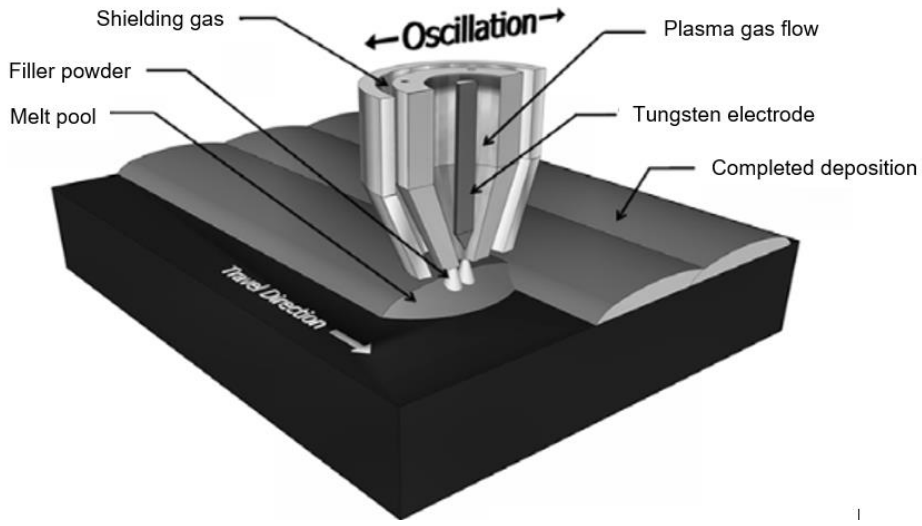

Figure 6.1: PTA welding process [57]-edited

Firstly, an electronic igniter provides voltage peaks to establish a non-transferred electric arc between the non-consumable tungsten electrode acting as a cathode, and the welding torch constrictor nozzle acting temporarily as the anode, in a so-called “pilot arc” mode. High density plasma is produced by the ionisation of an inert plasma gas passing through the pilot arc, resulting in an electrically conductive environment, due to the electrical properties of plasma, as described in Part 2.2. [53] [54]

The highly conductive plasma facilitates the completion of an electric circuit between the power source, the plasma itself, conductors, and the workpiece. The main, transferred electric arc is established between the tungsten electrode and the workpiece when a power source is added. In this transferred arc mode of operation, the plasma column reaches temperatures between 8 000 and 20 000 °C, depending on process parameters, and melts the substrate material (workpiece), thus creating a melt-pool. Filler material in the form of powder is carried to the plasma by an inert carrier gas. It is melted by the plasma arc and projected onto the workpiece, resulting in deposition in the weld pool. The plasma arc and filler material, as well as the melt pool are shielded by an inert shielding gas, eliminating contamination by the surrounding atmosphere. The relative movement of the welding torch over the workpiece, as well as the oscillation of the torch about a mean position results in the deposition of a continuous layer. [54] [55] [57]

6.2 Welding Torch Construction and Geometry

The PTA process as described above is realised by specialised equipment in mechanised or automated manners; automatic welding machines are commonly used, ensuring optimal process geometry, continuous supply of filler material as well as the supply of process gases. A schematic depiction of a PTA welding torch is shown in the following Figure 6.2:

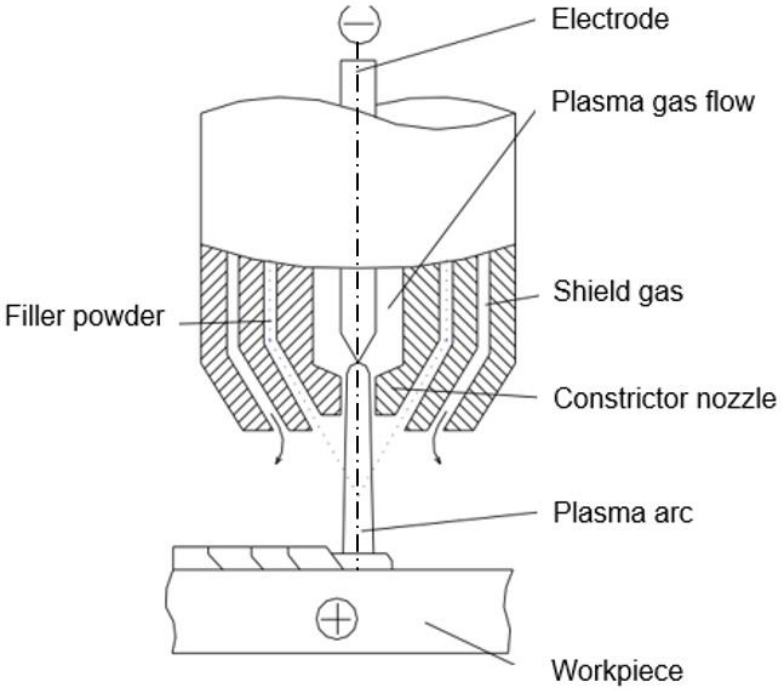

Figure 6.2: PTA welding torch [55]-edited

The tungsten electrode is contained within the central volume of the torch, with plasma gas flowing around it and through the constrictor nozzle at pressure. Once passing through the pilot arc, which is established between the electrode and the constrictor nozzle, this gas is ionized and a plasma arc is established between the electrode and the workpiece, as described in Part 6.1. Given the significant temperatures of the plasma, the torch is manufactured from a thermally conductive material, and is cooled by a cooling medium flow through cooling ducts within (not shown in Figure 6.2). Around the constrictor nozzle, there is an inner coaxial slit, through which the filler powder is delivered to the plasma arc, carried by an inert carrier gas. Given the volatility of the process, shielding gas is delivered through a second, outer coaxial nozzle, and creates a barrier against the surrounding atmosphere, thus preventing negative effects such as oxidation or the creation of pores. [53] [54] [55]

The geometry of the torch greatly influences the weld bead, and consequently, the resultant layer. The diameter of the constrictor nozzle directly influences the depth to which the substrate material is melted (penetration), as well as the width of the deposited weld bead. With a decreasing nozzle diameter, the

plasma is increasingly constricted and concentrated on a smaller area of incidence, thus producing a narrower, taller weld bead with a greater degree of penetration. The resultant weld bead is also influenced by the recess of the electrode into the welding torch; a higher degree of recess into the torch results in a more constricted plasma, with similar effects as a decrease in constrictor nozzle diameter. Electrode recess can be, for example, expected in the range of 0.8 to 2.6 mm.[9] The distance between the constrictor nozzle and the workpiece affects the deposited layer in a similar manner, the greater the nozzle-to-workpiece distance, the greater the width of the bead and the lesser the penetration. Furthermore, the degree of dilution also decreases with an increasing nozzle-to-workpiece distance. This distance should not exceed 15 mm to obtain a satisfactory deposition yield. [55]

6.3 Variables in the PTA Process

The PTA process is defined to a great extent by the selection of process parameters, as well as consumables such as gases and filler materials. The correct selection of parameters and consumables, as well as the optimal setup of the equipment, is of paramount significance in executing the deposition correctly and reaching the desired properties of the deposited layer. The observations mentioned in this Part were, where possible, utilised in the experimental Part 7, which subsequently follows.

6.3.1 Gases

As evident from the description of the PTA process above, three gases are necessary; a plasma gas, a carrier gas and a shielding gas. Either three or two different inert gases may be used, or all three functions may be fulfilled by a single gas. The gases described below can be used for all three applications, with the exception of pure helium, which is only used for shielding. [58]

The primary role of the plasma gas is the control of arc characteristics and the shielding of the tungsten electrode. Argon is the preferred plasma gas, especially for low current welding[10], primarily because of its low ionization potential of

[9] Electrode recess range of Thermal Dynamics Corporation PWM–300 torch.
[10] Welding current of 100 A or less.

15.7 eV. This allows for the convenient establishment of a stable, long-distance electric arc of significant current-carrying capacity. Argon is commercially available in purities ranging from 99,995 to 99,999%. The gas does however have a relatively low thermal conductivity. [56] [58] [59]

For applications requiring higher heat inputs at a higher current, argon-helium mixtures are used, usually in 70:30 to 30:70 ratios. With increasing helium-to-argon ratio, the voltage on the arc increases, as does the heat output. The higher thermal conductivity of helium improves the energetic properties of the arc, allows for deeper penetration, as well as higher travel speed. Nonetheless, due to the higher ionisation potential of helium (24.5 eV), more energy is required to establish an electric arc. Similarly, argon-hydrogen mixtures containing up to 10% hydrogen are used, especially for the high refining ability of hydrogen, which deoxidises, denitrifies, and decarbonises the weld pool. The highly thermally conductive hydrogen offers similar benefits to helium in terms of arc qualities. Furthermore, being highly flammable, hydrogen further increases the plasma temperature and thus contributes to the melting of the filler and substrate materials. Hydrogen has an ionisation potential of 13,5 eV, but being a diatomic element, the dissociation energy must also be considered. Resultantly, the energy required to ionise hydrogen is higher than that to ionise the argon gas. The use of hydrogen is limited for some materials sensitive to hydrogen contamination. [56] [58] [59] [60]

The same gases can be used for carrying the filler material, however, while the flow rate of the plasma gas is usually between 0,5 – 9 $\ell.min^{-1}$, the carrier gas flow rate is between 3 and 18 $\ell.min^{-1}$. For shielding, all of the above-mentioned gases may be used, with the added possibility of also using pure helium in certain applications. The flow rate of the shielding gas is between 2 and 20 $\ell.min^{-1}$, with active materials requiring up to 30 $\ell.min^{-1}$. [56]

6.3.2 Filler Material and Feed Rate

As mentioned, a specific characteristic of the PTA method is the filler material in powder form. As opposed to filler material in the form of a wire, the powder form

offers practically unlimited options in terms of filler material composition. By the commixing of multiple powders, specific filler materials can be prepared *in situ*, greatly expanding the potential of the PTA method. Among the most commonly used filler materials in industrial practice are cobalt, nickel and iron-based powders. During the PTA process, the powder is fed into the plasma arc through a specially designed powder feeder, and carried by a carrier gas, as described in Part 6.1. Given the nature of the powder delivery process, the powder should not be sharp-edged, and should be homogenous, in order to ensure a constant, steady feed rate. Grain size should be appropriate to the welding current, as overly large-grained powder will not be sufficiently melted in the plasma arc[11]. The range of suitable grain sizes for the PTA process is ~50 to ~180 µm. [54] [61] [62]

Powder feed rate also directly affects the resultant deposited layer, as selecting an appropriate supply volume of filler material results in defect-free layers. When a significantly larger amount of filler material is supplied, more energy is required to melt it, resulting in a possible insufficient melting of the substrate material and lower dilution. This is however only noticeable in significant volumes (see part 7.7.2). With the width of deposition being fixed by other parameters (see part 6.3.4), the height of the weld bead becomes a function of the feed rate. A higher feed rate results in a higher deposited layer, thus cushioning the effect of the plasma on the substrate material, preventing deeper penetration. [57]

6.3.3 Current

The welding current is of utmost significance, defining the resultant power of the plasma as well as its energy density, affecting the heat available to melt the filler and substrate materials. The welding current affects the characteristics of the weld bead, as well as the penetration of the substrate material and the dilution. With increasing current, the deposition rate increases, as does porosity in the deposited layers. The increased porosity resulting from the use of higher currents may also lead to a reduction in hardness as well as overall wear resistance. Pulsed direct

[11] Experiments revealed, when using a current of 100 A and an iron-based filler material, only grains smaller than 0.06 mm were fully melted in the arc, while at 200 A, this was true for grains smaller than 0.15 mm. [61]

current is preferable, as its use results in more homogenous structures and lower dilution levels. The frequency of the pulse also influences the structure's hardness, with higher frequencies resulting in harder structures. In contrast, higher current intensities result in higher dilution and a reduction in hardness. For the welding of 2-10mm thick alloyed steels, the welding current is between 110 and 300 A at a voltage of 28 to 40 V. [56] [57] [63] [64]

6.3.4 Torch Motion

The motion of the torch itself naturally influences the resultant layer. The travel speed, also called the transferred arc speed (corresponding to the arrow labelled "travel direction" in Figure 6.1), is the speed at which the torch travels over the workpiece and is usually between 20 to 85 $cm.min^{-1}$. At a higher travel speed, lower heat is supplied per unit length, which reduces the rate at which the substrate material melts, minimising dilution and resulting in shallow penetration. The travel speed is also inversely proportional to the deposition rate per unit length. The torch further oscillates perpendicularly to the travel speed about a mean position. The width of the weld bead, as well as the filler material distribution are influenced by the width of the oscillation, the oscillation frequency, and the time the torch is stationary at both ends of the oscillation range. A higher oscillation frequency also results in a lower heat input per unit of area, resulting in a decrease in dilution. [56] [57]

7 Experiment

The experiment, as described in the following Parts, follows the research done in the theoretical part of this thesis, and makes use of the experience gathered in prior works. To the extent of this research, very limited experience exists globally in fabricating a functionally graded material for plasma facing applications by the PTA method. In this respect, the presented experiment is one of the first in this field, and follows prior experiments at the Czech Technical University in Prague, which investigated the possibilities of fabricating a copper-tungsten and nickel-tungsten FGMs by the PTA method, referred to in Part 4.2.1. [33] [34]

7.1 Experiment Aims

The aim of the experiment is the verification of the possibility of fabricating a titanium-tungsten functionally graded material, ranging from pure tungsten to pure titanium, for plasma facing applications by the PTA method. Two aspects are considered:

1) The possibility and suitability of layering titanium and tungsten in an FGM by the PTA method, and
2) the possibility and suitability of using the PTA method for deposition on a tungsten substrate material.

7.2 Experiment Objectives

The objective of the experiment is the creation of an evenly layered, uniform FGM, without defects such as pores, cracks, weld lines, dusted material, oxidation, or damage to the substrate. The gradation should range from pure tungsten to pure titanium. Ideally, optimal deposition parameters should be gradually established for the process. After the deposition of each layer, the deposition is visually inspected for dusting, oxidation, unevenness, and other visually detectable defects, with respect to the course of the deposition, and adjustments are made to the parameters if necessary. The dynamics of the PTA process, the number of variables and inherent inconsistencies necessitate adjustments to be made on an empirical basis. After the complete deposition of all layers, a metallographic sample is made, allowing for more detailed inspection. Similarly, the results of this inspection are used in the

empirical optimisation of parameters for the next deposition. Prior to attempting a graded structure, depositions to test and establish process parameters are carried out.

7.3 Equipment Used

The equipment used for the realisation of the experiment is listed in Part 7.3.2, while special attention is given to the PTA machine itself in Part 7.3.1.

7.3.1 PTA Cladding Machine

The machine used was a PPC 250 R6 numerically controlled automatic plasma cladding machine, manufactured by KSK, s.r.o., shown below in Figure 7.1. The machine was designed for the cladding of the circumference as well as faces of rotary parts, and as such, the welding torch can be operated in four axes; besides movement in the Cartesian X, Y and Z axes, it can also be rotated. The machine can either be programmed to follow a pre-set cycle, or can be operated manually, as it was for the purpose of this experiment. [65]

Figure 7.1: KSK PPC 250 R6 cladding machine [65]

The machine used for the experiment was significantly modified, to allow for the simultaneous use of two filler powders, which are mixed in volume ratios pre-set in the machine control interface. The powders are dosed by rotary feeders, with the resulting ratio of filler powders determined by the difference in the speed of rotation of the feeders. The powders are carried by the carrier gas to a mixer, where they are mixed together, and subsequently jointly carried by the carrier gas to the welding torch.

Given the high affinity of titanium to oxygen, especially at high temperatures, the machine was further modified with the addition of a specialised cladding chamber, shown below in Figure 7.2. The chamber is composed of an octagonal metal base with a groove, in which glass panels are set, held in place at the top by an octagonal metal strip also containing a groove. The top of the octagonal strip is covered by a graphite seal to minimise leakage. The cladding chamber is covered by a metal plate, containing an opening for the free movement of the welding torch, and is sealed around the torch with leather. Threaded rods protrude from the base, to allow for the anchoring of the workpiece. Crucially, the chamber is separately connected to a supply of the shielding gas, which is fed into the chamber through an opening at the bottom, ensuring immersion of the workpiece in the shielding gas. The constant flow of the shielding gas results in the slight pressurisation of the chamber. The chamber is mounted to the worktable through a cooling element to increase heat dissipation. It was purposely designed for the cladding of titanium in prior works. [66]

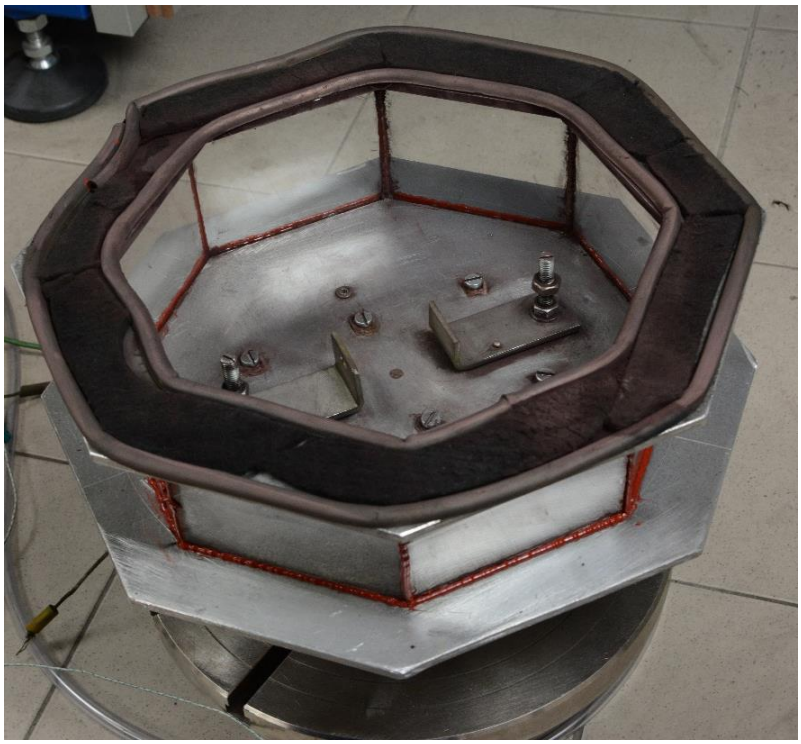

Figure 7.2: Cladding chamber

7.3.2 Other Equipment Used

A list of the equipment used, besides the PTA machine, follows below:

1) Recording and documentation:

- SLR digital camera; mfr.: Nikon Inc., type: D7100,
- Data logger; mfr.: AHLBORN GmbH, type: ALMEMO 5690-2,
- Thermocouple attachment unit; mfr.: BT Instruments, type: BT 2,
- Type K thermocouples (temp. range: –270 – 1260°C)

2) Substrate and filler preparation:

- Laboratory tabletop cutter; mfr.: Struers Inc., type: Labotom 3,
- Laboratory oven; mfr.: LAC, s.r.o., type: LE 09/11

3) Sample preparation:

- Metallographic sample mounting press; mfr.: Struers Inc., type: CitoPress 1,
- Metallographic sample polisher; mfr.: Buehler Ltd., type: BetaVector.

4) Analysis and evaluation:

- Scanning electron microscope; mfr.: Carl Zeiss AG, type: EVO MA 15,
- SDD detector unit; mfr.: Bruker AXS GmbH, type: XFlash 5010.
- X-ray diffractometer; mfr.: Bruker AXS GmbH, type: D8 Discover.
- Optical metallographic microscope; mfr.: VEB Carl Zeiss Jena, type: Neophot32.

7.4 Consumables Used

The consumables used for the experiment are described in the following Parts:

7.4.1 Filler Materials

1) Titanium powder

The titanium powder was manufactured by TLS Technik GmbH & Co. Spezialpulver KG. The grains are of variable asymmetric shapes and non-consistent size, which presented severe difficulties in feeding the powder by the PTA machine. The volumetric density of the powder was calculated to be 1.97 g.mℓ^{-1}. A microscope image of the powder grains is shown in Figure 7.3.

2) Tungsten powder

The tungsten powder was manufactured by Alldyne Powder Technologies Inc. The grains are sharp-edged and vary considerably in size and shape. Like in the case of the titanium powder, this presents significant difficulties in feeding the powder. The volumetric density of the powder was calculated to be 8.59 g.mℓ^{-1}. A microscope image of the powder grains is shown in Figure 7.4:

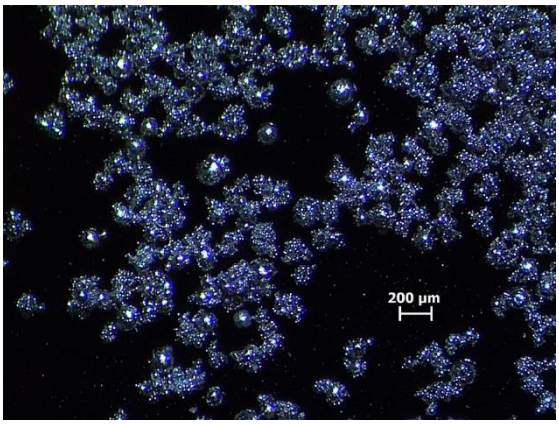

Figure 7.3: Microscope image of titanium powder (black background)

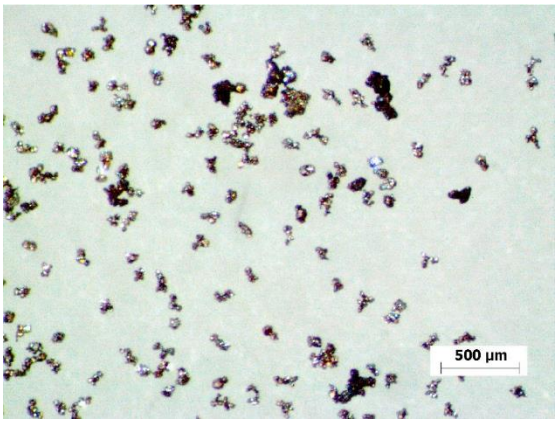

Figure 7.4: Microscope image of tungsten powder (white background)

7.4.2 Base Material

The base material (substrate) was pure tungsten, in the form of a plate, which was divided by a tabletop cutter into individual substrates. Six individual substrates labelled A, B, C, D, E, F[12] were created. The plate was manufactured using powder metallurgy by Porexi s.r.o.

7.4.3 Gases

1) Plasma gas

Argon with a purity of 99.999 (Ar 5.0) was used as the plasma gas.

2) Shielding and carrier gas

A mixture of 95 % argon with 5% hydrogen (95Ar-5H_2) was used as the carrier and shielding gas.[13]

Basic thermophysical properties of argon, being the primary constituent of both the plasma and shielding/carrier gas, are given in Table 7.1 below:

[12] One of the substrates was damaged during a flawed deposition and is not included in the results in Part 8.

[13] Contrary to recommended use of argon and helium and their mixtures for the PTA welding of titanium. [58]

Table 7.1: Thermophysical properties of argon [67]

Density	[kg.m^{-3}]	1400
Melting point	[°C]	-189.2
Boiling point	[°C]	-186.0
Specific heat capacity	[J.kg^{-1}.K^{-1}]	523
Thermal conductivity	[W.m^{-1}.K^{-1}]	0.0172

7.5 Experiment Setup

The experiment consisted of depositing several layers of titanium and tungsten in varying ratios on a tungsten substrate. The deposition was conducted by the PTA machine described above in Part 7.3.1, in a specialised cladding chamber; also described above. In the chamber, the substrate was placed on copper blocks acting as heat sinks and held in place by metal clamps fastened with nuts on the threaded rods. At first, the substrate was held down by clamps at the edges, however due to the repeated damage to the steel clamps, this was changed to samples being held down by the corners. Thermocouples, shielded in ceramic tubes, were welded on the substrate and directed out of the chamber under the lid to the adjacent data logger. Despite efforts in protecting the thermocouples, they repeatedly detached from the substrate during the process due to effects of the plasma arc. The lid on the chamber was weighed down with metal blocks to increase the sealing between the lid and the chamber. Welding parameters (incl. powder ratios and feed rate) were *a priori* set through the machine's digital interface. The workspace was ventilated, and a fume extractor was in operation during the deposition and shortly after the chamber was opened. The chamber was illuminated by halogen reflectors. Photographs of the work area, and of the sample positioned and fastened in the cladding chamber, prepared for deposition, are show below in Figure 7.5 and Figure 7.6 respectively.

Figure 7.5: PTA machine work area

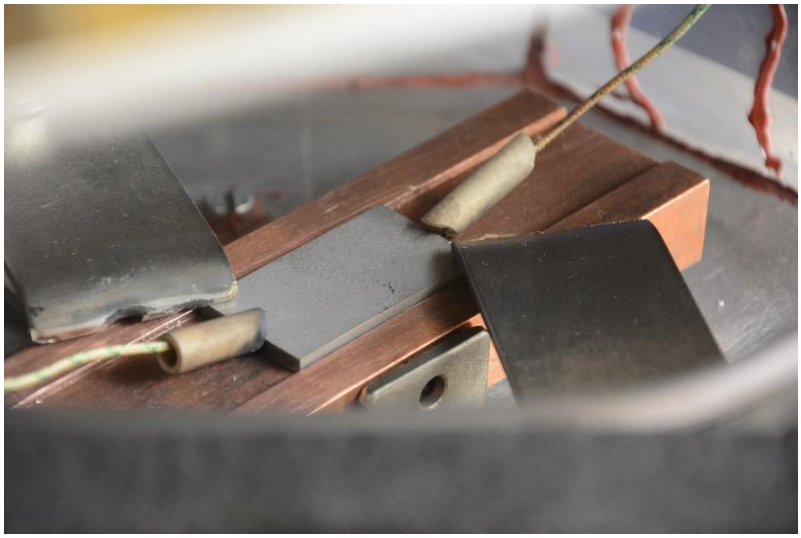

Figure 7.6:Substrate material in place in the cladding chamber

7.6 Experimental Method

1. Powders were dried overnight.
2. Powder reservoirs were filled with adequate amounts of both powders.
3. The mass flow rate of powders for various settings was established by measuring the volume flow over a time period.
4. The relationship between the pre-set volume ratio and resultant mass ratio of powders was established. (see Part 7.7.4).
5. Parameters were established for the first deposition (see Part 7.7).
6. Welding parameters were pre-set into the machine interface.
7. The substrate was degreased with technical alcohol.
8. The substrate was placed in the chamber on copper blocks and fastened down with clamps (see Part 7.5).
9. Thermocouples were welded onto the substrate.
10. The substrate was photographed.
11. The chamber was covered by the lid and weighed down with metal blocks.
12. The welding torch was positioned to the starting position.
13. The fume extractor was started.
14. The chamber was pressurised with the shielding gas. The lid was repeatedly lifted under pressure to allow remaining air to escape.
15. The pilot and subsequently transferred arc were established.
16. The torch made a pass over the substrate, depositing the filler material. For preheating, no filler was deposited.
17. The chamber continued to be supplied and pressurised by the shielding gas until the temperature of the substrate decreased below ~350°C. This was monitored through the thermocouples.
18. The chamber was opened, the substrate was photographed, cleaned by a metal brush, and allowed to cool.
19. The fume extractor was stopped.
20. Parameters for the next layer were selected considering the results of prior deposition, and steps 6 and 11 to 19 were repeated for every subsequent layer.
21. The substrate was taken out of the chamber.
22. Steps 6 to 21 were repeated for every subsequent substrate.

7.7 Input Parameters

Given the fact that no prior experience existed with the PTA cladding of a titanium-tungsten mixture on tungsten, the initial parameters were taken from prior works on similar materials and adjusted. Experience from prior substrates and prior layers was used in determining parameters for the next substrate or layer. Given the volatility and relative inconsistency of the process, the welding current and powder feed rate were sometimes modified *ad hoc* during deposition, within a limited range, if the deposition was evidently flawed.

The following Table 7.2 lists the parameters that define the welding process and are pre-set through the machine interface. An indication is made if the parameter was altered or remained constant throughout the experiment. Parameters are addressed in general in following Parts, as indicated in Table 7.2:

Table 7.2: Parameters set for the PTA cladding process

Parameter	Unit	Description	Alteration
CURRENT – see Part 7.7.2.			
Equivalent current	[A]	Mean between high and low currents.	Yes
Current-high	[A]	Pulsed current high.	Yes
Current-low	[A]	Pulsed current low.	Yes
Pulse frequency	[Hz]	Frequency of the current pulsation.	No
Pulse period-high	[s]	Period for which high current is held.	No
Pulse period-low	[s]	Period for which low current is held.	No
TORCH MOTION – see Part 7.7.3.			
Travel speed	[$mm.s^{-1}$]	Speed of torch motion over substrate.	Yes
Oscillation range	[mm]	Range of perpendicular motion of the torch.	Yes
Oscillation speed	[$mm.s^{-1}$]	Speed of perpendicular motion of the torch.	Yes
Stop-time pos.	[s]	Time torch is stopped at oscillation range end.	Yes
Stop-time neg.	[s]	Time torch is stopped at oscillation range end.	Yes
FILLER FEED – see Part 7.7.4.			
Powder feed rate	[-]	Set discrete level of feed rate.	Yes
Powder feed ratio	[vol.%]	Ratio of tungsten powder in total volume.	Yes

7.7.1 Constant parameters

The parameters that remained constant were current-defining; the pulse frequency and the low and high pulse periods. The values selected for these

parameters are given in Table 7.3 below, and remained constant throughout the experiment:

Table 7.3: Constant current-defining parameters

Pulse frequency [Hz]	Pulse period - high [s]	Pulse period - low [s]
200	0.0025	0.0025

7.7.2 Current

The current high and low, as well as the frequency for the first sample was selected based prior experience with the cladding of tungsten on the PTA machine. For subsequent depositions, the frequency remained constant, while the current high and low was altered to increase or decrease the arc energy, based on experience with the prior deposition. [33]

7.7.3 Torch motion

The initial travel speed was selected based on prior experience with the PTA machine and was altered based on the resultant deposited layer. The oscillation range was defined by the substrate width and was altered throughout the experiment depending on the layer being deposited. The oscillation speed was altered depending on the resultant powder distribution, as were the stop-times at both extremes of the oscillation range.

7.7.4 Feed Rate and Powder Ratios

The filler feed rate is expressed in the machine interface in terms of discrete setting levels from 0 to 40. The volume flow of the powders was determined by measuring the volume collected over a period of time. The volumetric density of the powders was determined *a priori* by the weighing of known volumes. The mass flow rates for different setting levels are presented in Figure 7.7 below:

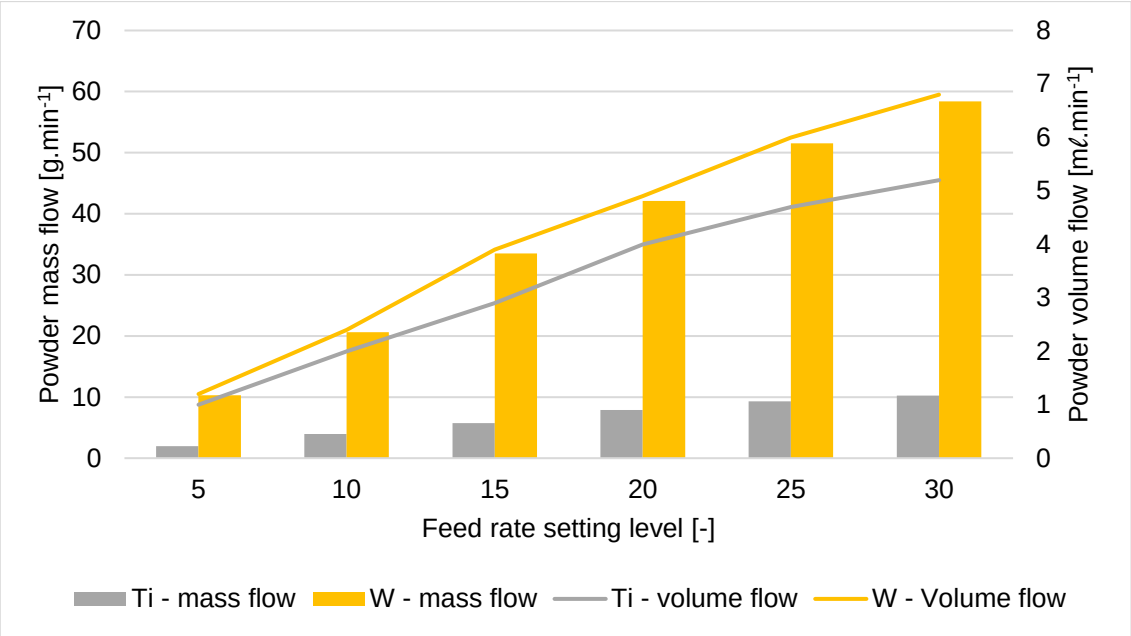

Figure 7.7: Graph to show the relationship between the feed rate setting level and the powder mass and volume flows

The graph shows that the volume flow rate is higher for the tungsten powder. The difference is caused by the different rheological properties of the two powders (see Part 7.4.1), and increases with higher setting levels. Due to the high density of tungsten, the mass flow rate of the tungsten powder is significantly higher than that of the titanium powder.

Approximate linear relationships were determined between the setting level and the mass flow rate. These are true for mid-range setting levels (5-20), as the relationship is no longer linear for higher feed rates due to the dynamics of the feeding process. These linear relationships are expressed by Equations 5 and 6 for titanium and tungsten respectively:

$$\dot{m}_{Ti} \approx 0{,}3909 \cdot SL \quad \text{for } SL \in \langle 5; 20 \rangle \tag{5}$$

$$\dot{m}_{W} \approx 2{,}1646 \cdot SL \quad \text{for } SL \in \langle 5; 20 \rangle \tag{6}$$

where:

SL.....setting level [-],
$\dot{m}_{Ti}$.....mass flow rate of titanium [g.min^{-1}], and
$\dot{m}_{W}$.....mass flow rate of tungsten [g.min^{-1}].

To achieve the desired ratios of the mass of filler materials in each layer, they have to be deposited in known mass flows and mutual ratios. However, the PTA machine handles ratios by volume, and adjusts powder ratio by adjusting the difference in speed of rotary feeders. Given the significantly different densities of both powders, the mass flow ratio is not proportional to the volume flow ratio. To compensate for this and allow for defining the powder mixture by the ratio of masses, the volume flow ratio was expressed in terms of mass flow ratio and densities of the filler powders. The corresponding volume flow ratio was determined based on the desired mass flow ratio and was then pre-set into the machine.

The difference in volume flow between the titanium and tungsten powder was omitted. This is acceptable, as it was planned to preform depositions with a filler feed rate setting below 10, at which the difference in volume flows is less significant[14]. As it later turned out however, the feeding process was impaired due to the unsuitable rheological properties of both powders, and the overall accuracy was thus adversely affected (see discussion in Part 8), making this omission altogether negligible. The resultant relationship between volume and mass flow ratios is expressed in Equation 7 below:

$$\%v_W = 100 \cdot \frac{\%m_W \cdot \rho_{Ti}}{\%m_W \cdot \rho_{Ti} + (100 - \%m_W) \cdot \rho_W} \qquad (7)$$

where:

$\%v_W$ ... volume ratio of tungsten [vol. %],
$\%m_W$ .. mass ratio of tungsten [wt. %],
ρ_{Ti} ..... volumetric density of titanium powder [g.mℓ^{-1}], and
ρ_W ..... volumetric density of tungsten powder [g.mℓ^{-1}].

[14] Due to difficulties with feeding the tungsten powder, this was later increased to 17.

7.8 Evaluation Methods

The samples were subjected to analysis by various methods:

1) Visual inspection

Firstly, a sample was submitted to visual inspection, in which the overall quality of the sample and the presence of defects such as pores, cracks and dusted material in the outer layer can be evaluated. Based on the visual inspection of the sample, process parameters could be optimised for the next deposition.

2) Optical microscope

The samples were then cut, and metallographic samples were prepared. These were subjected to analysis through optical microscope. This allowed for the initial analysis of layering, as well as defects such as pores, cracks, and visible voids.

3) Scanning electron microscope (SEM)

The samples were further analysed by SEM, set to detecting backscattered electrons. In this mode, high-Z elements appear lighter, with visible progression to darker, low-Z elements. Images captured from the SEM allow for the clear visual distinction between phases and show the microstructure in high resolution.

4) Energy dispersive spectroscopy (EDS)

Evaluation by EDS was carried out on selected samples. This elemental analysis of composition was carried out in selected points, as well as over the entire height of the samples. The results are expressed as the percentage of each element in the discrete points, while over the height of the sample, the results are displayed as one-dimensional graphs, showing the representation of the elements throughout the layers of the sample. This allows for the visualisation of compositional gradation.

5) X-ray diffraction (XRD)

Evaluation by XRD was carried out on one sample in several distinct layers, to determine and quantify the phases present in the layers. The analysis was performed by matching detected diffraction spectra to those of individual phases from a crystallographic database.

6) Immediate temperature logging

The thermocouples connected to the substrate were used partly to monitor the substrate temperature during the deposition, but were primarily used to monitor the cooling of the substrate. This was done to ensure that the shielding gas was supplied in sufficient quantity to prevent oxidation, until the temperature of the substrate decreased below a threshold temperature of ~350°C. This measurement was performed for guidance only, and because the temperature limit of the measurement was ~1370°C (data logger limit, 1260°C thermocouple limit) the recorded data is not consistent and is not presented.

8 Results and Discussion

The following Part is divided into individual sub-parts, each dedicated to one sample. The sub-parts are structured to include the parameters used to deposit each layer, along with a commentary about the course of the deposition. A photograph of the resultant sample is included, while photographs of individual layers are shown in Appendix A. Subsequently, the results of evaluation methods, as listed in Part 7.8, are presented, along with commentary.

Due to the complicated dynamics of the PTA process, the fact that the titanium-tungsten interactions are not yet fully explored and defined, and the fact that the deposition process was set on an empirical basis, the hypotheses presented are only estimates and should be taken as such. Further research, beyond the scope of this thesis, is required in order to fully understand and describe the processes that led to the creation of structures presented below, and to describe the structures themselves.

8.1 Sample I

Sample I was the first documented deposition of the experiment, and was deposited on Substrate A. The aim of this deposition was to explore the settings to ensure proper bonding of the deposition to the base material. As such, only one layer was deposited. No thermocouples were connected and no analysis apart from visual inspection was carried out on this sample. The deposition of the single layer was carried out with parameters set as per Table 8.1:

Table 8.1: Sample I - deposition parameters

Sample *I*	FILLER		CURRENT			TORCH MOTION				
Substrate *A*	Powder ratio	Feed rate	Current high	Current low	Current equiv.	Travel speed	Osc. range	Osc. speed	Stop pos.	Stop neg.
Layer	[wt.%W]	[-]	[A]	[A]	[A]	[mm.s^{-1}]	[mm]	[mm.s^{-1}]	[s]	[s]
1	100	8	170	120	145.0	1.0	8	16	0.2	0.2

The substrate was held down by clamps along the edges. The layer was deposited, without preheating, to test the parameters for the bonding of the deposited layer of pure tungsten to the base material. It was clear during deposition

that the set current is too low, and the heat is insufficient to melt the base material. The deposition is shown below in Figure 8.1, on the right:

Figure 8.1: Photograph of substrate A with deposited Samples I (right) and II (left)

It can be concluded from the visual inspection that the selected current was too low, as was evident during the deposition, resulting in insufficient energy to melt the base material. Furthermore, the filler material was only partially molten, and was partly deposited in powder form. The conclusion to be made from Sample I is that higher current values must be selected to ensure proper bonding between the base material and the deposited layer, as well as proper melting of the filler material. The amount of filler material deposited was sufficient.

8.2 Sample II

Sample II was deposited on the same Substrate A as Sample I. Like Sample I, the objective of this deposition was to establish parameters to ensure bonding between the filler and base materials. Given the experience with Sample I, the current was increased. The filler feed rate along with all other parameters was kept constant. Only one layer of pure tungsten was deposited, without preheating and thermocouples were not connected to the substrate. The deposition was carried out with parameters set as per Table 8.2:

Table 8.2: Sample II - deposition parameters

Sample *II*	FILLER		CURRENT			TORCH MOTION				
Substrate *A*	Powder ratio	Feed rate	Current high	Current low	Current equiv.	Travel speed	Osc. range	Osc. speed	Stop pos.	Stop neg.
Layer	[wt.%W]	[-]	[A]	[A]	[A]	[mm.s^{-1}]	[mm]	[mm.s^{-1}]	[s]	[s]
1	100	8	215	130	172.5	1.0	8	16	0.2	0.2

The substrate was held down by clamps along the edges. During the deposition, the clamps holding the substrate down were partially melted. When removing one of the clamps, a portion of the damaged base material along with the deposited filler material was removed with it – this can be seen above in Figure 8.1, in Part 8.1. This revealed that the base material has melted during the process, as has as the filler material, which fell in liquid form into an existing melt pool.

The sufficient melting of the filler and base materials was an improvement over the results achieved in Sample I, however, the current was set too high, which, along with the inconvenient position of the clamps, resulted in the melting of these steel clamps. Based on the results from Sample II, it was established that the high and low currents for the next deposition would be set as the mean value between Sample I and Sample II, while other parameters would be kept constant, as the amount and layout of deposited material seemed favourable.

8.3 Sample III

Sample III was the first experimental deposition in which multiple layers were deposited, and the primary purpose of this sample was to empirically test different parameter settings for the inter-layer bonding between multiple layers of pure tungsten, as well as bonding to the tungsten substrate. Like Samples I and II, Sample III was monitored during the deposition, and was subjected to visual inspection only. The deposition was carried out with parameters set as per Table 8.3:

Table 8.3: Sample III - deposition parameters

Sample *III*	FILLER		CURRENT			TORCH MOTION				
Substrate *B*	Powder ratio	Feed rate	Current high	Current low	Current equiv.	Travel speed	Osc. range	Osc. speed	Stop pos.	Stop neg.
Layer	[wt.%W]	[-]	[A]	[A]	[A]	[mm.s^{-1}]	[mm]	[mm.s^{-1}]	[s]	[s]
1	100	8	192	125	158.5	1.0	8	16	0.2	0.2
2	100	8	195	125	160.0	0.9	8	12	0.2	0.2
3	100	10	205	130	167.5	0.8	8	12	0.1	0.1

The substrate was held down by clamps along the edges. For the deposition of the first layer on the tungsten substrate, the mean value of the high and low currents used for Samples I and II was selected. All other parameters were not modified. The substrate was not preheated. During the deposition of the first layer, the surface of the substrate material has melted sufficiently, and bonded satisfactorily with the filler material, which however retained distinctive powder structure in some areas. The deposition was relatively uneven, with more filler material concentrated at the extremes of the oscillation range.

For the second layer, the currents were increased slightly to eliminate the dusting of filler material and ensure its complete melting. During the deposition of the second layer, the flow rate of the filler material was insufficient and gradually decreased. To counter this, the filler material was stirred, and the feeding system was emptied and refilled for the deposition of the third layer. The feed rate was increased, and the currents were also increased. However, even during the third deposition the feeding was not sufficient, and proper layering only occurred at the ends of the oscillation range, where the torch stopped. Sample III is seen in the left side of Figure 8.2, partly covered by Sample IV.

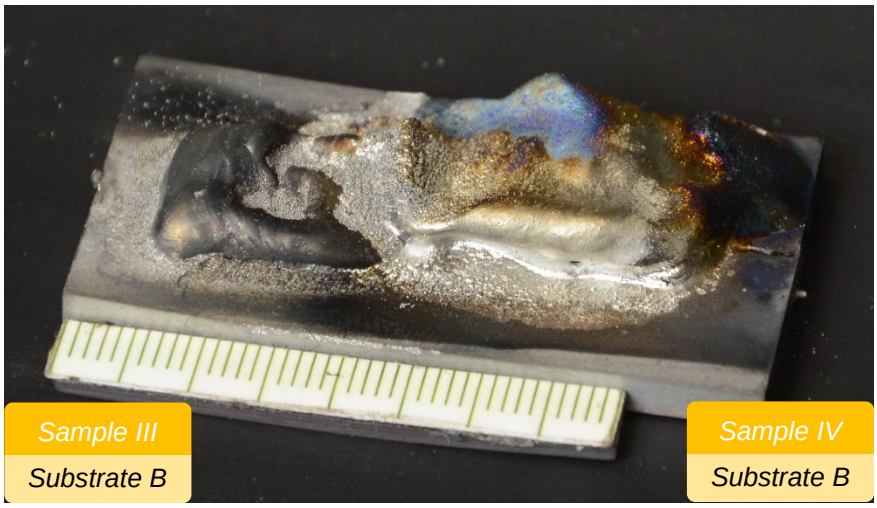

Figure 8.2: Photograph of substrate B with deposited Samples III (left) and IV (right)

Based on observations made during the deposition and the results of visual inspection, it can be stated that while a layered structure was achieved, the insufficient and inconsistent feeding of the filler material resulted in uneven layering. The best results were achieved at the extremes of the oscillation range, where the largest amount of filler material was deposited. Powdered structure visibly remains in parts of the top layer, which is partly the result of the deposition of Sample IV on the same substrate. Despite the problems with feeding the filler material, the layers are apparently sufficiently bonded together, as is the first layer to the substrate material.

8.4 Sample IV

Sample IV was the first sample on which a functionally graded structure was attempted, ranging from a deposition of a layer of pure tungsten on the substrate to a layer of 25 wt. % tungsten to 75 wt. % titanium at the surface. The sample was deposited on the same Substrate B as Sample III. The purpose of this sample was to test the properties of depositing layers of various composition, the interlayer adhesion, and the suitability for the parameters empirically tested before on pure tungsten for layers containing titanium. The current parameters were deliberately left constant if possible, to see the results with the increasing ratio of titanium in the filler material, and are listed in the following Table 8.4:

:

Table 8.4: Sample IV - deposition parameters

Sample *IV*	FILLER		CURRENT			TORCH MOTION				
Substrate *B*	Powder ratio	Feed rate	Current high	Current low	Current equiv.	Travel speed	Osc. range	Osc. speed	Stop pos.	Stop neg.
Layer	[wt.%W]	[-]	[A]	[A]	[A]	[mm.s^{-1}]	[mm]	[mm.s^{-1}]	[s]	[s]
1	100	7	192	125	158.5	0,9	8	16	0.2	0.2
2	85	6	192	125	158.5	1.0	8	16	0.2	0.2
3	70	6	192	125	158.5	1.0	8	16	0.3	0.3
4	50	6	192	125	158.5	1.0	8	16	0.3	0.3
5	25	6	150	98	124.0	1.0	8	16	0.3	0.3

The substrate was held down by clamps along the edges. Due to the unsuitable position of the clamps and relative width of the sample, clamps were partially melted during all depositions. During the deposition of the first layer, some filler material partly remained in powder form, and the substrate material seemingly melted only partially. The second layer was deposited with the same current parameters, but the filler feed rate was decreased. After the deposition of the second layer, the flow of the shielding gas was prematurely terminated, resulting in visible oxidation on the layer. For subsequent layers, the stop times were increased to distribute the filler material more evenly at the extremes of the oscillation range. Current was only decreased for the final layer, which contained a majority of titanium, due partly to the lower melting point of titanium, but mostly due to the fact that the work area and heatsinks have already accumulated significant heat. The final layer was also improperly shielded, resulting in visible oxidation to the titanium, clearly seen above in Figure 8.2 in Part 8.3.

The sample is visibly severely oxidised, uneven, and is dusted by filler material in powder form, showing that insufficient heat was delivered during the deposition of the final layer. Furthermore, Sample IV was partly deposited over Sample III, due to delays in stopping the deposition due to manual control.

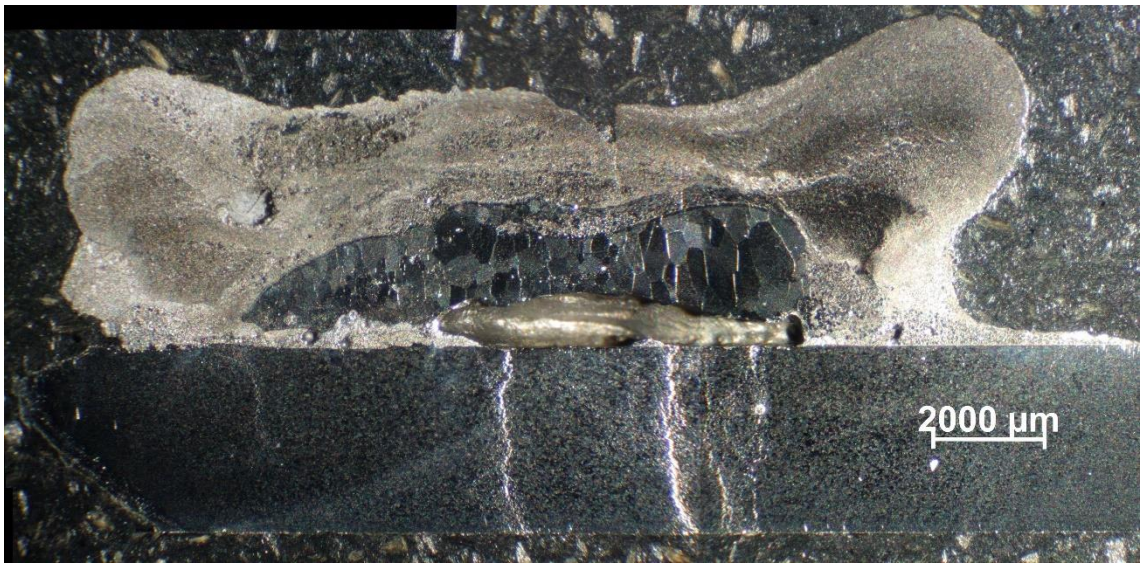

Figure 8.3: Macroscopic photograph of Sample IV cross-section

The macroscopic image above distinctly shows several layers, indicating that gradation was achieved to some degree. Directly on the substrate however, there is a layer of material that is not pure tungsten, as was expected, given the first deposition was carried out with tungsten filler only. Furthermore, a clear void is visible directly above the substrate in the centre. The material present directly on the substrate may partly originate from the steel clamps holding down the substrate, which were melted even during the deposition of the first layer. Given that Sample IV was deposited on the same substrate as Sample III and partially covers it, the material present could also be a result of any titanium accidentally present in Sample III. The void is likely the result of the evaporation of this material during the deposition of the layers.

The edge of the substrate itself is clearly distinguishable, indicating limited penetration. The layer directly above is likely mostly pure tungsten, as evidenced by the grained structure. The grains have grown to considerable size, and evidence that the layer cooled relatively slowly. This may indicate that the void and interlayer formed during the deposition of the first layers and limited the thermal conductivity from the tungsten layer to the substrate and the heat sinks. A clear interface is however visible between the pure tungsten layer and the layer above, indicating that the pure tungsten layer has not remolten during subsequent depositions. The over-

deposition of filler materials in the outermost layers at the extremes of the oscillation range is also clearly visible.

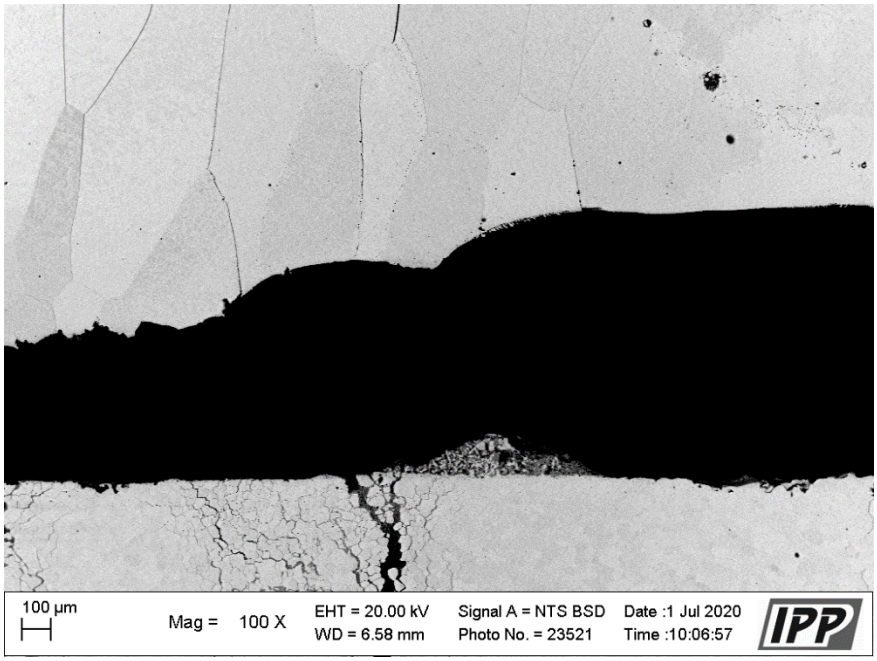

Figure 8.4: SEM photograph of Sample IV (substrate and first layer I/F, centre) [J. Matějíček, IPP]

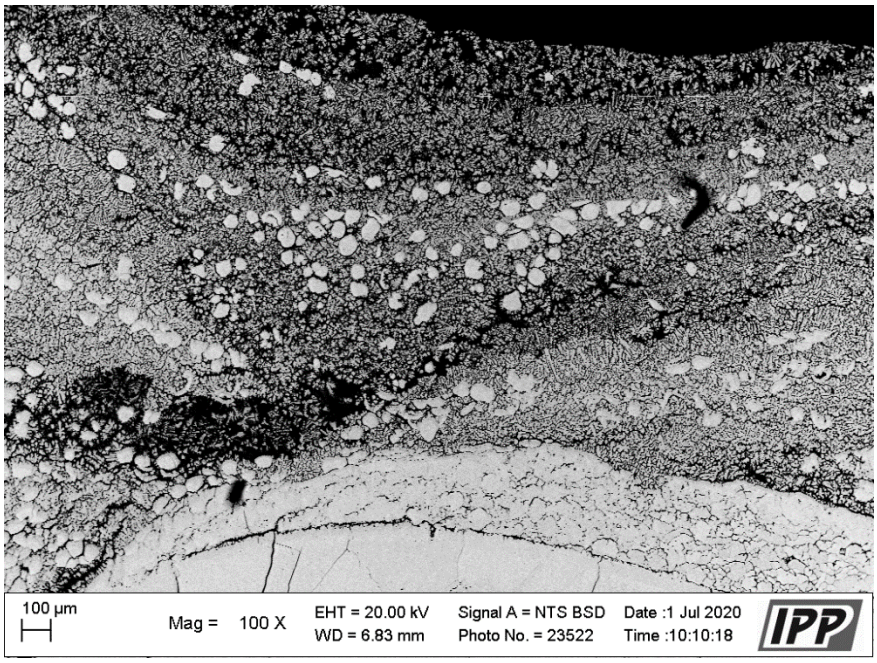

Figure 8.5: SEM photograph of Sample IV (outer layers, surface, centre) [J. Matějíček, IPP]

The SEM images above confirm the pure tungsten composition of the layer above the void, and clearly show the grained structure. The first image reveals that

the layer directly on the substrate contains both tungsten and another lower-Z element – titanium or iron. Visible damage to the substrate is the result of thermal stress, possibly due to the fact that two samples were deposited on one substrate.

Multiple distinguishable layers are visible above the tungsten layer, clearly progressing from tungsten-rich to more titanium-rich compositions. This indicates that gradation was achieved in these layers, and the mixing of layers was not severe. The relatively large tungsten structures in these layers could be, given their size, remains of original grains of the tungsten powder, evidencing limited melting of the tungsten filler. There is a visible gap between the pure tungsten and further layers, and interlayer adhesion in this location is not good. While tungsten seems to have retained its pure form in the remainders of the filler grains, the rest of the material in the outer layers is a mixture of Ti-richer and W-richer phases, with possible regions pure titanium in the outermost layers. A mixture of HCP α-phase titanium with a BCC tungsten-rich phase would be expected as per the Ti-W equilibrium diagram (Figure 5.1), (if assuming the cooling process occurred under equilibrium conditions), but no analysis was carried out on the sample to determine the structure. XRD analysis was performed on Sample VII (see Part 8.7 below).

Overall, it can be stated that a degree of gradation was achieved in Sample IV. This is mostly true for the outer layers, while most of the area in the centre of this cross section of the sample is pure tungsten. Adhesion between the first tungsten layer and the substrate is practically non-existent, as an interlayer was formed on the substrate, likely during the deposition of the tungsten layer. As such, this Sample is not successful in terms of composition. The fact that the tungsten filler material has not fully melted in the outermost layer should not however pose problems in terms of properties of the material. This sample is visibly severely oxidised, on the surface of multiple layers, and further likely includes iron and other alloying elements from the steel clamps which partially melted.

8.5 Sample V

Sample V is a full-scale deposition on an individual substrate, utilising its full width. A full gradation from pure tungsten to pure titanium was attempted on this

sample, in six layers. The initial current parameters were the same as in the first deposition of Sample IV. However, based on experience with Sample IV, Sample V was the first where the substrate was preheated prior to deposition. The deposition was carried out with parameters set as per Table 8.5:

Table 8.5: Sample V - deposition parameters

Sample V	FILLER		CURRENT			TORCH MOTION				
Substrate C	Powder ratio	Feed rate	Current high	Current low	Current equiv.	Travel speed	Osc. range	Osc. speed	Stop pos.	Stop neg.
Layer	[wt.%W]	[-]	[A]	[A]	[A]	[mm.s^{-1}]	[mm]	[mm.s^{-1}]	[s]	[s]
PH	N/A	N/A	192	125	158.5	2.0	18	16	0.4	0.4
1	100	6	192	125	158.5	1.0	18	16	0.4	0.4
2	85	6	192	125	158.5	1.0	16	16	0.4	0.4
3	70	6	192	125	158.5	1.0	16	16	0.4	0.4
4	50	7	172	112	142.0	1.0	14	16	0.4	0.4
5	25	9	172	112	142.0	1.0	14	16	0.4	0.4
6	0	9	172	112	142.0	1.0	14	16	0.2	0.2

The substrate was held down by clamps in the corners. The substrate was preheated with a single pass of the torch, with current parameters equal to those used for the subsequent deposition. This was done to decrease the amount of energy needed to melt the surface layer of the substrate material during the deposition of the first layer and ensure bonding between the substrate and the filler. During the deposition, melting of the filler material was seemingly sufficient, as was the melting of the substrate material in the first deposition. The currents were reduced for the deposition of the final three layers, as significant heat was already accumulated in the heat sink elements supporting the substrate. Furthermore, the layers with a higher titanium ratio have, on average, a slightly lower melting point and require less energy to melt the surface. The filler feed rate was seemingly sufficient for the first three layers, but was increased as problems with feeding the filler started occurring again during the deposition of the fourth layer. A photograph of Substrate C with Sample V deposited is shown below in Figure 8.6:

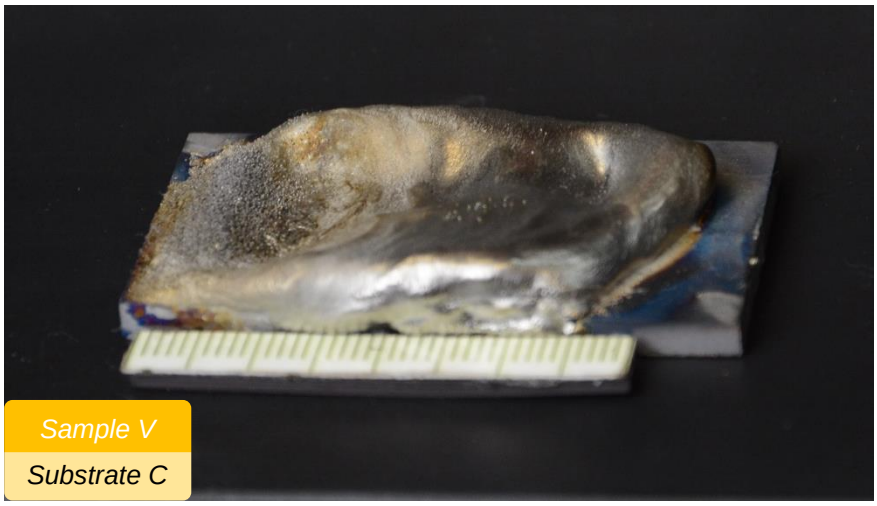

Figure 8.6: Photograph of substrate C with deposited Sample V

From the visual inspection it can be seen that the deposited layer is relatively even, except for the area to the left in Figure 8.6. The surface layer of titanium was well protected by the shielding gas, and oxidation is not visible. However, oxidation is visible at the edges of the second layer, as the shielding gas flow was prematurely terminated. Residues of filler material in powder form are visible at the left side of Figure 8.6 – evidence of localised insufficient melting of the filler material.

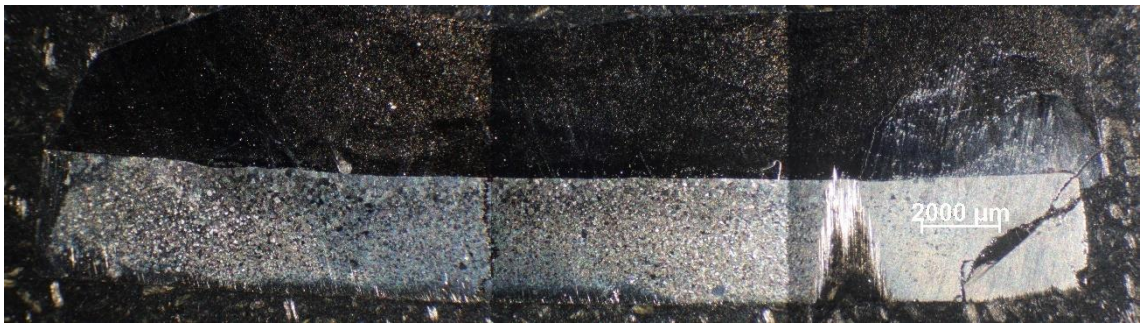

Figure 8.7: Macroscopic photograph of Sample V cross-section

The macroscopic image, seen above in Figure 8.7, reveals that no individual layers can be clearly distinguished. This shows that large sections of the previous layer were melted during the deposition of the subsequent layer, and a sharp interface is not distinguishable between them. This is evidence of significant heat delivered during deposition. The mixing of the materials was likely also enhanced by the dynamic effects of the plasma. Furthermore, the substrate material is evidently deformed and damaged, which is further evidence of significant heat.

Evident cracks attest to large stresses induced in the substrate during deposition, at the interface with the first layer.

Nonetheless, the edge of the substrate is distinctly visible and relatively straight, indicating limited penetration. The SEM image seen below in Figure 8.8 however reveals that a ~20µm layer containing titanium was formed on the surface of the substrate, showing sufficient bonding between the substrate and the first layer occurred.

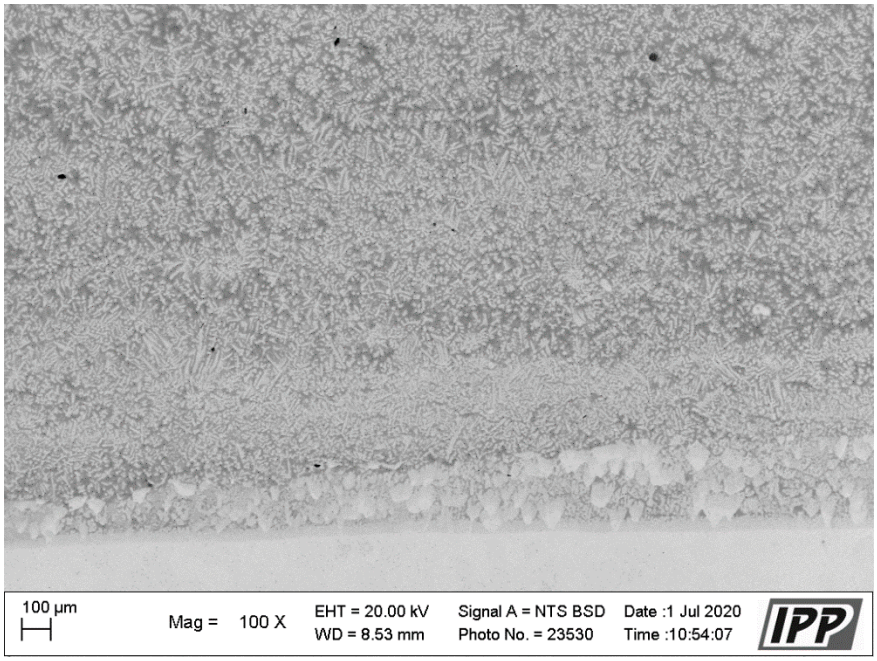

Figure 8.8: SEM photograph, Sample V (substrate and first layer I/F, centre) [J. Matějíček, IPP]

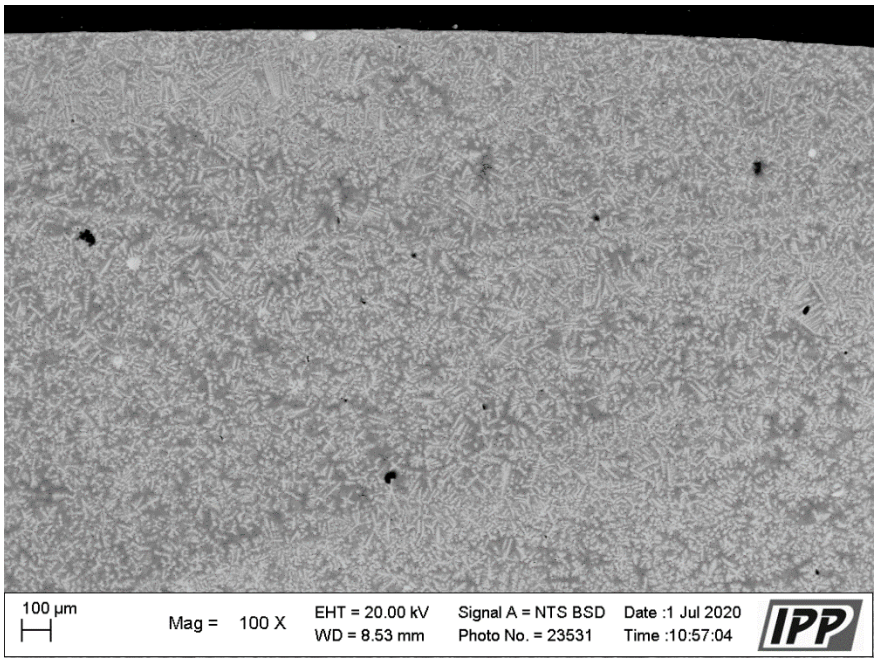

Figure 8.9: SEM photograph, Sample V (outer layers, surface, centre) [J. Matějíček, IPP]

The SEM images above show that the structure is indeed relatively homogenous, with no sharp interfaces and a slight gradation in structure. Two clear boundaries between slightly different structures can be distinguished in Figure 8.9, showing limited evidence of layering. The structure in various regions is shown in detail in the SEM images below:

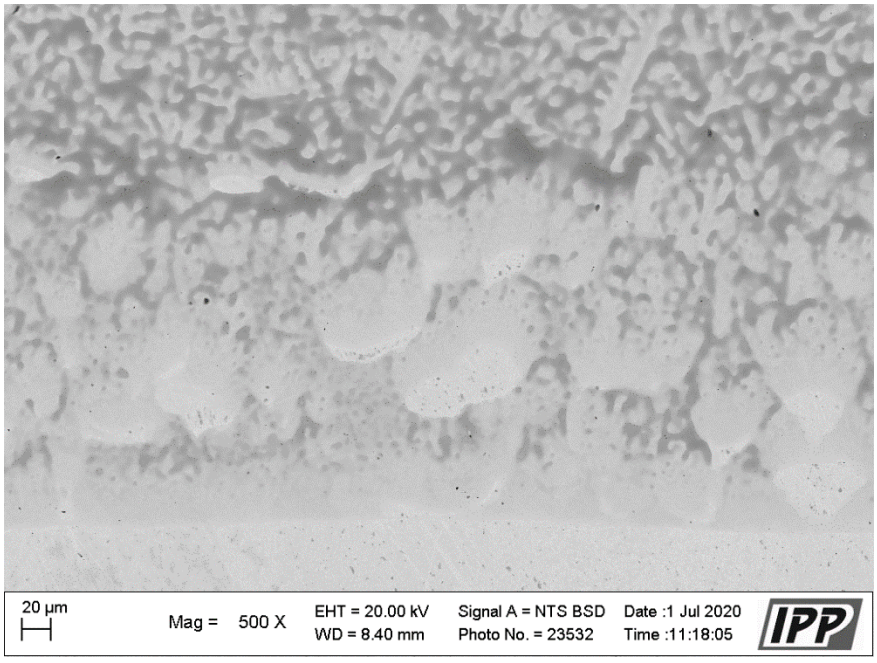

Figure 8.10: SEM photograph, Sample V (detail, substrate and first layer I/F, centre) [J. Matějíček, IPP]

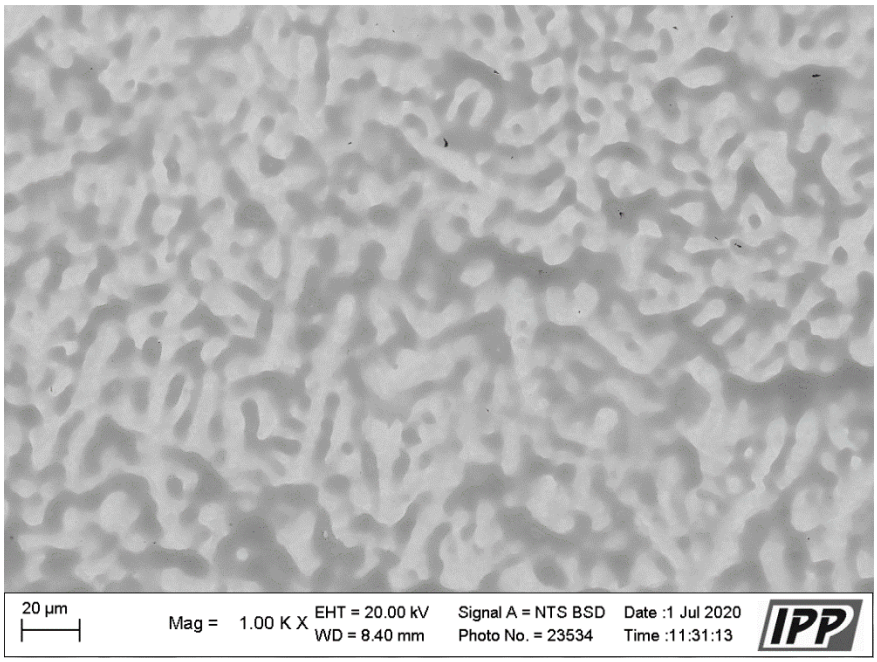

Figure 8.11: SEM photograph, Sample V (detail, structure of central layer, centre) [J. Matějíček, IPP]

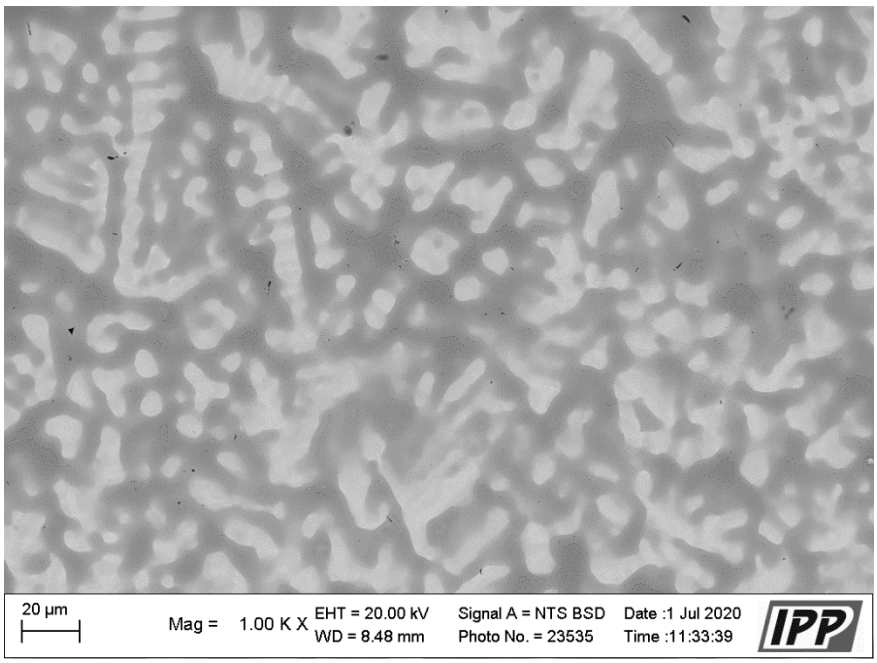

Figure 8.12: SEM photograph, Sample V (detail, structure of outer layer, centre) [J. Matějíček, IPP]

In the layer immediately next to the substrate, tungsten forms the basis of the material in this region, and tungsten-rich alloys are concentrated in relatively large, concise areas. The central layer, while still seemingly tungsten-rich, shows a more dendritic-like structure. The same is true for the layer furthest from the substrate,

which apparently contains tungsten in lower concentrations. The dendritic-like structure is likely the result of the completely molten alloy redistributing by diffusion into tungsten and titanium-rich areas. The original constituents are practically no longer present in their pure form, and the material is a mixture of Ti-richer and W-richer phases.

EDS was performed on Sample V, both in discrete locations, and continuously across the entire height of the sample. The continuous analysis was performed over a straight line, shown in Figure 8.13, in the centre of the sample, connecting the substrate and the surface of the sample.

The results of the continuous scan (Figure 8.14) show limited gradation and two distinct transitions. The amount of titanium does eventually surpass the amount of tungsten in the uppermost region, however the ratio of the two materials remains close to 50% throughout the height of the sample. The EDS does nonetheless show that a continuously graded material was achieved.

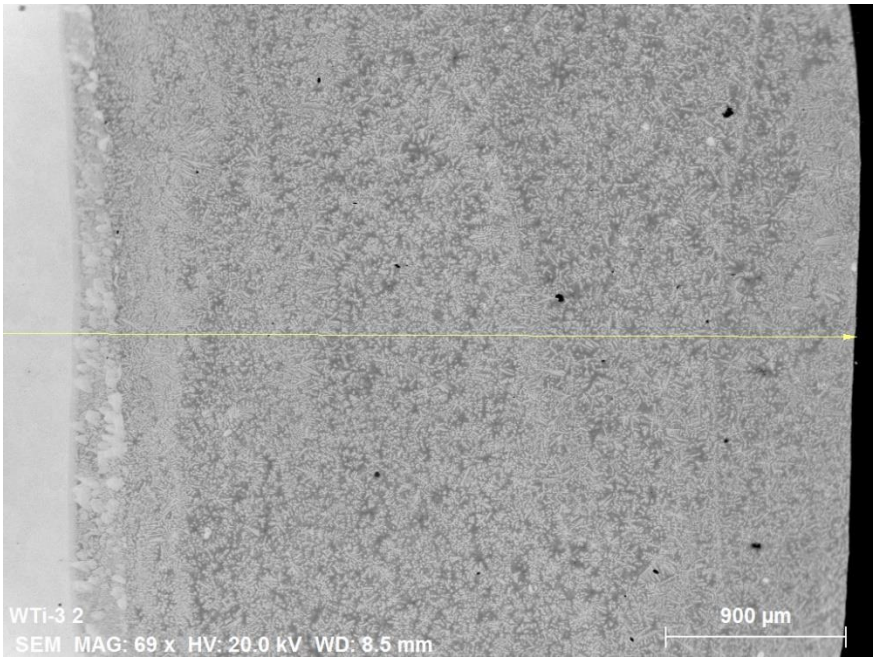

Figure 8.13: Location of linescan EDS analysis, Sample V [J. Matějíček, IPP]

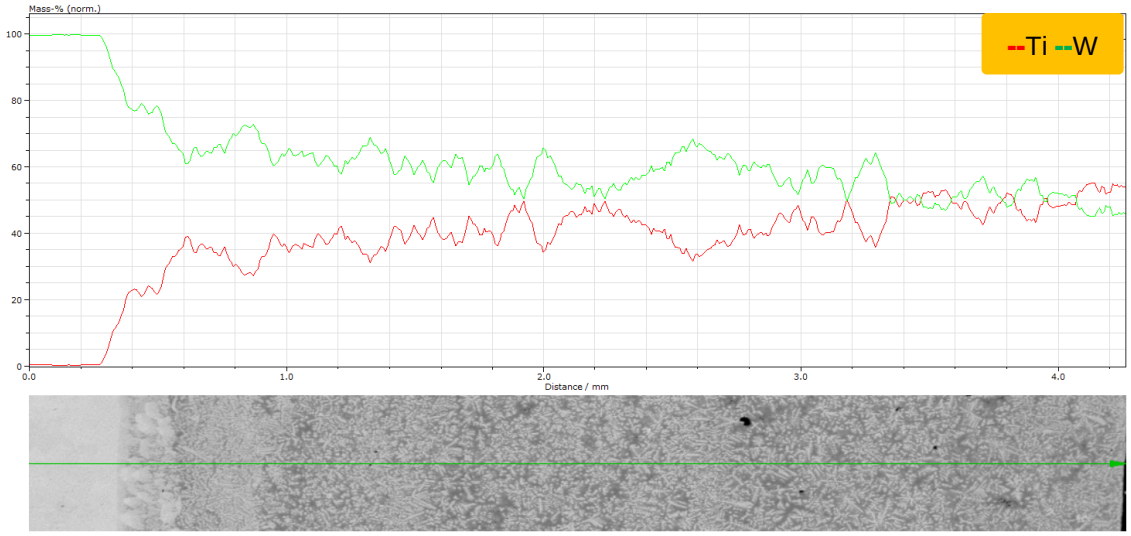

Figure 8.14: Linescan EDS analysis, Sample V [J. Matějíček, IPP]

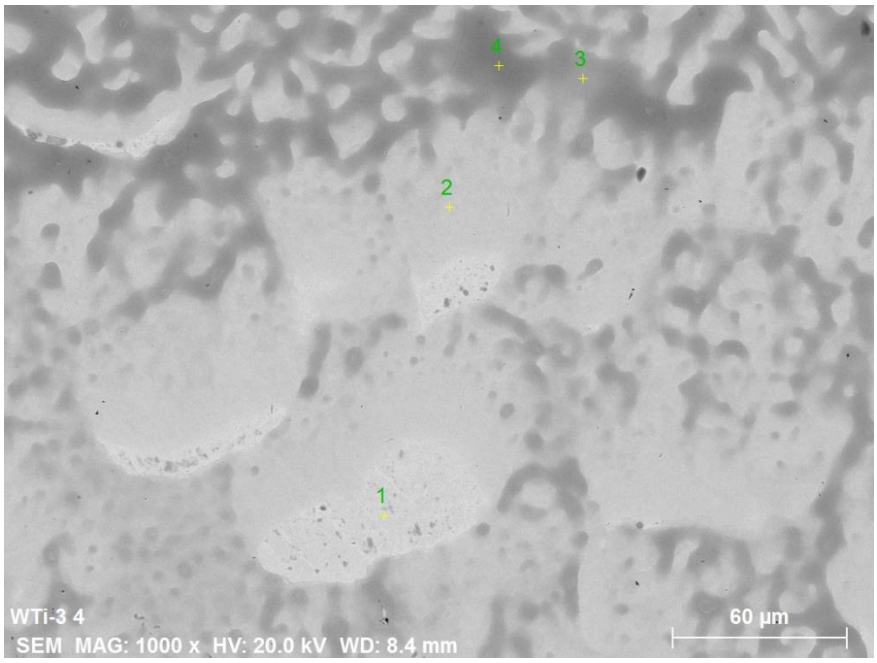

Figure 8.15: Locations of discrete EDS analysis, Sample V [J. Matějíček, IPP]

Discrete EDS analysis was performed in four points, marked in Figure 8.15 above, ranging from the most tungsten-rich to the most titanium-rich. The location in the sample is in the innermost layer, and corresponds to the area of Figure 8.10. The results are presented in Table 8.6 below:

Table 8.6: Results of discrete EDS analysis, Sample V

Location [-]	Conc. of Oxygen [wt.%]	Conc. of Titanium [wt.%]	Conc. of Tungsten [wt.%]
1	1.5	0.7	97.7
2	1.1	14.5	84.4
3	0.0	46.3	53.7
4	6.1	60.7	33.2

The results for this innermost layer show that in the most tungsten-rich area, the concentration of tungsten is 97.7 wt. % of tungsten, while in the most titanium-rich area, the concentration of titanium is 60.7 wt. % titanium. The presence of oxygen suggests imperfect shielding during the deposition process but is at an acceptable level.

Overall, the deposition of Sample V was relatively successful. Continual gradation, albeit slight, was achieved in the material, and as such it can be called a graded material. No discrete interfaces between layers are immediately recognisable, and as such the material should theoretically perform well under thermal stress. The bonding between the substrate and the first layer is satisfactory. The heat used for the deposition was however seemingly too high, resulting in the damage to the substrate material, and intense mixing of layers. This may have been caused in part by the initial bending deformation of the substrate, which resulted in the reduction of the area of thermal contact between the substrate and the copper heatsink below.

8.6 Sample VI

Sample VI was deposited on a recycled substrate (D). The substrate was used in a prior deposition which failed shortly into the deposition of the first layer due to problems with feeding the filler material. The remains of this deposition were mechanically removed. During the removal, the substrate was damaged in one corner (visible in Figure 8.16). No other visible damage or deformation existed on the substrate prior to the deposition.

Sample VI was intended as an optimisation of the relatively successful Sample V. The parameters for the first layer were kept constant, as were the parameters for preheating, which proved successful in Sample V. The substrate was fastened down more firmly by clamps, which were moved slightly towards the centre of the sample from the corners, to prevent the deformation of the sample and subsequent overheating. The position of the clamps was however still limited by the potential damage caused by the plasma. Sample VI was intended to be graded in six layers from pure tungsten to pure titanium, and was deposited with parameters as per Table 8.7:

Table 8.7: Sample VI - deposition parameters

Sample *VI*	FILLER		CURRENT			TORCH MOTION				
Substrate *D*	Powder ratio	Feed rate	Current high	Current low	Current equiv.	Travel speed	Osc. range	Osc. speed	Stop pos.	Stop neg.
Layer	[wt.%W]	[-]	[A]	[A]	[A]	[mm.s^{-1}]	[mm]	[mm.s^{-1}]	[s]	[s]
PH	N/A	N/A	192	125	158.5	2.0	16	16	0.2	0.2
1	100	6	192	125	158.5	1.0	18	16	0.2	0.2
2	85	8	192	125	158.5	1.0	18	16	0.2	0.2
3	70	8	200	133	166.5	1.0	18	16	0.2	0.2
4	50	8	200	133	166.5	1.0	16	16	0.2	0.2
5	30	8	200	133	166.5	1.0	16	16	0.2	0.2
6	0	8	175	112	143.5	1.0	16	16	0.2	0.2

The substrate was held down by clamps in the corners. Preheating was performed as in the case of Sample V. During the deposition of the first layer, it was immediately clear that filler material was practically not being delivered. To counter this, the flow of the carrier gas was increased for the second layer, as was the feed rate. However, the deposition of the first layer served practically only as a second preheat pass. Further layers were deposited using the same filler feed rate. After the second layer, the currents were increased as the filler material was seemingly not melting sufficiently. This was changed for the deposition of the last layer, which was of pure titanium, for reasons described above in respect to Sample V. A photograph of Substrate D with Sample VI deposited is shown below in Figure 8.16:

Figure 8.16: Photograph of substrate D with deposited Sample VI

From visual inspection, it is clear that the amount of filler material delivered was inadequate, as the sample is significantly lower (in terms of height) than Sample V, also composed of six layers, despite similar filler feed rates. Furthermore, there is an evident accumulation of material at the extremes of the oscillation range, despite the reduction of stop-times by half. Like in the case of Sample V, there is filler material in powder form on one side of the sample. In this case this is caused by the fact that the arc was terminated before the filler material feed, due to manual control, resulting in the deposition of unmolten filler into the solidifying melt pool. Oxidation is visible at the edges of the deposition, indicating imperfect shielding.

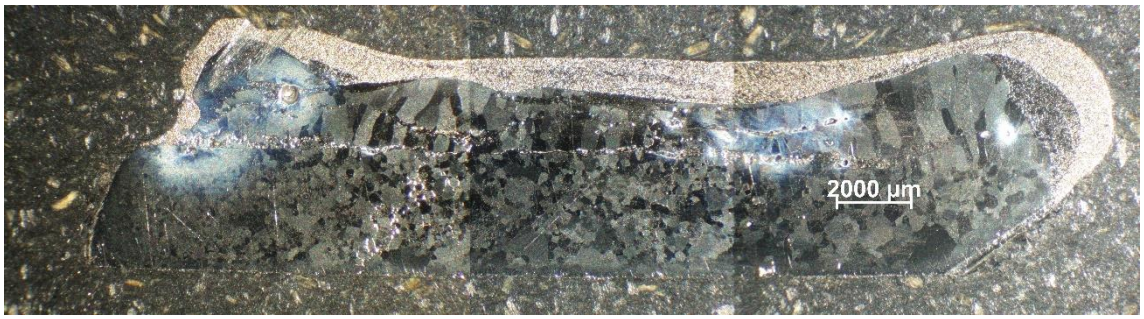

Figure 8.17: Macroscopic photograph of Sample VI cross-section

The macroscopic image above distinctly shows three layers; the middle layer is most profound in the top right corner. It is clear, based on the similarity of the structure of the first layer to the substrate material, that the inner distinct layer is composed practically only of pure tungsten. This seems to indicate that titanium was

not being delivered during the deposition of the first layers. Due to the increased current, it is also possible that some titanium may have evaporated prior to deposition.

The crack visible half-way through the height of the sample does not seem to fully respect the original interface between the substrate and the first layer. This suggests that the substrate and the first layer were perhaps in fact fully bonded (this is evident in the right section of the image) and the crack was formed later. The fact that material from the outer layer visibly enters the crack (seen on the left side of the image) suggests that the crack was formed during the deposition of the final layers, possibly due to stress induced by thermal cycling.

The sharp interface between the layers suggests that titanium was in fact not delivered at all until a certain point in the deposition of the final layers, when a blockage in the feeding system could have been released – this is however only speculation.

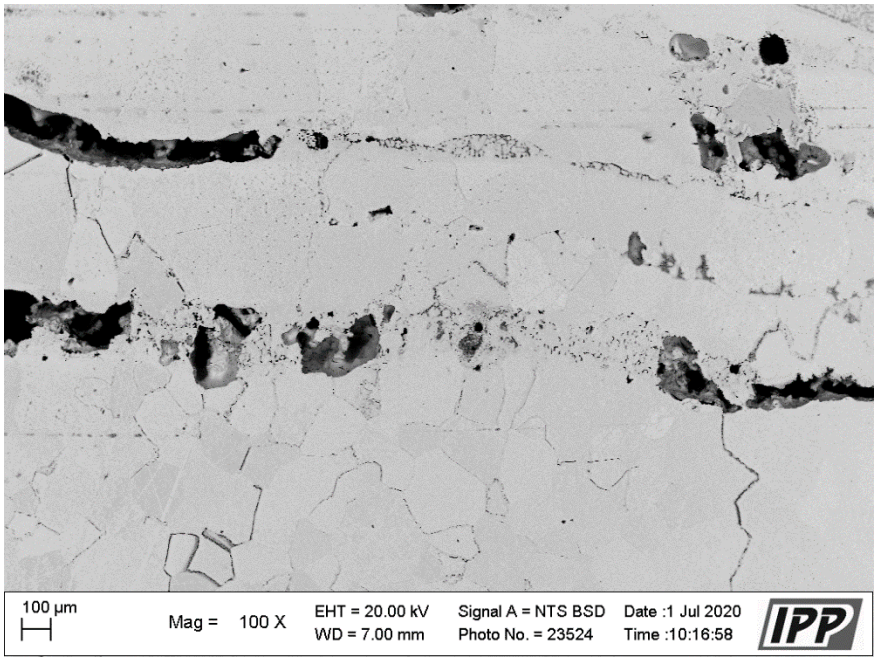

Figure 8.18: SEM photograph, Sample VI (substrate and first layer I/F, centre) [J. Matějíček, IPP]

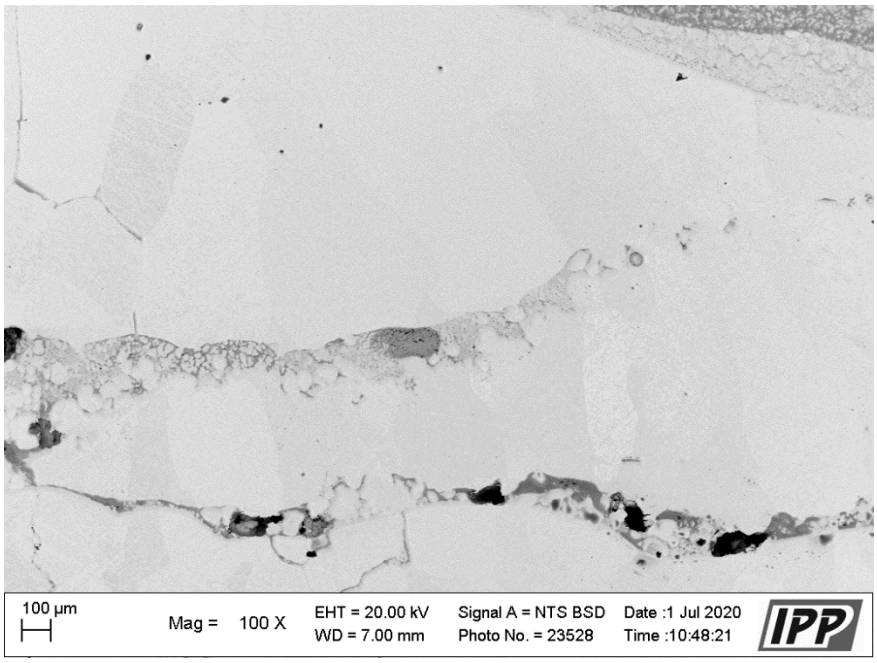

Figure 8.19: SEM photograph, Sample VI (substrate and first layer I/F, right side) [J. Matějíček, IPP]

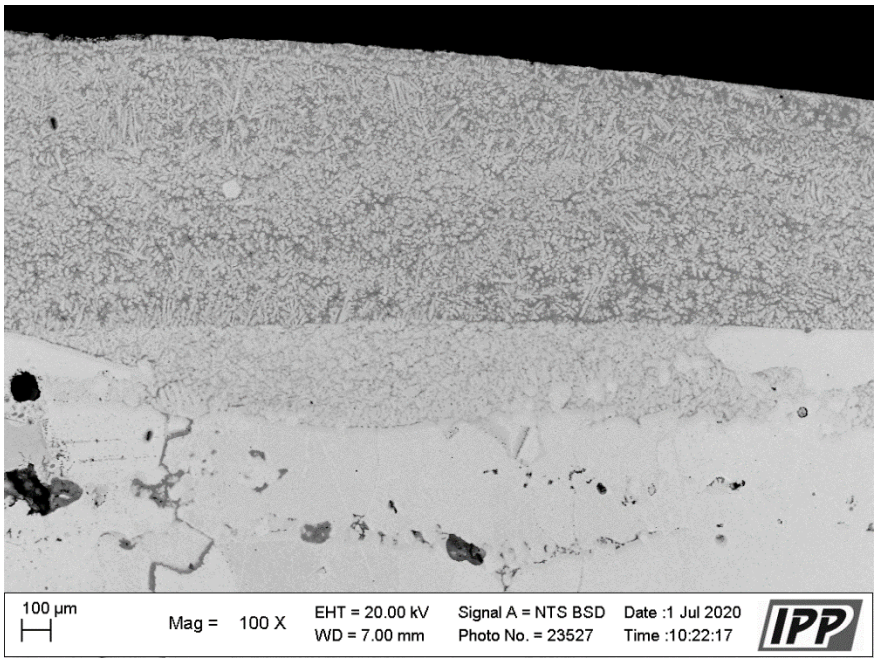

Figure 8.20: SEM photograph, Sample VI (outer layers, surface, centre) [J. Matějíček, IPP]

The SEM images distinctly show the three layers described above and confirm that the visible cracks do not follow the interface between the substrate and the first layer. The cracks do in fact seem to connect pre-existing pores, which may be the result of the evaporation of titanium, mentioned above. Furthermore, the fact

that the first layer is composed of pure tungsten is confirmed by the visibly similar structure of the grains between the substrate and the first layer.

The fact that the grains have grown to considerable size in the first layer suggests significant thermal inertia during cooling. This may point to the fact that thermal conductivity was reduced by the crack that formed, slowing down the cooling of the substrate after the final depositions. In contrast, the fact that a sharp interface exists between layers suggests that the inner layer was not melted during the deposition of the final layers, which would indicate that thermal conductivity was in fact sufficient to disperse heat into the heat sinks, and prevent the inner layer from melting, despite an increase in the currents. In the outer layer, dendritic-like structures similar to those found in Sample V are visible, and probably formed through diffusion during the solidification of the outer layer.

EDS was performed on Sample VI continuously across the entire height of the sample, over a straight line, shown in Figure 8.21, in the centre of the sample, connecting the substrate and the surface of the sample.

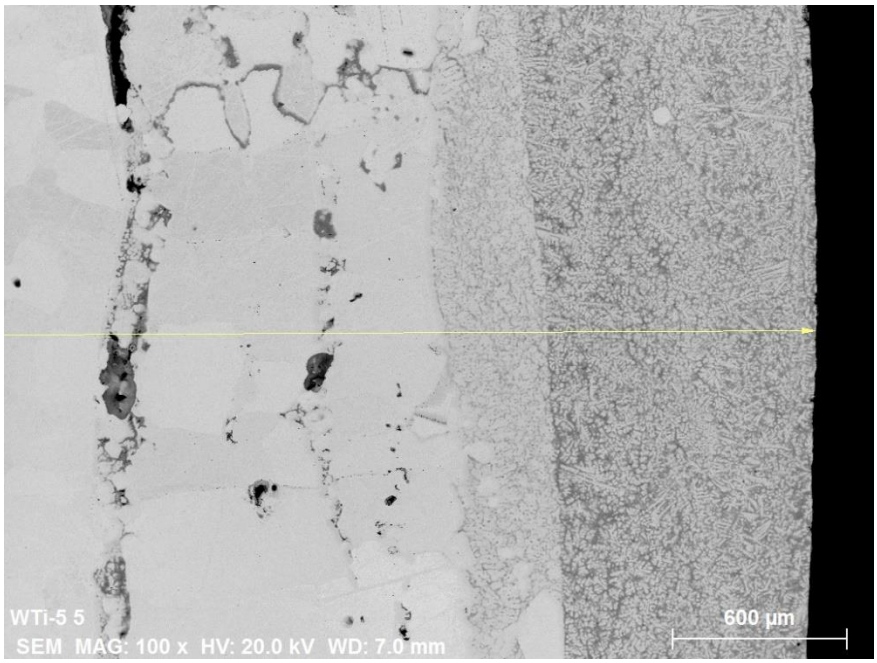

Figure 8.21: Location of linescan EDS analysis, Sample VI [J. Matějíček, IPP]

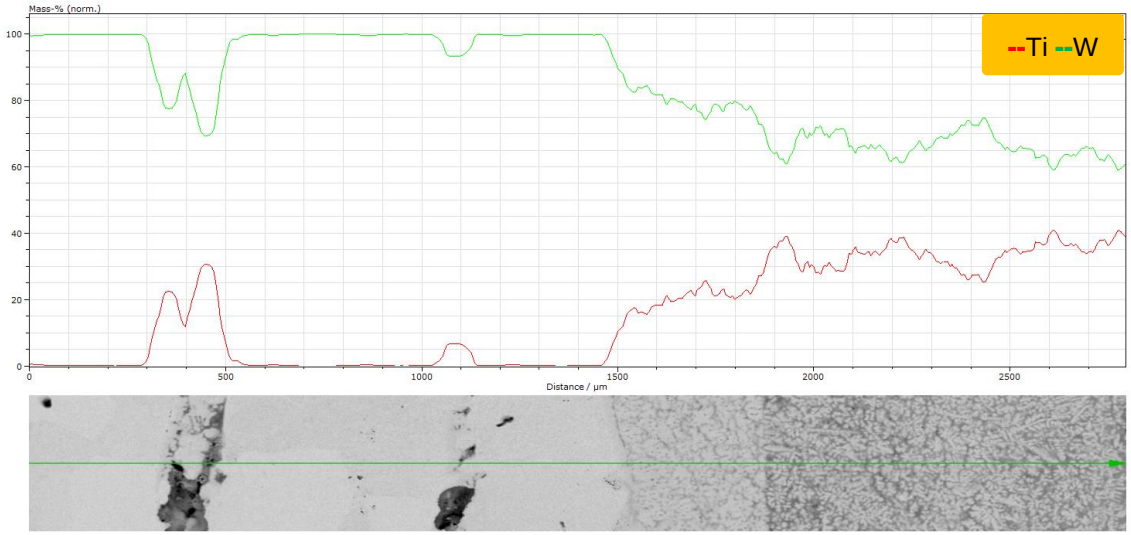

Figure 8.22: Linescan EDS analysis, Sample VI [J. Matějíček, IPP]

The results confirm the statements made above: The inner layer contains pure tungsten only, while titanium is only present in the central and outer layers, between which a titanium peak is visible. The central and outer layers contain a mixture of Ti-richer and W-richer phases. The material can be described as slightly graded from the interface between the inner and central layer. The EDS also confirms the presence of titanium in the visible crack. Discrete EDS was not performed on this sample.

Overall, it seems that the deposition of Sample VI was significantly impaired by problems with feeding the titanium filler material. While limited gradation is recognizable in the outer layers, the inner layer is composed of pure tungsten. The bonding between the pure tungsten layer and the substrate is however very good, possibly as a result of preheating made *de facto* in two passes. The substrate does not show signs of stress induced damage, suggesting that the increased grip, resulting in better thermal contact with the heatsink, did indeed alleviate this problem, present in Sample V.

8.7 Sample VII

Sample VII was the final experimental deposition. It was deposited on Substrate E. The first, pure tungsten layer was omitted as opposed to previous samples, and a layer of 85 wt. % tungsten to 15 wt. % titanium was deposited

directly on the substrate, to test the bonding of a layer containing titanium to the tungsten substrate. In this sample, parameters were optimised *ad hoc* within a limited range to attempt a continuously graded structure with optimal deposition parameters. The feed rate was increased significantly compared to previous samples, to try and alleviate the persistent problems with feeding the filler materials. Sample VII was deposited in five layers with parameters as per Table 8.8:

Table 8.8: Sample VII - deposition parameters

Sample *VII*	FILLER		CURRENT			TORCH MOTION				
Substrate *E*	Powder ratio	Feed rate	Current high	Current low	Current equiv.	Travel speed	Osc. range	Osc. speed	Stop pos.	Stop neg.
Layer	[wt.%W]	[-]	[A]	[A]	[A]	[mm.s^{-1}]	[mm]	[mm.s^{-1}]	[s]	[s]
PH	N/A	N/A	192	125	158.5	2.0	18	16	0.2	0.2
1	85	17	192	125	158.5	1.0	18	16	0.2	0.2
2	70	17	188	125	156.5	1.0	16	16	0.2	0.2
3	50	17	153	125	139.0	1.0	16	16	0.2	0.2
4	30	17	145	112	128.5	1.0	14	16	0.2	0.2
5	0	17	124	92	108.0	1.0	14	16	0.2	0.2

The substrate was held down by clamps in the corners. The preheating pass was realised with the same parameters as in the previous cases, and the current was kept the same for the deposition of the first layer. During the deposition, the filler material was melting sufficiently, and the surface of the substrate seemed to melt sufficiently as well. The current however seemed too high, melting large portions of previous layers, and was gradually reduced as the ratio of titanium was increased. Some oxidation occurred during the deposition of the first and second layers. In multiple layers, towards the end of the pass, filler material was deposited in powder form into an existing melt pool. This was once again due to the way in which the machine was manually controlled, where the arc was terminated before the feed of the filler material. A photograph of Substrate E with Sample VII deposited is shown below in Figure 8.23:

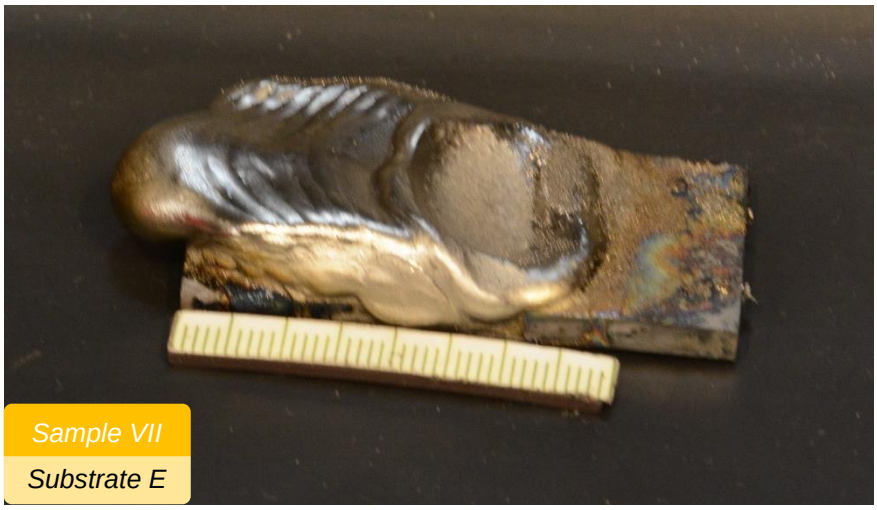

Figure 8.23: Photograph of substrate E with deposited Sample VII

From the visual inspection of the sample, the oxidation of the first layer on the substrate surface is immediately visible, as is the dusted filler material on the right side of the photograph. The results of the dynamic effects of the plasma are also visible on the right side, where multiple layers were melted and spread on the substrate. The portion of the sample towards the left of the photograph however shows desirable structure, characteristic of cladding processes, showing even, consistent deposition.

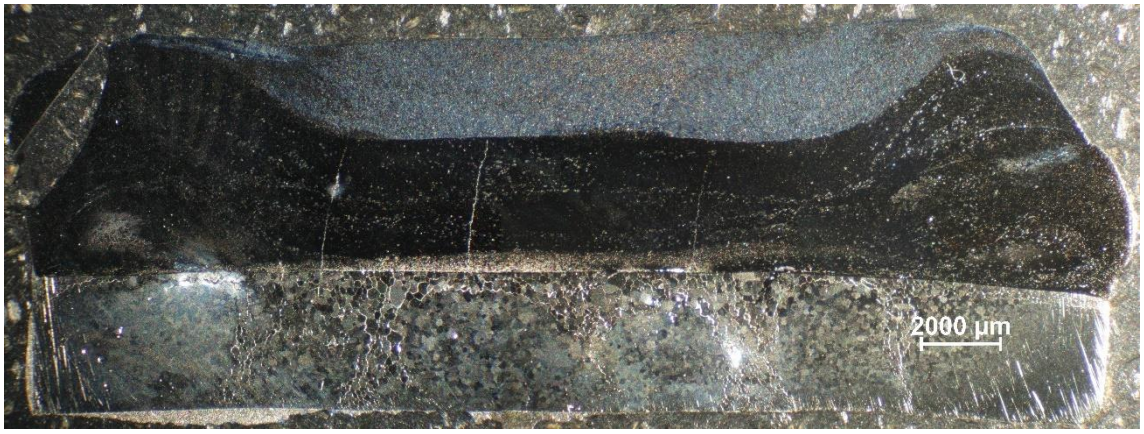

Figure 8.24: Macroscopic photograph of Sample VII cross-section

The macroscopic image above clearly shows three distinct layers, evidencing successful gradation. The structures of the layers show that the filler material was fully melted, and the layers are relatively homogenous. The edge of the substrate is clearly visible, but the substrate is evidently deformed and damaged. Cracks are also visible in the innermost and central layer, indicating that significant heat acted on

the material. This can once again be explained by the bending of a substrate fastened down by clamps in the corners, which greatly reduced the area of thermal contact with the heatsinks, adversely affecting heat dissipation.

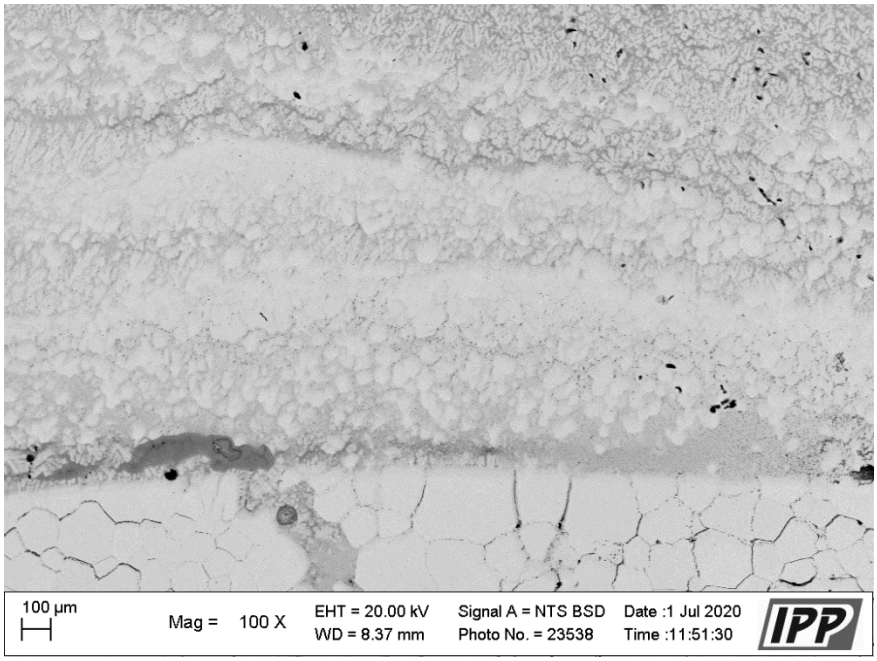

Figure 8.25: SEM photograph, Sample VII (substrate and first layer I/F, centre) [J. Matějíček, IPP]

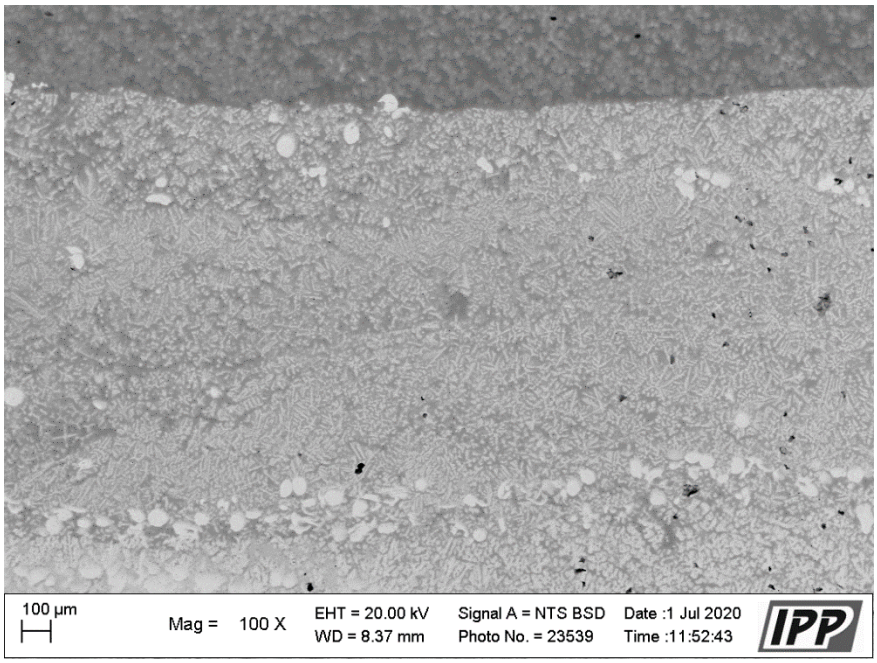

Figure 8.26: SEM photograph, Sample VII (central layers, centre) [J. Matějíček, IPP]

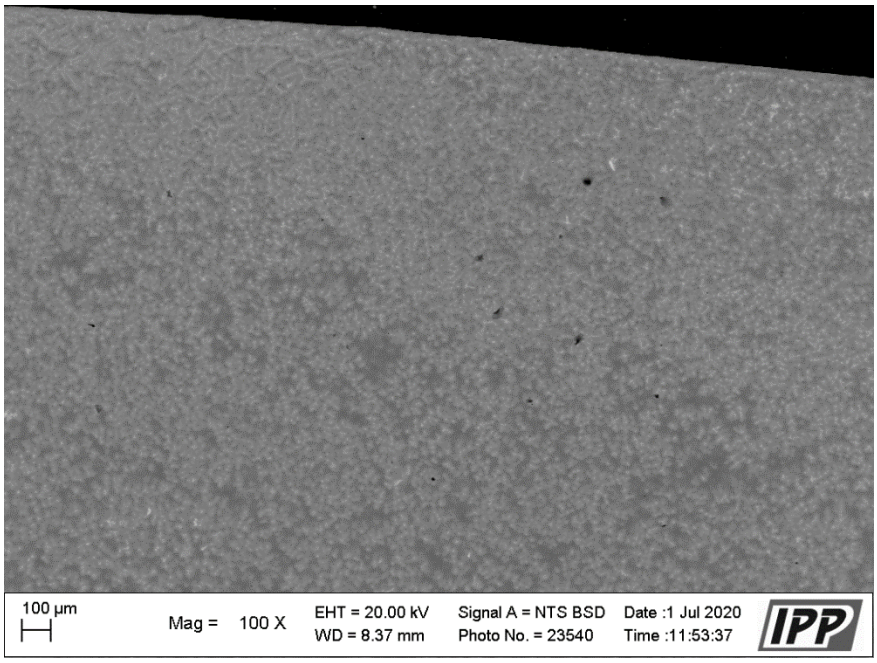

Figure 8.27: SEM photograph, Sample VII (outer layers, surface, centre) [J. Matějíček, IPP]

The SEM photographs above show distinct layering from tungsten-rich towards titanium-rich layers. The gradation is relatively smooth, apart from a significant transition, visible clearly in the top part of Figure 8.26. This may have been caused by a sporadic change in the filler powder feed and the fact that the decreasing current was not sufficient to re-melt a depth of the relatively tungsten-rich material, as the titanium-rich layers were deposited. The damage to the substrate material is clearly visible in Figure 8.25. The crack visible in the substrate continues along the interface of the substrate and the first layer. A region of poor bonding along the substrate-first layer interface is visible in detail in Figure 8.28 below:

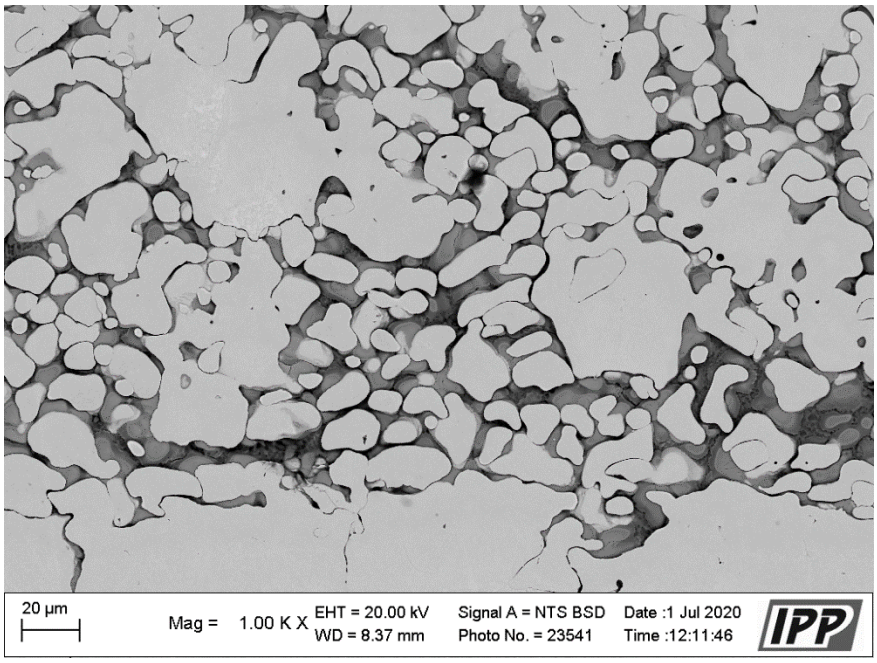

Figure 8.28: SEM photograph, Sample VII (detail, substrate and first layer I/F, right side) [J. Matějíček, IPP]

The following series of SEM photographs show the transition from the innermost layers to the surface in detail. The transition from the tungsten-rich first layer to the titanium-rich fifth layer is clearly visible from the backscattered electron detection. In all layers, titanium and tungsten are not present in pure form, but once again, a mixture Ti-richer and W-richer phases forms the majority of the volume. The visible structures show diffusion interfaces and were likely formed by diffusion in the cooling liquid. Sharp interfaces can be seen in Figure 8.29, showing localized imperfect bonding.

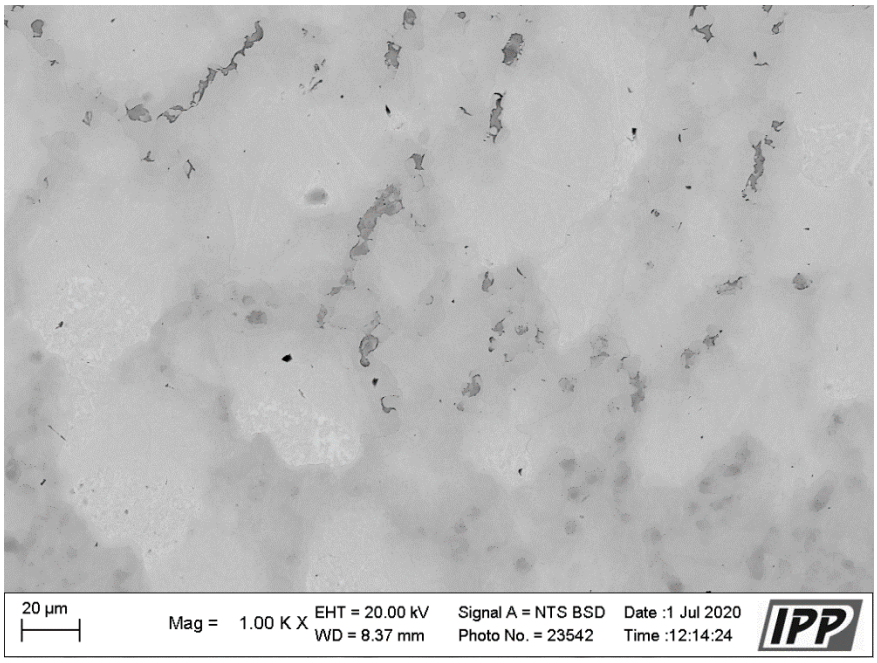

Figure 8.29: SEM photograph, Sample VII (detail, first and second layer, centre) [J. Matějíček, IPP]

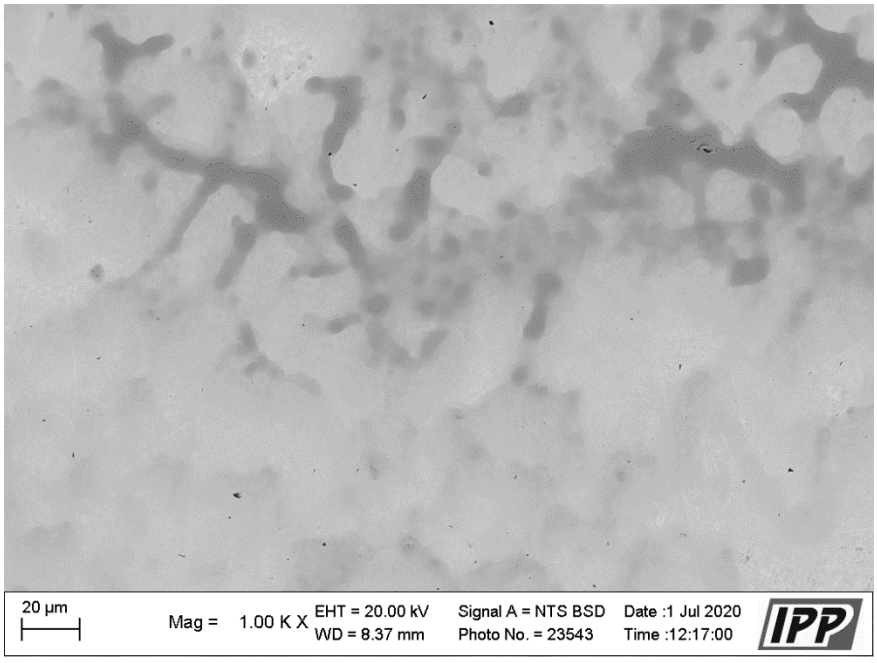

Figure 8.30: SEM photograph, Sample VII (detail, second and third layer, centre) [J. Matějíček, IPP]

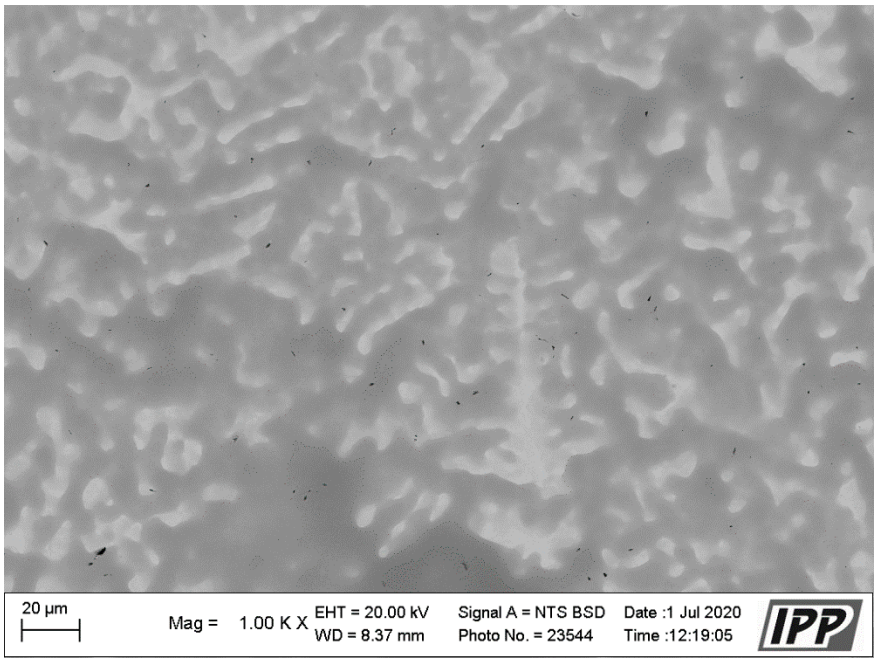

Figure 8.31: SEM photograph, Sample VII (detail, fourth layer, centre) [J. Matějíček, IPP]

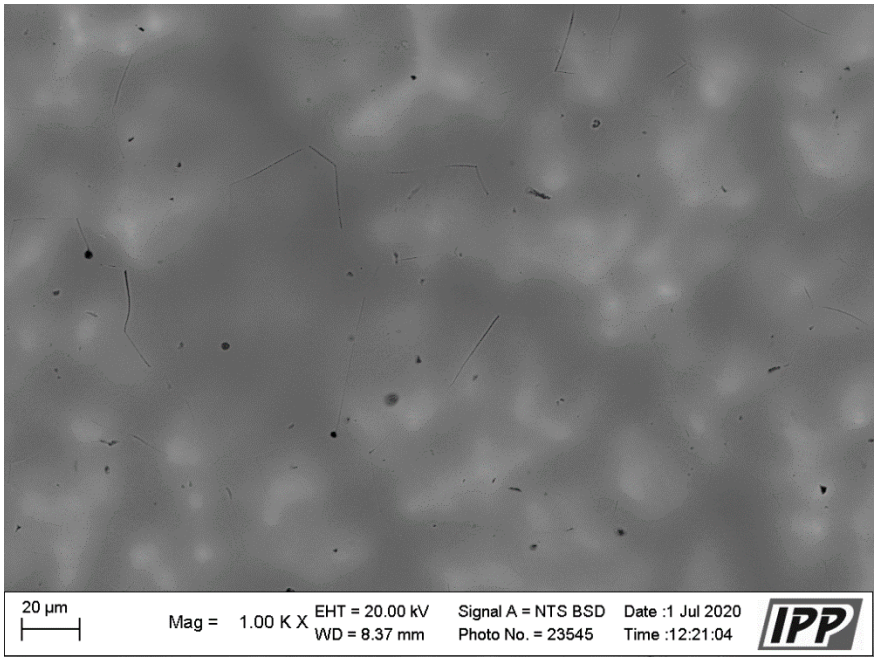

Figure 8.32: SEM photograph, Sample VII (detail, fifth layer, centre) [J. Matějíček, IPP]

EDS was performed on Sample VII; in discrete locations, and continuously across the height of the sample. The continuous analysis was performed over a straight line, shown in Figure 8.33, in the centre of the sample, connecting the substrate and the surface of the sample.

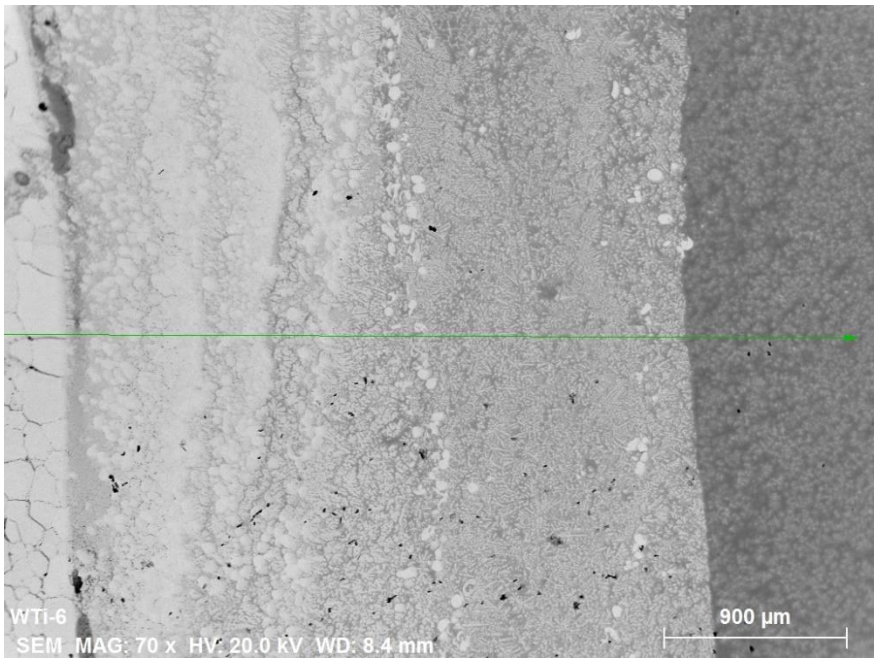

Figure 8.33: Location of linescan EDS analysis, Sample VII [J. Matějíček, IPP]

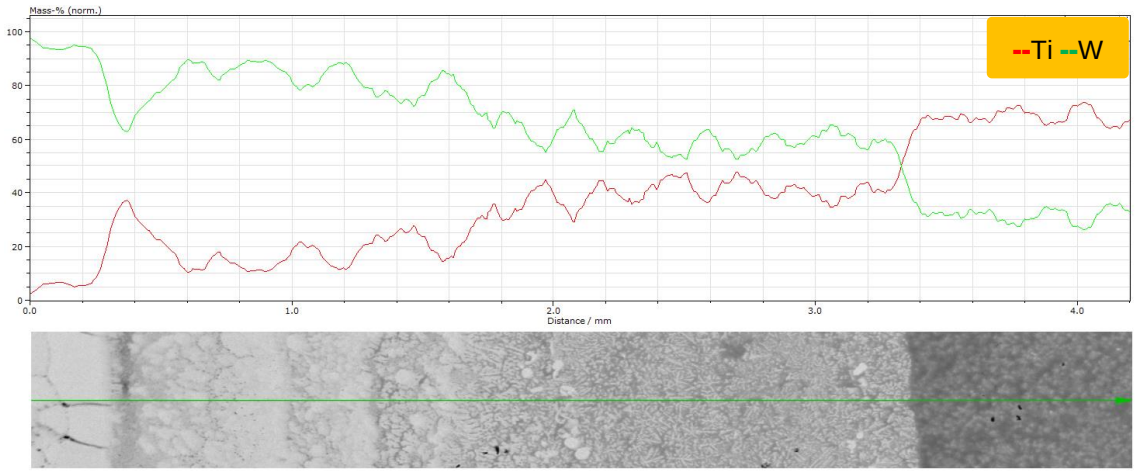

Figure 8.34: Figure 8.22: Linescan EDS analysis, Sample VII [J. Matějíček, IPP]

The results clearly show the graded structure, which was achieved across the entire height of the sample. The titanium peak seen immediately on the substrate is likely the result of liquid titanium filling a forming crack as the tungsten already solidified. Two more significant transitions are visible, where in the second transition, titanium begins to constitute the majority of the material. This second transition is significant enough to be clearly visible not only in the SEM images, but also in the macroscopic image.

Discrete EDS analysis was performed in three points, marked in Figure 8.35 below, ranging from the most tungsten-rich to the most titanium-rich. The location in the sample is in the outermost layer, and corresponds to the area of Figure 8.32. The results are presented in Table 8.9.

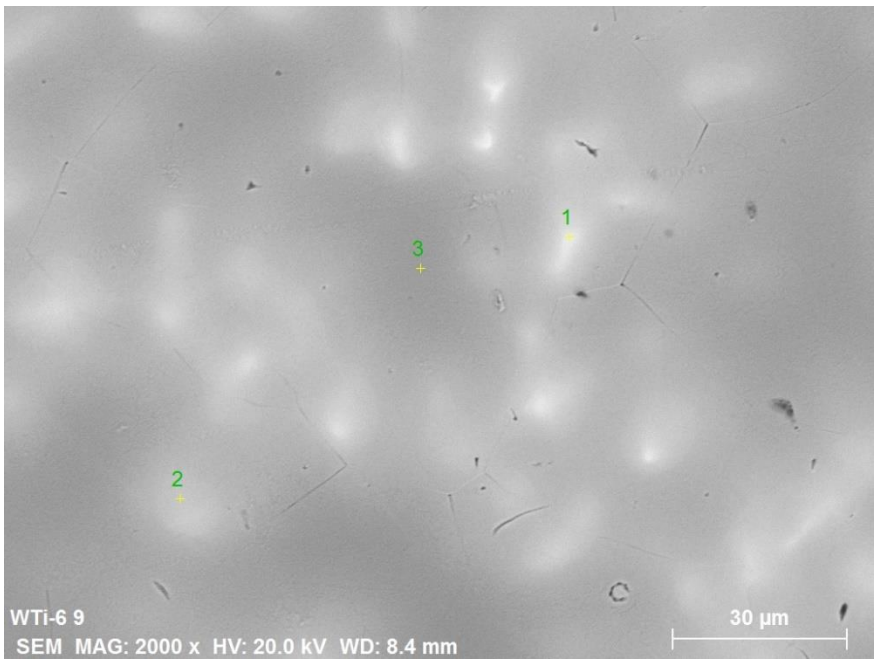

Figure 8.35: Locations of discrete EDS analysis, Sample VII [J. Matějíček, IPP]

Table 8.9: Results of discrete EDS analysis, Sample VII

Location [-]	Conc. of Oxygen [wt.%]	Conc. of Titanium [wt.%]	Conc. of Tungsten [wt.%]
1	2.9	36.4	60.7
2	3.9	54.2	41.9
3	3.9	70.7	25.4

The results show that in the most tungsten-rich area of the outermost layer, the concentration of tungsten is 60.7 wt. % of tungsten, while in the most titanium-rich area of the outermost layer, the concentration of titanium is 70.7 wt. % titanium. The presence of oxygen suggests imperfect shielding during the deposition.

XRD analysis was performed on Sample VII, to determine the phase composition of the layers. The diffraction spectrum was detected in three points in three distinct layers. The first spectrum was detected in the centre of the outermost

layer, near the surface (corresponding to Figure 8.27), the second in the central layer (corresponding to Figure 8.26) and the third in the innermost layer (corresponding to Figure 8.25), near the interface with the substrate. The detected spectra are shown below, in blue:

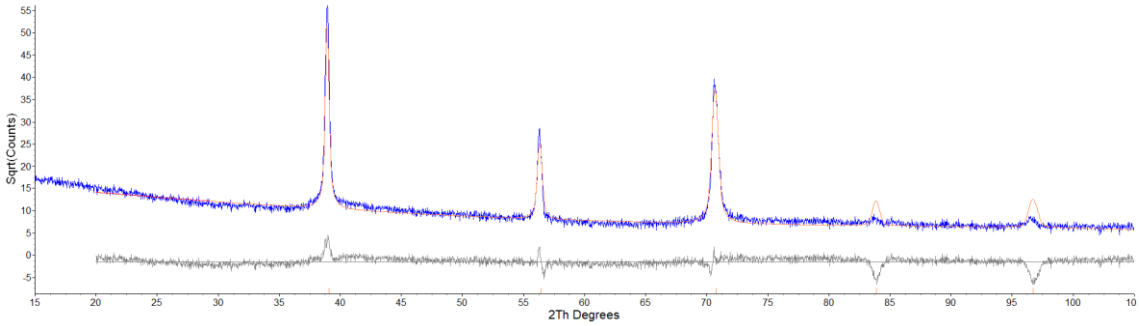

Figure 8.36: XRD spectrum, Sample VII (detected in outer layer, centre) [J. Matějíček, IPP]

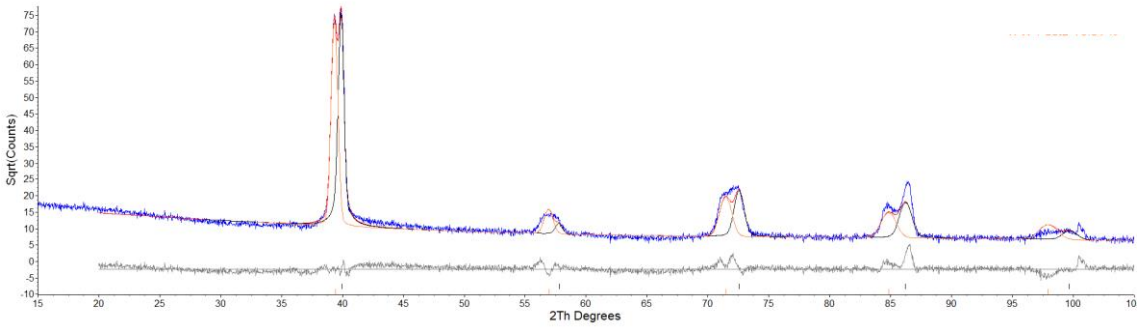

Figure 8.37: XRD spectrum, Sample VII (detected in central layer, centre) [J. Matějíček, IPP]

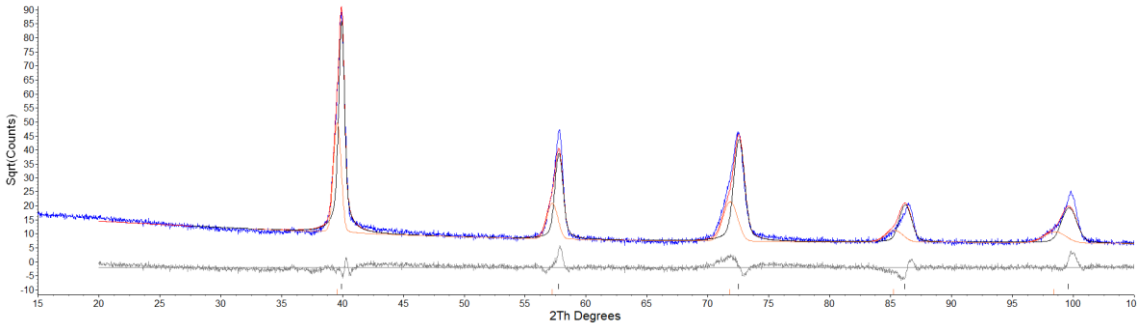

Figure 8.38: XRD spectrum, Sample VII (detected in inner layer, centre) [J. Matějíček, IPP]

The spectra were best fitted by the Rietveld method with pre-defined spectra of pure β-phase titanium (orange) and a 50Ti-50W alloy (black), with permitted modification of the lattice parameters, corresponding to variation of the

composition. The modification of the 50Ti-50W spectrum is as close as possible, given the limited availability of data on Ti-W alloys – the realistic composition of the structure is approximated by Vegard's law in Appendix B. The modification in the β-phase titanium spectrum corresponds to β-phase titanium enriched with tungsten (W content approximated in Appendix B). Calculated concentrations of the approximation phases in each layer, with their calculated lattice parameters, are also given in Appendix B.

Titanium was expected in the α-phase at room temperature according to the equilibrium phase diagram. The fact that the spectrum was matched with β-phase titanium would indicate that the cooling and solidification in this process was faster than what would correspond to equilibrium conditions, and the titanium remained in the β-phase. The results of the XRD analysis of Sample VII are likely true for other samples as well, given the similarity of the cooling process, and the existence of the β-phase is thus probable in the other samples. No explicit conclusions can however be drawn from this, as the spectrum was modified, and no further research was carried out.

Sample VII was overall the most successful deposition. Gradation was achieved from the substrate all the way to the surface, with titanium becoming the dominant constituent in the outer layers. The desired pure-titanium top layer was however not achieved. Except for the relatively abrupt transition from tungsten-rich to titanium-rich composition at ~3mm from the substrate, the gradation was progressive and continuous, indicating beneficial properties in terms of interlayer stress. The bonding of the layers to the substrate material seems to be adequate in most parts, visible damage is however present at the interface in certain locations. The structure in most layers is relatively homogenous, indicating sufficient melting and mixing of the filler materials. Visible damage to the substrate was likely caused by the deformation of the substrate due to inadequate fastening. The fact that diffraction spectra in the sample were matched with β-phase titanium spectra is indicative of the fact that the titanium was in fact stabilised in the β-phase.

9 Conclusion

Based on the performed research, it can be stated that while nuclear fusion is theoretically a viable energetic source with few downsides, the technological challenges to be overcome are vast. A particular problem is that of PFCs and PFMs, which must endure extreme conditions and significant stresses, and the design of which is limited by the constraints of the conventional materials available today. A possible direction of research to alleviate such problems is the use of FGMs, which can be manufactured by several more or less feasible methods. The PTA technology, which was used as the base technology for the experiment, offers multiple benefits in the context of manufacturing FGMs for PFCs. The combination of titanium and tungsten, which is a result of the limited prior research made in this area, seems to be a viable option for such an application. The results of the theoretical part form a contextual background for the realisation of the experimental part.

The aim of the experimental part was the fabrication of an FGM, satisfactorily bonded to a tungsten substrate, continuously and evenly layered from pure tungsten to pure titanium, without significant defects. A total of seven samples were deposited on five substrates and were subjected to inspection by various methods.

As a general conclusion to the experimental part of the thesis, it can be stated that this aim was achieved to significant extent. A fully or partially graded structure was achieved on multiple samples, even though a full gradation range from pure tungsten to pure titanium was not achieved. Furthermore, the depositions were, on some samples, sufficiently bonded to the substrate, contained relatively few defects, and were layered evenly and continuously.

The deposition of Sample VII was overall the most successful, where gradation was achieved throughout the entire height of the sample. The gradation was continuous, except for two distinctly visible interfaces where discrete transitions occurred. The structure of the layers was homogenous, evidencing satisfactory melting and mixing of the layers. This implies that FGMs manufactured by the PTA method should offer superior properties in terms of thermal stress, as opposed to other manufacturing methods. Despite occasional visible cracks in the

substrate and deposited layers, which were likely caused by improper thermal contact with heatsinks, the overall quality of the deposition is good throughout most of the volume. Similar results were also achieved in Sample V.

Process parameters were optimised, with Samples I – III specifically deposited to establish process parameters. However, due to the complicated dynamics of the PTA process and the significant number of variables and unknown properties, no explicit causal relationship could be established between the parameters and the resulting deposition. The increase in currents resulted in the increased melting of the filler and substrate materials, but the extent of this correlation was limited by the multitude of other variables in the process.

A problem that manifested itself repeatedly throughout the experiment was the continual difficulty in feeding the filler materials in powder form. The feed rate was often significantly constrained, and at times, one filler powder was not being delivered at all. This presented an inconsistency and inaccuracy in the actual composition of the deposited filler material and made it difficult to make any conclusions directly related to the quantity of constituents in the deposited layers. The problems were caused by the inappropriate shapes and consequent rheological properties of both filler powders, to which the feeding system of the PTA machine is highly sensitive. To alleviate such problems, powders of appropriate grain size, shape and consistence must be used in future experiments.

Overall, the suitability of the PTA method in the manufacturing of Ti-W FGMs was demonstrated to significant extent. It can be argued, given the resulting structure of the depositions, that FGMs manufactured in this way may surpass FGMs manufactured using other methods in multiple areas, namely in the bonding between layers and resulting thermal stress properties. The PTA method also offers significant productivity, making it suitable for the cladding of larger areas. A drawback in using the PTA method is the inherent dynamic nature of the process and resulting inconsistency. This can however be eliminated to a certain extent by repeated experimentation with a large number of depositions, resulting in a better understanding and description of the specific processes, and the establishment of

empirical relationships. This could not be achieved on the limited number of substrates available.

In terms of the actual applicability of the resulting materials in PFCs, significant research, beyond the scope of this work, is required to determine the suitability of such a FGM. While the composition was determined by EDS in some locations and XRD analysis was carried out on a single sample, the actual structures that were formed – and most importantly – their properties with respect to applications in PFCs, would need to be experimentally determined and evaluated. To date, only very limited information is available on the properties of Ti-W alloys throughout the entire range of concentrations, especially with regard to their use as PFMs.

Based on the limited information available, the combination of titanium and tungsten does seem to possess certain beneficial properties that indicate the possibility of their use as PFMs. The use of FGMs in general is a highly perspective direction of research on PFM possibilities, as is the use of PTA technology in the manufacturing of such materials. As such, it is my sincere hope that the results achieved in this work may be indicative of possible future applications of titanium-tungsten FGMs in fusion reactors – the successful realisation of which may in itself be fundamental to the future well-being of humankind.

Bibliography

[1] ŘÍPA, Milan, Jan MLYNÁŘ, Vladimír WEINZETTL a František ŽÁČEK. *Řízená termojaderná fúze pro každého* [online]. 3. přepr. vydání. Praha: Ústav Fyziky Plazmatu AV ČR, 2011 [cit. 2020-05-04]. ISBN 80-902724-7-9. Available at: https://www.cez.cz/edee/content/file/vzdelavani/fuze_sceeen.pdf

[2] RUYS, Andrew. Functionally Graded Materials (FGM) and Their Production Methods. *AZO Materials* [online]. Manchester: AZoM, 2002 [cit. 2020-05-04]. Available at: https://www.azom.com/article.aspx?ArticleID=1592

[3] GIRKA, Igor, ed. *Nuclear Fusion: One Noble Goal and a Variety of Scientific and Technological Challenges* [online]. 1. vydání. IntechOpen, 2019 [cit. 2020-05-04]. ISBN 978-1-83962-115-4. Available at: https://www.intechopen.com/books/nuclear-fusion-one-noble-goal-and-a-variety-of-scientific-and-technological-challenges

[4] MCCRACKEN, Garry a Peter STOTT. *Fúze: Energie vesmíru*. 1. vydání. Praha: Mladá fronta, 2006. Kolumbus. ISBN 80-204-1453-3.

[5] HOMER, David a Michael BOWEN-JONES. *Physics Course Companion*. 2014 Edition. Oxford: Oxford University Press, 2014. ISBN 978-0-19-839213-2.

[6] EINSTEIN, Albert. Ist die Trägheit eines Körpers von seinem Energieinhalt abhängig?. *Annalen der Physik*. Bern, 1905, **1905** (323/13), 639-641. DOI: https://doi.org/10.1002/andp.19053231314.

[7] SCHUMACHER, Uwe. Status and problems of fusion reactor development. *Die Naturwissenschaften*. 2001, **2001** (88/3), 102-112. DOI: https://doi.org/10.1007/s001140100214.

[8] HABJANEC, Davor. Deuterium-Tritium fusion reaction. In: *Interesting energy facts: Nuclear fusion facts* [online]. 2010 [cit. 2020-05-05]. Available at: https://interestingenergyfacts.blogspot.com/2010/04/nuclear-fusion-facts.html

[9] KOTRÍK, Tomáš, Milan AFTANAS a Michael KOMM. Termonukleární fúze. *Fyzikální sekce - Matematicko-fyzikální fakulta - Univerzita Karlova* [online].

Praha [cit. 2020-05-05]. Available at: https://physics.mff.cuni.cz/kfpp/s4r/plazma/?p=6

[10] ENTLER, Slavomír a Jan MLYNÁŘ. *Spoutání Slunce* [online]. 1. vydání. Praha: Středisko společných činností AV ČR, v. v. i., 2016 [cit. 2020-05-06]. ISBN 2464-6245. Available at: http://www.vedakolemnas.cz/miranda2/export/sitesavcr/data.avcr.cz/academia/vedakolemnas/sys/galerie-download/vkn_50_web.pdf_1987196848.pdf

[11] ELIEZER, Shalom a Yaffa ELIEZER. *The Fourth State of Matter: An introduction to Plasma Science* [online]. Second Edition. Bristol and Philadelphia: Institute of Physics Publishing, 2001 [cit. 2020-08-15]. ISBN 0 7503 0740 4. Available at: https://www.researchgate.net/publication/247157205_S_Eliezer_and_Y_Eliezer_The_Fourth_State_of_Matter_Institute_of_Physics_Bristol_England_2001_2nd_updated_edition

[12] Fúze, to není jen vtip II: Čtvrté skupenství hmoty. *AtomInfo* [online]. 2013 [cit. 2020-07-15]. Available at: https://atominfo.cz/2013/12/fuze-to-neni-jen-vtip-ii-ctvrte-skupenstvi-hmoty/

[13] RUTHERFORD, Paul a Robert GOLDSTON. *Introduction to Plasma Physics*. 1. vydání. Bristol: Institute of Physics Publishing, 1995. ISBN 0 7503 0183.

[14] ENTLER, Slavomír. Jaderná Fúze - budoucnost energetiky. *Energetika*. 2015, **2015** (3), 136-142.

[15] TRAN, Minh Quang a Mitsuru KIKUCHI, ed., Karl LACKNER. *Fusion Physics*. 1. vydání. Vienna: IAEA Publishing, 2012. ISBN 978–92–0–130410–0.

[16] ITER PROJECT. The ITER Tokamak. *ITER.org* [online]. St Paul lez Durance, 2020 [cit. 2020-05-06]. Available at: https://www.iter.org/mach

[17] DOLAN, Thomas, ed. *Magnetic Fusion Technology* [online]. London: Springer, 2014 [cit. 2020-05-06]. ISBN 978-1-4471-5556-0. Available at: https://link.springer.com/book/10.1007/978-1-4471-5556-0#about

[18] NORAJITRA, Prachai. *Divertor Development for a Future Fusion Power Plant*. Karlsruhe, 2011. Disertační. Karlsruher Institut für Technologie. Vedoucí práce Prof. O. Kraft.

[19] COTRELL, G. A. A survey of plasma facing materials for fusion power plants. *MAterials Perspective*. 2013, **2006** (22/8), 869-880. DOI: https://doi.org/10.1179/174328406X111110.

[20] RUBELL, Marek. Fusion Neutrons: Tritium Breeding and Impact on Wall Materials and Components of Diagnostic Systems. *Journal of Fusion Energy*. 2019, **2019** (38), 315-329. DOI: https://doi.org/10.1007/s10894-018-0182-1.

[21] FEDERICI, G. et al. European DEMO design strategy and consequences for materials. *Nuclear Fusion*. 2017, **2017** (57/9). DOI: OI https://doi.org/10.1088/1741-4326/57/9/092002.

[22] AUBERT, J., G. AIELLO, N. JONQUERES, A. LI PUMA, A. MORIN a G. RAMPAL. *Report for TA WP12-DAS-02 – T03 - DEMO1 WCLL blanket concept design description*. European Fusion Development Agreement, 2013.

[23] WENNIGER, R. et al. The DEMO Wall Load Challenge. *Nuclear Fusion*. 2017, **2017** (57/4). DOI: https://doi.org/10.1088/1741-4326/aa4fb4.

[24] MATĚJÍČEK, Jiří. Materials for Fusion Applications. *Acta Polytechnica*. 2013, **2013** (53/2), 197-212.

[25] KHRIPUNOV, B. et al. Study of tungsten as a plasma-facing material for a fusion reactor. *Physics Procedia*. 2015, **2015** (71), 63-67. DOI: https://doi.org/10.1016/j.phpro.2015.08.313.

[26] NEU, R. Investigations on tungsten heavy alloys for use as plasma facing material. *Fusion Engineering and Design*. 2017, **2017** (124), 450-454. DOI: https://doi.org/10.1016/j.fusengdes.2017.01.043.

[27] NEU, R. Results on the use of tungsten heavy alloys in the divertor of ASDEX Upgrade. *Journal of Nuclear Materials*. 2018, **2018** (511), 567-573. DOI: https://doi.org/10.1016/j.jnucmat.2018.05.066.

[28] NAEBE, Minoo a Kamyar SHIRVANIMOGHADDAM. Functionally graded materials:: A review of fabrication and properties. *Applied Materials Today*. 2016, **2016** (5), 223-245.

[29] NIKBAKHT, S., S. KAMARIAN a M. SHAKERI. A review on optimization of composite structures Part II:: Functionally graded materials. *Composite Structures*. 2019, **2019** (214), 83-102.

[30] EL-GALY, Islam, Bassiouny SALEH a Mahmoud AHMED. Functionally graded materials classifcations and development trends from industrial point of view. *SN Applied Sciences*. **2019** (1). DOI: https://doi.org/10.1007/s42452-019-1413-4.

[31] GE, Chang-Chun. Development of functionally graded plasma-facing materials. *Journal of Nuclear Materials*. 2000, **2000** (283-287), 1116-1120. DOI: https://doi.org/10.1016/S0022-3115(00)00318-4.

[32] CHAUBEY, A. K. Fabrication and characterization of W-Cu functionally graded material by spark plasma sintering process. *Fusion Engineering and Design*. 2018, **2018** (135), 24-30.

[33] ANTOŠ, Jakub. *Plazmové navařování materiálů pro první stěnu fúzních reaktorů*. Praha, 2018. Master's thesis. Czech Technical University. Vedoucí práce Ing. Pavel Rohan, Ph. D.

[34] VÝLETOVÁ, Karolína. *Plazmové navařování wolframu na kovovou podložku*. Praha, 2019. Bachelor's thesis. Czech Technical University. Vedoucí práce Ing. Pavel Rohan, Ph. D.

[35] Melting temperatures of common metals and alloys. *The Engineering Toolbox* [online]. 2005 [cit. 2020-07-09]. Available at: https://www.engineeringtoolbox.com/melting-temperature-metals-d_860.html

[36] Thermal conductivity of common metals, metallic elements and Alloys. *The Engineering Toolbox* [online]. 2005 [cit. 2020-07-09]. Available at: https://www.engineeringtoolbox.com/thermal-conductivity-metals-d_858.html

[37] LARIONOV, V., V. VARLACHEV a Xu SHUPENG. Accumulation of hydrogen in titanium exposed toneutron irradiation. *International Journal of Hydrogen Energy*. 2020, **2020** (45), 15294-15301. DOI: https://doi.org/10.1016/j.ijhydene.2020.04.014.

[38] ISHIDA, T. *Study of the radiation damage effect on Titanium metastable beta alloy by high intensity proton beam*. 2018, **2018** (15), 169-174. DOI: https://doi.org/10.1016/j.nme.2018.04.006.

[39] WEBBER, T. a J. AKTAA. Numerical assessment of functionally graded tungsten/steel joints for divertor applications. *Fusion Engineering and Design*. 2011, **2011** (86), 220-226. DOI: https://doi.org/10.1016/j.fusengdes.2010.12.084.

[40] MATĚJÍČEK, Jiří. Overview of processing technologies for tungsten-steel composites and FGMs for fusion applications. *Nukleonika*. 2015, **2015** (60/2), 267-273. DOI: https://doi.org/10.1515/nuka-2015-0049.

[41] Titanium: Chemical Element. *Encyclopedia Brittanica* [online]. Chicago, 2009 [cit. 2020-07-25]. Available at: https://www.britannica.com/science/titanium

[42] Titanium (Ti) - The Different Properties and Applications. *AZO Materials* [online]. 2013 [cit. 2020-07-25]. Available at: https://www.azom.com/article.aspx?ArticleID=9118

[43] Materials Thermal Properties Database. *Thermtest Instruments* [online]. Fredericton, NB, 2019 [cit. 2020-07-25]. Available at: https://thermtest.com/materials-database#titanium

[44] STRÁSKÝ, Josef. *Titanium and Titanium Alloys: PowerPoint Presentation*. FRVŠ 559/2013, 2013.

[45] MURRAY, J. L. The Ti-W (Titanium-Tungsten) System. *Bulletin of Alloy Phase Diagrams volume*. 1981, **1981** (2), 192-196. DOI: https://doi.org/10.1007/BF02881477.

[46] MOTYKA, Maciej, Waldemar ZIAJA a Jan SIENIAWSKI, ed. *Titanium Alloys: Novel Aspects of Their Manufacturing and Processing* [online]. IntechOpen, 2019 [cit. 2020-08-15]. ISBN 978-1-83962-554-1. Available at:

https://www.intechopen.com/books/titanium-alloys-novel-aspects-of-their-manufacturing-and-processing

[47] BRADFORD, Alina. Facts About Tungsten. *Live Science* [online]. 2016 [cit. 2020-07-25]. Available at: https://www.livescience.com/38997-facts-about-tungsten.html

[48] Tungsten: Chemical Element. *Encyclopedia Brittanica* [online]. Chicago, 2017 [cit. 2020-07-25]. Available at: https://www.britannica.com/science/tungsten-chemical-element

[49] Tungsten - Mechanical Properties And Material Applications. *AZO Materials* [online]. 2012 [cit. 2020-07-25]. Available at: https://www.azom.com/article.aspx?ArticleID=7641#:~:text=Tungsten%20has%20high%20electrical%20and,glass%20seals%2C%20and%20dimensional%20stability.

[50] AGUIRRE, Maria. Mechanical Behavior of W-Y2O3 and W-Ti Alloys from 25 A degrees C to 1000 A degrees C. *Metallurgical and Materials Transactions A*. 2009, **2009** (40), 2283-2290. DOI: https://doi.org/10.1007/s11661-009-9956-4.

[51] CATARINO, N. Helium and deuterium irradiation effects in tungsten-based materials with titanium. *Surface and Coatings Technology*. 2018, **2018** (355), 143-147. DOI: https://doi.org/10.1016/j.surfcoat.2018.03.015.

[52] BUZI, L. Deuterium and helium ion irradiation of nanograined tungsten and tungsten–titanium alloys. *Nuclear Materials and Energy*. 2019, **2019** (21). DOI: https://doi.org/10.1016/j.nme.2019.100713.

[53] The PTA Process. *Commersald* [online]. Modena: Commersald [cit. 2020-07-14]. Available at: https://www.commersald.com/the-pta-process-plasma-transferred-arc.htm

[54] ROHAN, Pavel. Navařování plazmatem - ochranné povlaky ve výrobě i výzkumu. *MM Průmyslové spektrum*. 2015, **2015** (1), 86. ISSN 1212-2572.

[55] SUDNIK, Wladislav. *Arc Welding* [online]. 1. IntechOpen, 2011 [cit. 2020-07-14]. ISBN 978-953-51-6083-0. Available at: https://www.intechopen.com/books/arc-welding

[56] AMBROŽ, Oldřich, Bohumil KANDRUS a Jaroslav KUBÍČEK. *Technologie svařování a zařízení*. 1. vydání. Ostrava: ZEROSS, 2001. Svařování. ISBN 80-857-7181-0.

[57] DESHMUKH, D. a V. KALYANKAR. Recent status of overlay by plasma transferred arc welding technique. *International Journal of Materials and Product Technology*. 2018, **2018** (56/1,2), 23-83.

[58] OLSON, D. L. *ASM Handbook Volume 6: Welding, Brazing and Soldering*. 10th edition. Materials Park, OH, USA: ASM International, 2016. ISBN 978-0-87170-382-8.

[59] OH, J., K. ROH a J. LIM. Brief review of removal effect of hydrogen-plasma arc melting on refining of pure titanium andtitanium alloys. *International Journal of Hydrogen Energy*. 2016, **2016** (41/48), 23033-23041. DOI: https://doi.org/10.1016/j.ijhydene.2016.09.082.

[60] KUBÍČEK, Jaroslav. *Technologie II - Část Svařování: Speciální metody tavného svařování - Tlakové svařování*. Brno, 2006. Sylabus přednášek. Vysoké učení technické v Brně.

[61] XIBAO, Wang a Liu HUA. Metal powder thermal behaviour during the plasma transferred arc surfacing process. *Surface and Coatings Technology*. 1998, **1998** (106), 156-161. DOI: https://doi.org/10.1016/S0257-8972(98)00521-0.

[62] Atomized Powders. *Cogne USA Speciality Steel, Inc.* [online]. [cit. 2020-07-18]. Available at: http://cogneusa.com/wp-content/uploads/2016/02/ptapowder_en.pdf

[63] D'OLIVIERA, A., R. PAREDES a R. SANTOS. Pulsed current plasma transferred arc hardfacing. *Journal of Materials Processing Technology*. 2006, **2006** (171/2), 167-174. DOI: https://doi.org/10.1016/j.jmatprotec.2005.02.269.

[64] ROHAN, P., T. KRAMÁR, K. KOVANDA a J. URBAN. High speed steel cladding by PTA - Influence of parameters. In: *METAL 2016 - 25th Anniversary International Conference on Metallurgy and Materials, Conference Proceedings*. 2016, s. 946-950. Available at: https://www.scopus.com/inward/record.uri?eid=2-s2.0-

85010824756&partnerID=40&md5=11b36174fb827fc135260272af41b2e8

[65] KSK, s.r.o. *KSK - český výrobce navařovacích automatů, kooperant v oboru navařování tvrdokovů* [online]. Česká Třebová: KSK, s.r.o., 2016 [cit. 2017-11-30]. Available at: http://www.kskct.cz/cs/navarovani/

[66] BOXANOVÁ, Monika. *Aditivní výroba polotovarů pulzní PTA metodou*. Praha, 2019. Master's thesis. Czech Technical University in Prague.

[67] Argon - Thermophysical Properties. *The Engineering Toolbox* [online]. 2008 [cit. 2020-07-20]. Available at: https://www.engineeringtoolbox.com/argon-d_1414.html

[68] METCALFE, J. a M. QUIGLEY. Heat Transfer in Plasma-Arc Welding. *Welding Journal*. 1975, **1975** (54/3), 99-103.

APPENDICES

Appendix A: *Photographs of individual layers in multi-layer samples*

Sample III

Sample III, Layer 1

Photograph N/A

Sample III, Layer 2

Sample III, Layer 3

Sample IV

Sample IV, Layer 1

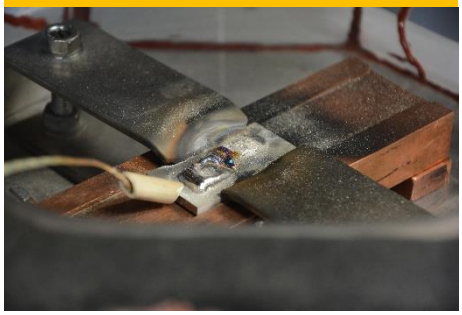

Sample IV, Layer 2

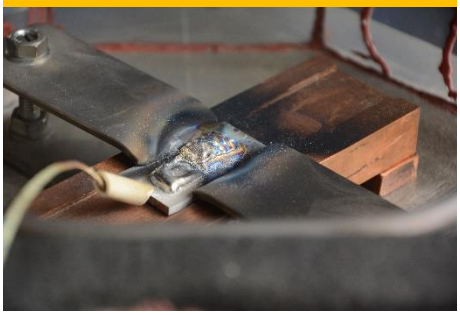

Sample IV, Layer 3

Sample IV, Layer 4

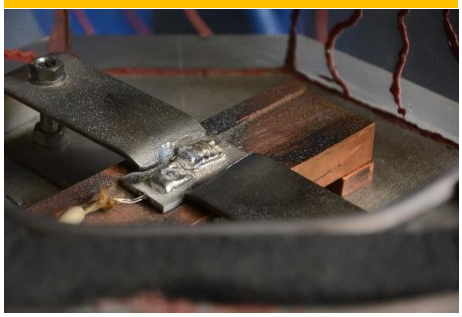

Sample IV, Layer 5

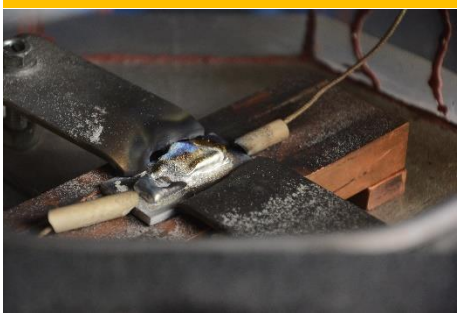

Sample V

Sample V, Layer 1

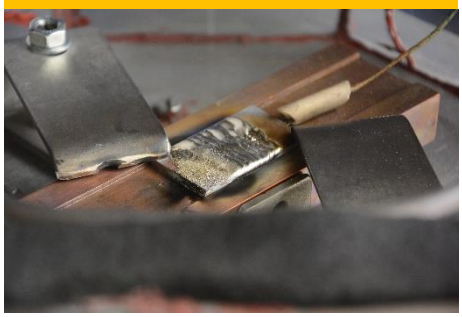

Sample V, Layer 2

Sample V, Layer 3

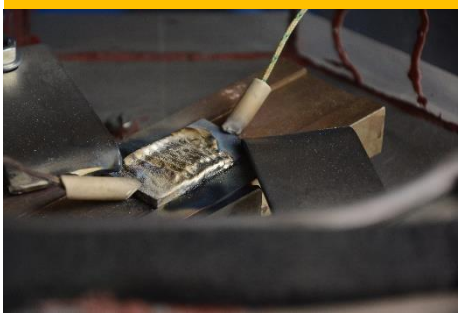

Sample V, Layer 4

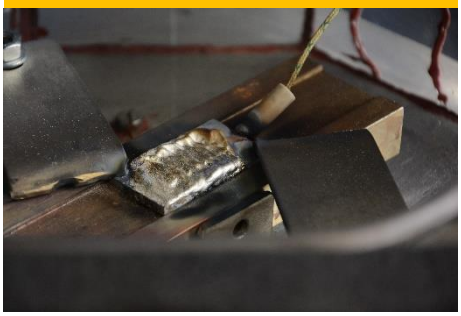

Sample V, Layer 5

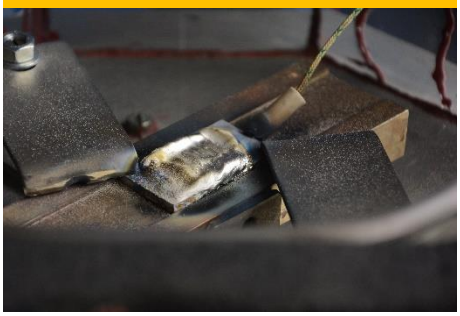

Sample V, Layer 6

Sample VI

Sample VI, Layer 1

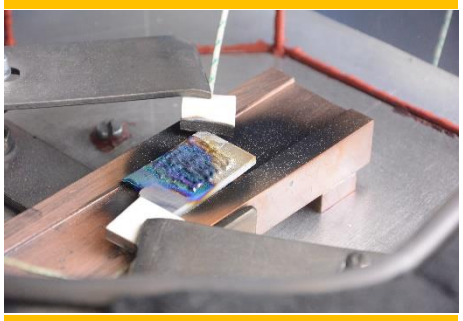

Sample VI, Layer 2

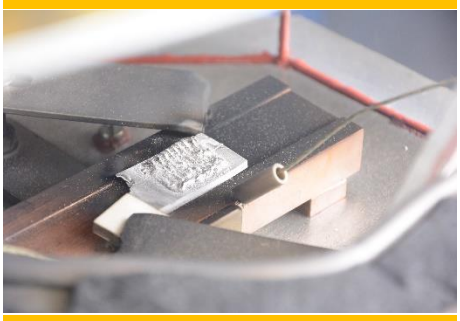

Sample VI, Layer 3

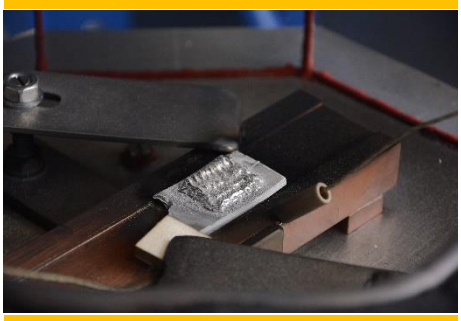

Sample VI, Layer 4

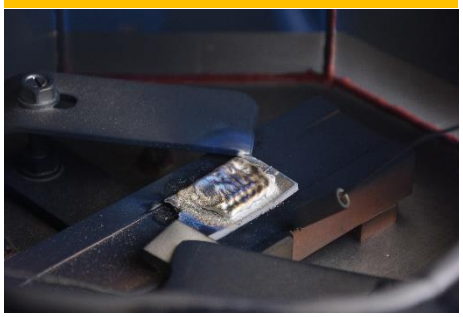

Sample VI, Layer 5

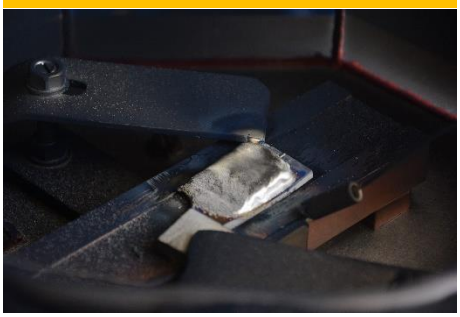

Sample VI, Layer 6

Sample VII

Sample VII, Layer 1

Sample VII, Layer 2

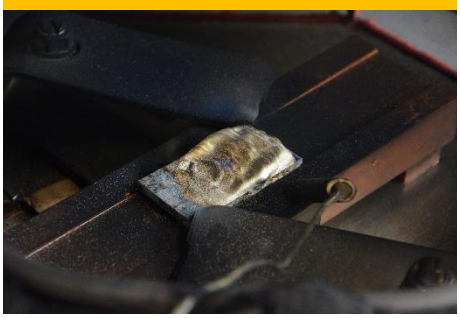

Sample VII, Layer 3

Sample VII, Layer 4

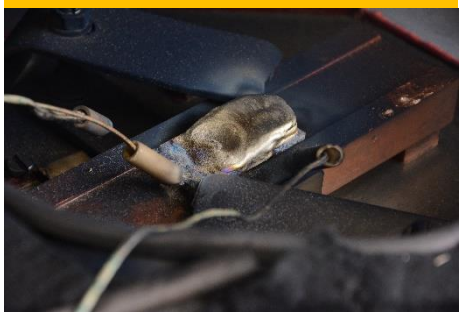

Sample VII, Layer 5

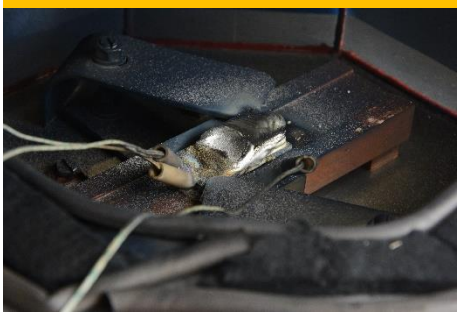

Appendix B: *Approximation of phase composition by Vegard's law*

Table 1: Calculated content of the approximation phases in each layer, with lattice parameters, Sample VII

Location [-]	Conc. of β-Ti(+W) [wt. %]	Lattice par. [-]	Conc. of 50Ti-50W [wt. %]	Lattice par. [-]
Outer	100.0	3,25923	0.0	N/A
Central	70.84	3,229909	29.16	3,187748
Inner	30.92	3,217562	69.08	3,189882

Table 2: Results of approximation of concentrations by Vegard's law, Sample VII

Phase	β-Ti(+W)		50Ti-50W	
Location [-]	Conc. of Ti [at.%]	Conc. of W [at.%]	Conc. of Ti [at.%]	Conc. of W [at.%]
Outer	67	33	-	-
Central	46	54	16	84
Inner	37	63	18	82